NUMERICAL INVESTIGATION OF THE IMPACT OF APPLIED MAGNETIC FIELDS WITH VARIED INTENSITIES AT DIFFERENT LOCATIONS ON FERRONANOFLUID FLOW IN A SMOOTH PIPE

2023
MASTER THESIS
MECHANICAL ENGINEERING

Hani MOHAMAD HAMIDO

Thesis Advisor
Prof. Dr. Kamil ARSLAN

NUMERICAL INVESTIGATION OF THE IMPACT OF APPLIED MAGNETIC FIELDS WITH VARIED INTENSITIES AT DIFFERENT LOCATIONS ON FERRONANOFLUID FLOW IN A SMOOTH PIPE

Hani MOHAMAD HAMIDO

Thesis Advisor

Prof. Dr. Kamil ARSLAN

T.C.

Karabük University

Institute of Graduate Programs

Department of Mechanical Engineering

Prepared as

Master Thesis

KARABÜK

August 2023

I certify that in my opinion the thesis submitted by Hani MOHAMAD HAMIDO titled "NUMERICAL INVESTIGATION OF THE IMPACT OF APPLIED MAGNETIC FIELDS WITH VARIED INTENSITIES AT DIFFERENT LOCATIONS ON FERRONANOFLUID FLOW IN A SMOOTH PIPE" is fully adequate in scope and in quality as a thesis for the degree of Master of Science.

Prof. Dr. Kamil ARSLAN .....

Thesis Advisor, Department of Mechanical Engineering

This thesis is accepted by the examining committee with a unanimous vote in the Department of Mechanical Engineering as a Master of Science thesis. August 9, 2023

Examining Committee Members (Institutions)	Signature
Chairman : Assist. Prof. Dr. Mehmet GÜRDAL (KU)	.....
Member : Prof. Dr. Kamil ARSLAN (KBU)	.....
Member : Assist. Prof. Dr. Mutlu TEKİR (KBU)	.....

The degree of Master of Science by the thesis submitted is approved by the Administrative Board of the Institute of Graduate Programs, Karabük University.

Prof. Dr. Müslüm KUZU .....

Director of the Institute of Graduate Programs

“I declare that all the information within this thesis has been gathered and presented in accordance with academic regulations and ethical principles and I have according to the requirements of these regulations and principles cited all those which do not originate in this work as well.”

Hani MOHAMAD HAMIDO

ABSTRACT

M.Sc. Thesis

NUMERICAL INVESTIGATION OF THE IMPACT OF APPLIED MAGNETIC FIELDS WITH VARIED INTENSITIES AT DIFFERENT LOCATIONS ON FERRONANOFLUID FLOW IN A SMOOTH PIPE

Hani MOHAMAD HAMIDO

Karabük University
Institute of Graduate Programs
Department of Mechanical Engineering

Thesis Advisor:
Prof. Dr. Kamil ARSLAN
August 2023, 101 pages

This master thesis presents a numerical investigation for determination of the effect of location and intensity of applied magnetic field on the ferronanofluid flow in a smooth pipe. The study focuses on laminar flow condition with Reynolds numbers ranging from $1000 \leq Re \leq 2000$. Hydrodynamically and thermally developing flow condition has been considered for this study. The ferronanofluid flowing into a smooth pipe with a length of $L=1500$ *mm* and diameter of $D=16$ *mm* has been considered. The selected nanofluid is a distilled water-based ferronanofluid consisting of Fe_3O_4, chosen for its attraction to magnetic fields. The nanoparticle volume fractions of the ferronanofluid have been considered as ($\varphi = 0.5, 1,$ and 2 vol. %). The analyses have encompassed three different magnetic field intensities as *0.01, 0.05,* and *0.1 T*. To identify the optimal scenario, the magnetic field location has been varied within three distinct sections of the pipe, each measuring *100 mm* and located at distances from the inlet as

follows: *300 - 400 mm, 750 - 850 mm,* and *1200 - 1300 mm*. Initially, the behavior of the ferronanofluid was examined without the presence of a magnetic field, considering different nanoparticle volume fraction values. Subsequently, the study investigated the flow of ferronanofluid under the influence of a magnetic field with three different intensity magnitudes and three different locations. The optimal case has been identified as the case of ferronanofluid flow with nanoparticle volume fraction of *2 %* under a magnetic field with a strength of *0.01 T*, with the magnetic field positioned at the third location distancing *1200 mm – 1300 mm.* This configuration yields the highest value for the performance evaluation criteria.

Key Words **:** ferronanofluid, magnetic field, laminar flow, convective heat transfer, *CFD*.

Science Code : 91411

ÖZET

Yüksek Lisans Tezi

FARKLI LOKASYONLARDA DEĞİŞKEN YOĞUNLUKLARA SAHİP MANYETİK ALANLARIN PÜRÜZSÜZ BİR BORUDAKİ FERRONANOAKIŞKAN AKIŞI ÜZERİNDEKİ ETKİSİNİN SAYISAL OLARAK İNCELENMESİ

Hani MOHAMAD HAMIDO

Karabük Üniversitesi
Lisansüstü Eğitim Enstitüsü
Makine Mühendisliği Anabilim Dalı

Tez Danışmanı:
Prof. Dr. Kamil ARSLAN
Ağustos 2023, 101 sayfa

Bu yüksek lisans tezi, düz bir borudaki ferronanoakışkan akışı üzerine uygulanan manyetik alanın konumu ve yoğunluğunun etkisinin belirlenmesi için sayısal bir araştırma sunmaktadır. Çalışma, $1000 \leq Re \leq 2000$ arasında değişen Reynolds sayıları ile laminer akış durumuna odaklanmaktadır. Bu çalışma için hidrodinamik ve termal olarak gelişen akış durumu dikkate alınmıştır. Uzunluğu $L=1500$ *mm* ve çapı $D=16$ *mm* olan düz bir boruda akan ferronanoakışkan ele alınmıştır. Seçilen nanoakışkan, manyetik alanlara olan etkileşimi nedeniyle seçilen, Fe_3O_4'den oluşan, damıtılmış su bazlı bir ferronanoakışkandır. Ferronanoakışkanın nanoparçacık hacim oranları (φ = *0,5, 1,0* ve *2,0* %hacimce) olarak kabul edilmiştir. Analizler, *0,01, 0,05* ve *0,1 T* olmak üzere üç farklı manyetik alan yoğunluğunu kapsamaktadır. Optimum senaryoyu belirlemek için manyetik alan konumu, borunun her biri *100 mm* ölçülerinde ve

girişten uzaklıklarda bulunan üç ayrı bölümünde değiştirilmiştir (*300 - 400 mm, 750 - 850 mm ve 1200 - 1300 mm*). Başlangıçta, farklı nanoparçacık hacim oranı değerleri dikkate alınarak, manyetik alan olmadan ferronanoakışkanın davranışı incelenmiştir. Ardından, çalışma, üç farklı yoğunluk değeri ve üç farklı konumdaki manyetik alanın etkisi altındaki ferronanoakışkan akışı incelenmiştir. Optimal durum, manyetik alan *1200 mm – 1300 mm* mesafedeki üçüncü konumda konumlandırılmış, *0,01 T*'lık bir manyetik alan yoğunluğu altında %2'lik nanoparçacık hacim oranına sahip ferronanoakışkan akışı durumu olarak tanımlanmıştır. Bu durum, performans değerlendirme kriterleri için en yüksek değeri vermektedir.

Anahtar Kelimeler : Ferronanoakışkan, manyetik alan, laminer akış, taşınımla ısı transferi, *HAD*.

Bilim Kodu **:** 91411

ACKNOWLEDGMENT

I would like to express my deepest appreciation and gratitude to my thesis advisor, Prof. Dr. Kamil ARSLAN. His guidance, expertise, and unwavering support throughout the entire research process have been invaluable. Professor Arslan's commitment to academic excellence, his insightful feedback, and his dedication to my intellectual growth have greatly influenced the quality and success of this thesis. I would also like to thank Professor Arslan for providing me with numerous opportunities to expand my knowledge and skills in the field of nanofluids. His encouragement and belief in my abilities have been instrumental in shaping my academic and professional development. I am truly grateful for his mentorship and the valuable lessons I have learned under his guidance. Additionally, I would like to acknowledge Professor Arslan's continuous encouragement and motivation, which inspired me to overcome challenges and persevere in my research. His constructive criticism and attention to detail have significantly enhanced the rigor and precision of this work.

I want to express my gratitude to my colleague Hayati KADIR PAZARLIOGLU for his assistance, even though he is occupied. I am appreciative of his support during the early stages of my thesis, where he provided me with guidance in a seamless manner.

I would like to express my sincere gratitude to my wife, Dr. Riham IDLBI, for her unwavering support and understanding throughout the entire process of completing this thesis. Her love, patience, and encouragement have been a constant source of motivation and strength.

I extend my heartfelt gratitude to my friend Hasan YASSIN for his unwavering support during my thesis. His encouragement and insights were invaluable. Hasan's friendship played a pivotal role in my success.

TABLE OF CONTENTS

Page

THESIS APPROVAL PAGE ..... **Hata! Yer işareti tanımlanmamış.**
ABSTRACT iv
ÖZET vi
ACKNOWLEDGMENT viii
TABLE OF CONTENTS ix
LIST OF FIGURES xi
LIST OF TABLES xv
SYMBOLS AND ABBREVITIONS INDEX xvi

PART 1: INTRODUCTION 1
1.1. Heat Transfer Methods 1
1.1.1. Active method 1
1.1.2 Passive method 2
1.1.3 Mixed method 3
1.2. The Nanofluids 3
1.2.1. The structure of the nanofluids 4
1.2.2. The ferronanofluids 5
1.3. The Application of Nanofluids 5
1.3.1. Industrial and domestic cooling/heating 6
1.3.2. Nuclear reactors 6
1.3.3. Smart fluids 6
1.3.4. Drilling technology 7
1.3.5. Electronic applications 8
1.3.6. Automobile applications 8
1.3.7. Biomedical applications 9
1.3.8. Other applications 9

PART 2: LITERATURE REVIEW 10

Page

PART 3: METHODOLOGY 19
3.1. PHYSICAL MODEL. 21
3.2. GOVERNING EQUATIONS 24
3.3. SOLUTION PROCEDURE 27
3.4. MESH INDEPENDENCE STUDY 28

PART 4: RESULTS AND DISCUSSION 32
4.1. Water Flow in Smooth Pipe 33
4.2. Ferronanofluid Flow in Smooth Pipe with the Absence of Magnetic Field 36
4.2.1. Convection heat transfer coefficient 37
4.2.2. Nusselt number 38
4.2.3. Darcy friction factor 39
4.2.4. Performance evaluation criteria 39
4.3. Ferronanofluid Flow in Smooth Pipe Under the Effect of Magnetic Field 43
4.3.1. Ferronanofluid Flow Under the Effect of MF at Location 1 (300 – 400) mm 45
4.3.2. Ferronanofluid Flow Under the Effect of MF at Location 2 (700 – 800) mm 57
4.3.3 Ferronanofluid Flow Under the Effect of MF at Location 3 (1200 – 1300) mm 70
4.4. Comparing the Cases 83
4.4.1. PEC for Different NPVFs at 1st Location 84
4.4.2. PEC for Different NPVFs at 2nd Location 85
4.4.3. PEC for Different NPVFs at 3rd Location 87
4.5. The best-case scenario of PEC. 89

PART 5: CONCLUSION 94
SUGGESTIONS FOR FUTURE WORK 95
REFERENCES 96

RESUME 101

LIST OF FIGURES

Page

Figure 1. 1: Heat exchanger with fan [3]. 2

Figure 1. 2: Heat exchanger [3]. 3

Figure 3. 1: The Study flow chart 19

Figure 3. 2: Front view of the smooth pipe under heat flux. 22

Figure 3. 3: Front view of the smooth pipe with magnetic field at 1st location. 22

Figure 3. 4: Front view of the smooth pipe with magnetic field 2nd location. 23

Figure 3. 5: Front view of the smooth pipe with magnetic field 3rd location. 23

Figure 3. 6: Explanation of computational domain and the boundary conditions 27

Figure 3. 7: Enableing MHD model. 28

Figure 3. 8: Mesh independence study at Re =1000 29

Figure 3. 9: Variation in the number of elements. 30

Figure 3. 10: Cross-section view of the meshed pipe. 30

Figure 3. 11: Mesh in the magnetic field area. 31

Figure 4.1: Variation of Nu number with Re number for pure water [45].....34

Figure 4. 2: Variation of Darcy friction factor with Re number for pure water [46]. .. 35

Figure 4.3: Surface Nusselt number distribution for water. 35

Figure 4. 4: Surface temperature and velocity distribution for water. 36

Figure 4.5: Variation of convection heat transfer with Reynolds number for different NPVF. 38

Figure 4. 6 Variation of Nusselt number with Reynolds number for different NPVF. 38

Figure 4. 7 Variation of Darcy friction factor with Re for different NPVF. 39

Figure 4. 8 Variation of PEC with Re for different NPVF. 40

Figure 4. 9 Variation of PEC with Re for 2.5 % NPVF. 41

Page

Figure 4. 10. Surface Nusselt number distribution for different NPVF. 42

Figure 4. 11. Surface temperature distribution for different NPVF..... 42

Figure 4. 12. Velocity distribution for different NPVF. 43

Figure 4.13. Variation of Nu number with Re number for different MF intensities. ... 47

Figure 4. 14 Variation of Pressure drop with Re number for different MF intensities. 47

Figure 4. 15 Variation of Darcy Friction with Re number for different MF intensities. 48

Figure 4. 16 Variation of PEC with Re number for different MF intensities. 49

Figure 4. 17. Variation of surface Nusselt number distribution for different MF intensities..... 49

Figure 4. 18. Variation of surface temperature distribution for different MF intensities 50

Figure 4. 19 Variation of velocity distribution for different MF intensities..... 50

Figure 4. 20 Variation of Nu number with Re number for different MF intensities. ... 51

Figure 4. 21 Variation of Pressure Drop with Re number for different MF intensities. 52

Figure 4. 22 Variation of Darcy friction with Re number for different MF intensities.53

Figure 4. 23 Variation of PEC with Re number for different MF intensities. 54

Figure 4. 24 Variation of Nu number with Re number for different MF intensities. ... 55

Figure 4. 25 Variation of Pressure drop with Re number for different MF intensities. 55

Figure 4. 26 Variation of Darcy friction with Re number for different MF intensities.56

Figure 4. 27 Variation of PEC with Re number for different MF intensities. 57

Figure 4. 28 Variation of Nu number with Re number for different MF intensities. ... 58

Figure 4. 29 Variation of Pressure drop with Re number for different MF intensities. 59

Figure 4. 30 Variation of Darcy friction with Re number for different MF intensities.60

Figure 4. 31 Variation of PEC with Re number for different MF intensities. 61

Figure 4. 32 Variation of Nu number with Re number for different MF intensities. ... 62

Page

Figure 4. 33 Variation of Pressure drop with Re number for different MF intensities. 63

Figure 4. 34 Variation of Darcy friction with Re number for different MF intensities.64

Figure 4. 35 Variation of PEC with Re number for different MF intensities. 64

Figure 4. 36 Variation of Nu number with Re number for different MF intensities. ... 65

Figure 4. 37 Variation of Pressure drop with Re number for different MF intensities. 66

Figure 4. 38 Variation of Darcy friction with Re number for different MF intensities.67

Figure 4. 39 Variation of PEC with Re number for different MF intensities. 68

Figure 4. 40. Variation of surface Nusselt number distribution for different NPVF.... 68

Figure 4. 41. Variation of surface temperature distribution for different NPVF. 69

Figure 4. 42. Velocity distribution streamline for different NPVF. 69

Figure 4. 43 Variation of Nu number with Re number for different MF intensities. ... 71

Figure 4. 44 Variation of Pressure drop with Re number for different MF intensities. 72

Figure 4. 45 Variation of Darcy friction with Re number for different MF intensities.73

Figure 4. 46 Variation of PEC with Re number for different MF intensities. 74

Figure 4. 47 Variation of Nu number with Re number for different MF intensities. ... 75

Figure 4. 48 Variation of Pressure drop with Re number for different MF intensities. 76

Figure 4. 49 Variation of Darcy friction with Re number for different MF intensities.77

Figure 4. 50 Variation of PEC with Re number for different MF intensities. 78

Figure 4. 51 Variation of Nu number with Re number for different MF intensities. ... 79

Figure 4. 52 Variation of Pressure drop with Re number for different MF intensities. 80

Figure 4. 53 Variation of Darcy friction with Re number for different MF intensities.81

Figure 4. 54 Variation of PEC with Re number for different MF intensities. 81

Figure 4. 55. Variation of surface Nusslet number distribution for different locations. 82

Figure 4. 56 Variation of Surface temperature distribution for different MF locations. 82

Figure 4. 57 Variation of velocity distribution for different MF locations..... 83

Page

Figure 4.58. Variation of PEC with Re number for various NPVFs. 84

Figure 4. 59 Variation of PEC with Re number for various NPVFs 86

Figure 4. 60 Variation of PEC with Re number for various NPVFs. 88

Figure 4. 61 Variation of PEC with Re number for different MF locations. 90

Figure 4. 62 PEC with Re number for 2 % NPVF under 0.01 T MF – 3rd location. 90

Figure 4. 63 Surface Nusselt number distribution. 91

Figure 4. 64 Surface temperature distribution. 91

Figure 4. 65 Pipe cross section temperature distribution on the 3rd location and outlet. 92

Figure 4. 66 Velocity streamline distribution. 92

Figure 4. 67 Pipe cross section velocity distribution on the 3rd location and outlet. 93

LIST OF TABLES

Page

Table 3. 1 Termophysical properties of the water and Fe_3O_4/water 20

Table 3. 2 Thermophysical properties of Aluminum. 21

Table 4.1. Cases of the study under the magnetic field.....45

Table 4.2. PEC of various NPVFs and MF intensities at 1st Location. 85

Table 4. 3 PEC of various NPVFs and MF intensities at 2nd Location..... 87

Table 4. 4 PEC of various NPVFs and MF intensities at 2nd Location..... 89

SYMBOLS AND ABBREVITIONS INDEX

SYMBOLS

TWh : Terawatt-hours

Fe_3O_4 : Iron Oxid

K_f : Thermal conductivity of nanofluid

MF : Magnetic Field, T

MHD : Magnetohydrodynamics

NPVF : Nanoparticles Volume Fraction

A : Area, m^2

D : Diameter, m

f : Darcy friction factor, -

h : Heat transfer coefficient, $W/m^2.K$

k : Thermal conductivity, W/m.K

L : Length, m

Nu : Nusselt number, -

p : Pressure, Pa

PEC : Performance Elevation Criteria, -

$\dot{q}$: Heat transfer rate, W

$\ddot{q}$: Heat flux, W/m^2

T : Temperature, K

V : Velocity, m/s

ρ : Fluid density, kg/m^3

μ : Dynamic viscosity, $N.s/m^2$

Re : Reynolds number, -

ΔP : Pressure drop, Pa

PART 1: INTRODUCTION

1.1. Heat Transfer Methods

With the rise of globalization, modern lifestyle, and an increasing global population, the demand for goods has experienced a significant surge. As a result, production capacities are growing exponentially, leading to the establishment of more factories and manufacturing plants across various industries to meet this demand. Moreover, in every industry, heat must be added, removed, or transferred to facilitate various processes. It is crucial for these operations to be executed efficiently, economically, and expeditiously. Consequently, researchers and engineers have been driven to explore innovative solutions and more effective techniques in the field of heat transfer.

Extensive research efforts have been dedicated to improving heat transfer and discovering more efficient methods in thermal systems. These methods and techniques have been categorized as active, passive, and mixed methods to facilitate comprehension and identification [1].

1.1.1. Active method

The active method represents the conventional approach to augment heat transfer, involving the utilization of an external power source to facilitate heat transfer [2]. This method typically requires additional energy consumption by the heat transfer medium or fluid. Numerous techniques fall under the category of actively enhancing convection heat transfer, including mechanical aids, surface vibration, fluid vibration, electrostatic fields, injection, suction, and jet impingement. A prominent example of the active method is illustrated in Figure 1.1, which depicts a heat exchanger equipped with a fan.

Figure 1. 1: Heat exchanger with fan [3].

1.1.2 Passive method

The passive method offers a more cost-effective approach as it does not require an external power supply or additional energy input to enhance heat transfer. This method focuses on optimizing the properties of working fluids or heat transfer surfaces to improve heat transfer efficiency [4]. It achieves this by modifying the fluid properties or developing more effective mediums for heat transfer, as well as by altering the surfaces of thermal systems. Various techniques fall under the passive method, including processed surfaces, uneven surfaces, enlarged surfaces, coiled tubes, swirl flow devices, additives for liquids and gases, and surface tension devices. An illustrative example of a passive method technique is the use of extended surfaces, such as fins, as depicted in Figure 1.2 within a heat exchanger.

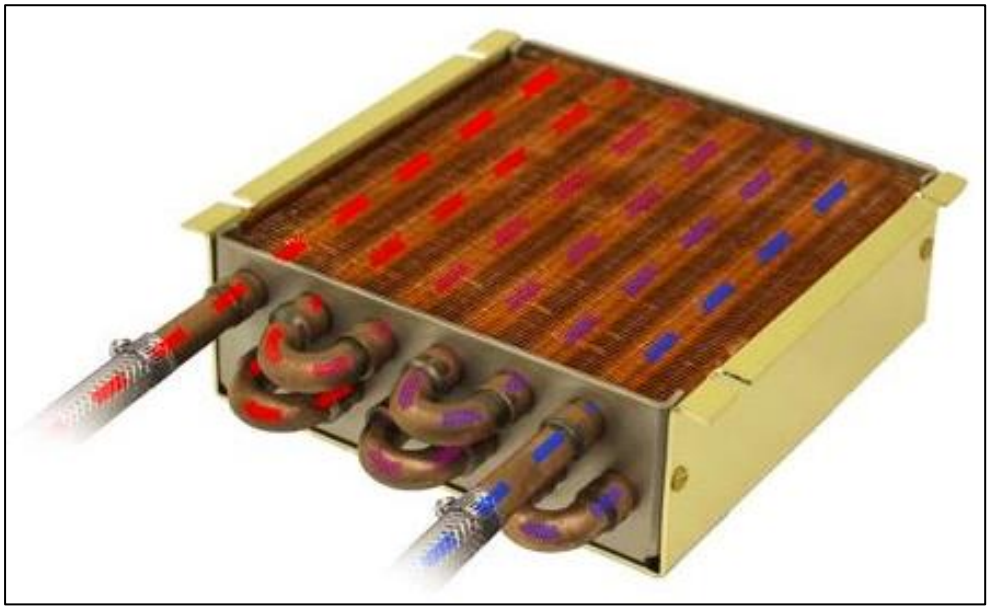

Figure 1. 2: Heat exchanger [3].

1.1.3 Mixed method

The mixed method in heat transfer combines elements from both active and passive techniques to optimize performance. Active methods hinge on external power sources to enhance heat transfer, while passive methods leverage intrinsic properties of fluids and surfaces. By integrating these approaches, engineers aim to maximize heat transfer rates while minimizing energy consumption and costs [5]. The mixed method employs advanced materials, intelligent control systems, and hybrid configurations to achieve desired outcomes. It encompasses techniques such as integrating active elements within passive systems or incorporating passive elements into traditionally active systems. This approach offers versatility and adaptability, leading to improved energy efficiency, enhanced thermal management, and increased system effectiveness in various industrial applications.

1.2. The Nanofluids

Fluids are commonly used as a medium for heat transfer, and enhancing their thermal properties is a passive methodology for enhancing the efficiency of thermal systems. Various industries, such as transportation, residential and non-residential buildings, oil

and gas, paper, casting, chemical, and food processing, rely on fluid conduction for heat transfer to reduce energy consumption and improve equipment efficiency. However, the thermal conductivity of standard convection heat transfer fluids poses limitations compared to metallic solids. For instance, the thermal conductivity of aluminum is ≈ 400 times greater than water and ≈ 1650 times higher than engine oil [6]. To overcome this constraint, the concept of metallic fluids emerged, where their thermal conductivity surpasses that of normal fluids. By incorporating suspended metallic particles, the thermal conductivity of these liquids is expected to be significantly enhanced compared to ordinary fluids. Over the years, many theoretical and experimental studies have been conducted on fluids containing suspended solid particles, with Maxwell's pioneering theoretical research dating back *141* years ago to *1882*.

1.2.1. The structure of the nanofluids

The concept of metallic fluids, which are a type of nanofluid designed to enhance heat transfer by incorporating solid or metallic particles into conventional fluids. Metallic fluids aim to impart solid-like thermal characteristics to the base fluid, thereby improving its heat transfer capabilities.

Metallic fluids consist of two primary constituents: a carrier fluid and suspended solid particles. The carrier fluid serves as the base medium and can be selected from substances such as distilled water, ethylene glycol, or engine oil. These fluids provide the necessary fluidity and compatibility with the heat transfer system.

The suspended solid particles in metallic fluids typically comprise metallic oxides or other solid materials, including iron oxide, aluminum oxide, copper oxide, silicon, and other suitable particles. These particles are chosen based on their thermal conductivity and stability, as they play a crucial role in enhancing the thermal properties of the fluid. The size of the suspended particles in metallic fluids can vary, ranging from millimeters to micrometers. The specific particle size distribution and concentration are important factors that influence the overall thermal performance and stability of the metallic fluid [7].

Research and development efforts in the field of metallic fluids have focused on optimizing the composition, particle size, and concentration of the suspended solids to achieve the desired thermal characteristics. By incorporating solid particles into conventional fluids, metallic fluids offer improved heat transfer performance and find applications in various areas where efficient heat dissipation is of utmost importance.

1.2.2. The ferronanofluids

Ferronanofluids are a distinctive class of liquids that consist of small magnetic particles, typically nanoparticles of magnetite, suspended in a carrier fluid, commonly an oil-based substance. These magnetic particles grant ferronanofluids distinctive characteristics, including the ability to be manipulated and controlled by magnetic fields [8].

The behavior of ferronanofluids in response to magnetic fields is intriguing and depends on factors such as the potency of the magnetic field. These fluids find diverse applications, with three prominent ones being sealing, damping, and heat transfer, which specifically interests us in this research endeavor.

In addition to these primary applications, ferronanofluids find utility in various fields, including electronics, sound systems, medical equipment, and artistic installations. They exhibit remarkable properties, such as the capability to form spiky structures known as "magnetic spikes". Furthermore, ferronanofluids have been employed in numerous scientific experiments and demonstrations. Given their fascinating attributes and expanding range of practical and scientific applications, ferronanofluids represent a captivating material worthy of exploration.

1.3. The Application of Nanofluids

Nanofluids, a class of fluids containing nanoparticles in suspension, possess exceptional physical and chemical properties that render them highly desirable for a range of applications across diverse fields. Notably, nanofluids exhibit pronounced benefits in enhancing heat transfer within thermal management systems, improving lubrication characteristics, and exhibiting potential in biomedical and energy-related domains. Their unique attributes have propelled significant interest in exploring their potential for

advancing technological advancements and addressing key challenges in these areas. By harnessing the capabilities of nanofluids, researchers and engineers aim to optimize heat transfer efficiency, reduce energy consumption, enhance lubrication performance, and explore novel opportunities in fields such as medicine and sustainable energy generation. Through comprehensive studies and experimentation, the intricate mechanisms underlying the behavior and performance of nanofluids are being unraveled, paving the way for their widespread application and the realization of their immense potential in diverse sectors [9].

1.3.1. Industrial and domestic cooling/heating

The nanofluids boost heat transfer effectively, thus increasing the efficiency of the thermal systems, which will end up with huge saving of energy and emission. A study has carried out in US to calculate the energy saving if the conventional coolant fluids replaced with nanofluids which result energy saving equal to the consumption of *50,000 – 150,000* households per year [10].

1.3.2. Nuclear reactors

Countable number of research have assessed the possibilities of using the nanofluids in the coolant systems of the nuclear reactors [11], the studies have focused on the improvement of the efficiency of removing the heat, where it is still limited by many factors. Authors have covered all the cooling systems in the nuclear plants. The nanofluids give significant changes in the cooling system and it helps to solve some of the challenges in the reactors.

On the other hand, these improvements still need more consideration when we look at these challenges from a safety perspective. Overall, replacing the traditional cooling fluids with nanofluids is promising and needs more research and development [12].

1.3.3. Smart fluids

The rapid advancement of technology has resulted in a heavy reliance on battery-powered devices, such as cars, phones, and laptops. This increased demand for energy,

coupled with limited energy resources, has prompted the exploration of innovative solutions. One promising avenue is the utilization of nanofluids as smart fluids to optimize energy consumption. Pioneering research projects have proposed the implementation of a specific type of nanofluid as a heat valve, offering a novel approach to regulate and control heat transfer processes.

By leveraging the unique properties of nanofluids, such as enhanced thermal conductivity and heat transfer capabilities, these smart fluids can effectively manage energy flow in various systems. The concept of utilizing nanofluids as heat valves opens up possibilities for more efficient energy utilization and improved thermal management. With further research and development, nanofluids have the potential to revolutionize energy conservation and enable the creation of advanced smart systems that optimize energy consumption based on specific requirements.

Exploring the capabilities of nanofluids as smart fluids represents a significant step towards sustainable and efficient energy utilization. By harnessing the advantages offered by nanofluids, researchers and engineers can pave the strategy for the development of innovative solutions technologies that address the growing demand for energy while minimizing waste and maximizing efficiency [13].

1.3.4. Drilling technology

Our planet earth has many energy resources that conserved under the crust, it has been announced by Massachusetts Institute of Technology MIT that the total geothermal energy of the earth is estimated by *13000 ZJ* and only *200 ZJ* can be extracted [14]. These energies are constituted as fusel fuel or geothermal, where extracting this energy has been limited by high temperature and pressure. Nevertheless, the nanofluids look promising in this field as well, the enhancement of transferring the heat will increase the performance of the drilling machinery. On the geothermal side, the nanofluids will help to improve the efficiency of the process and allow transferring higher temperature to the surface.

1.3.5. Electronic applications

The target in the Tech industry is to have smaller chips with higher performance, but that generates high temperature, thus the dissipation must be done rapidly. The expectation to have computer microchips that will generate confined heat flux of more than $10\ MW/m^2$ with power can ramp up to $300\ W$ [15]. The nanofluids possess high thermal conductivity, enabling the cooling system in the electronic chips to transfer the heat very effectively.

Manipulating and operating minimal volumes of liquid is necessary to operate fluidic digital display devices, optical microscopes, and other electromechanical devices. It turns out that, the wettability of the surfaces or even the surface tension can be engineered by nanofluids, and this process can be done whether by electrowetting or by using nanofluids with smaller nanoparticles [16].

1.3.6. Automobile applications

The vehicles manufacturers have been focusing all the time on how to reduce fuel consumption where the latter will result in good manners economically and environmentally. However, the main target for them is how to reduce the aerodynamic dragging force, where approximately *65%* of the truck speed is consumed to overcome this force. Therefore, the focus on how to design a truck with less wind resistance, subsequently the radiator is taking place in the front of the truck to remove the heat by convection. The researcher proof that, using nanofluids as a coolant fluid will help to reduce the size of the radiator by *105* which led to fuel saving by *5%*, considering the reduce in other operating equipment such as the pump and the compressor increased the saving up to *6%* [17].

The aluminum nanofluids can be produced by plasma arc system and using this aluminum nanofluids as additive to the diesel fuel can increase the total generated heat by the combustion [18].

The research showed that using the nanofluids instead of the conventional break fluids can increase the thermal properties of the break fluids, hence improve the efficiency of

the breaks. The nanofluids have been used in automatic transmission because of their thermal properties and the ability to dissipate the overheating in the system. One of the uses is lubrication, as the nanofluids have reduced the wear in the mechanical parts due to friction.

1.3.7. Biomedical applications

The nanofluids have been employed in the medical and pharmaceutical field at the beginning in the academia in *1990s*, but recently, some companies started commercial applications. The use of nanofluids is promising in drugs delivery, Cancer therapeutic, Cryopreservation, and some other advance applications.

1.3.8. Other applications

The classical physical concept about the normal fluids don’t apply on the nanofluids, especially in terms of adhesion and spreading, and that opens new horizons for other uses such as lubrication, soil redamation, and strainer. In short word, there will be many more engineering applications of nanofluids in the future.

PART 2: LITERATURE REVIEW

According to the International Energy Agency (IEA), global primary energy consumption has been steadily experiencing a rising trend over the past two decades, reaching *176,431 TWh* in *2021* compared to *124,821 TWh* previously. This surge in energy consumption, encompassing various sources such as oil, natural gas, coal, nuclear power, hydroelectricity, and renewable energy, reflects a significant global demand. As engineers and scientists, this trend highlights the need to effectively manage heat generation and transfer in various processes and industries. Numerous research studies have been dedicated to enhancing heat transfer efficiency in traditional methods and optimizing energy usage in these processes.

Heat transfer can be achieved through three methods: passive, active, and mixed. Passive methods, such as heat exchangers with extended surfaces to enhance convection, do not require an external energy source for heating or cooling. This makes them energy-efficient solutions. Active methods, on the other hand, rely on energy sources, such as fans, to facilitate heat removal or addition. Mixed methods combine aspects of both passive and active approaches, aiming to maximize efficiency while minimizing energy consumption.

Nanotechnology has emerged as a significant player in the passive heat transfer method. By incorporating solid particles into base fluids, nanotechnology enhances the thermal conductivity of these fluids. Common base fluids include distilled water and organic liquids like refrigerants, fuels, lubrication oils, and ethylene glycol. The higher thermal conductivity of the solid particles improves heat transfer efficiency in these nanofluids.

Overall, given the growing demand for energy and the need for efficient heat management, the application of nanotechnology and the exploration of passive heat

transfer methods present promising avenues for optimizing energy usage and enhancing overall process efficiency [19].

Choi [20], almost three decades ago, was one of the pioneers who had added the nanoparticles to the carrier fluids, he found out that there is always limitation in the thermal connectivity of the fluids so he decided to add copper and the results showed high potential of the use of nanofluids in the heat transfer systems and that'd been predicted this innovative idea will dramatically decrease the required pumping power in the heat exchanger, thus reducing the consumed energy, hence to improve the heat transfer by factor of *2x* times it needs to increase the pumping power by factor of *10x* where by using the nonfluids it requires only *3x* increase of the pumping power. The concept of nanofluids is all about comingling the nano-sized particles which could be aluminum, copper, silver, iron oxide, or any material with high thermal conductivity with the base fluids (water, oil, ethylene, etc.). The nanofluids field is a promising technology where there are considerable number of experimental studies have proven that the nanofluids noticeably increased the thermal conductivity of these fluids comparing to the normal fluids [6,21–24].

Ferronanofluids are suspensions consisting of magnetic particles dispersed in a nonmagnetic fluid medium. These magnetic particles, typically around *10 nm* in diameter, are monodomain, meaning they have a uniform magnetic alignment. To prevent particle aggregation and maintain stability, the Fe_3O_4 particles are coated with surfactant layers that adsorb onto their surfaces. These surfactant layers act as a protective barrier, preventing the particles from clumping together and maintaining the ferronanofluid's distinctive properties [25].

Despite the presence of surfactant layers, some particle aggregation can still occur due to attractive forces such as van der Waals forces and dipole-dipole interactions. However, the majority of particles remain dispersed in the carrier fluid due to the stabilizing effect of the surfactant layer [26].

In the lack of an external magnetic field, the particles within the ferronanofluid are randomly oriented, resulting in a lack of overall magnetization. However, when Exposed

to an external magnetic field, the dipole moments of the particles align with the field, causing the ferronanofluid to develop a net magnetic moment and become magnetized. This magnetization leads to a range of unique properties exhibited by ferronanofluids, including magnetization saturation (the maximum achievable magnetization under a given field strength) and magnetic anisotropy (the directional dependence of magnetic properties) [27].

Overall, ferronanofluids possess fascinating characteristics due to the interplay between the magnetic particles and the surrounding fluid medium. Grasping their behavior in the presence of magnetic fields is crucial for harnessing their potential applications in various fields, including electronics, medicine, and engineering [28].

Several studies have been conducted on nanofluids that consist of metallic, carbon nanotube *(CNTs)*, and nonmetallic materials. However, a significant portion of these studies have specifically investigated the thermal conductivities of ferronanofluids.

Gubin et al. and Li et al. systematically describes the primary techniques used to prepare ferronanofluid samples, along with presenting experimental data on the properties of ferronanofluids and discussing the primary theoretical perspectives on the magnetism of magnetic nanoparticles. Specifically, the article describes the experimental investigation of the viscosity and thermal conductivity of aqueous magnetic fluids in the presence and absence of external magnetic fields, specifically at low magnetic field intensities [29,30].

Poppelwell conducted measurements of the thermal conductivity of several ferronanofluids that contain colloidal dispersed Fe_3O_4 particles in carriers such as diester, hydrocarbon, water, and fluorocarbon, and it's been proven that when a magnetic field of *0.1 T* was applied, there was no observable impact on the thermal conductivities of the ferronanofluids [31].

Experimentally *Fe* nanofluids are produced using ethylene glycol and *Fe* nanocrystalline powder that was synthesized through a chemical vapor condensation method. In order to enhance the dispersion of nanoparticles, sonication with high-powered pulses is

utilized during the preparation of the nanofluids. After sonication, the nanofluids show an increase in thermal conductivity. By increasing the volume fraction of particles to *0.55 vol.%*, the thermal conductivity of a *Fe* nanofluid is non-linearly increased by up to *18%*. However, it has been discovered that the inclusion of highly thermally conductive materials, such as in the case of *Cu* nanofluids, does not always effectively improve the thermal transport properties of nanofluids [32].

Zhu et al. experimentally compared the thermal conductivity of the Fe_3O_4 aqueous nanofluids with the other oxide aqueous ones, where the results had proven that the thermal conductivity of the iron oxide was higher than other oxide aqueous nanofluids, the experiment carried over by observing the behavior of the particles with X-Ray scanner, and that attributed with the property of the clustering and alignment of the ferro particles [33].

Maryam et al. conducted an experiment to produce Magnetite Fe_3O_4 nanoparticles using a co-precipitation method at varying *PH* levels. They then analyzed the resulting products using X-ray diffraction *(XRD)*, Fourier transform infrared spectroscopy *(FTIS)*, and transmission electronic microscopy *(TEM)*. The study discovered that the particles were cubic in shape and displayed superparamagnetic properties when examined at room temperature. The researchers used Fe_3O_4 nanoparticles dispersed in water with tetramethyl ammonium hydroxide as a dispersant to make magnetic nanofluids. They then measured the thermal conductivity of the nanofluids at different volume fractions and temperatures and found that the thermal conductivity ratio increased as the temperature and volume fraction raised. The nanofluid containing *3 vol%* of nanoparticles at *40°C* exhibited the most significant increase in thermal conductivity, which was *11.5%*. The experimental findings were also compared to theoretical models [34].

Philip et al. observed a significant increase in thermal conductivity within a nanofluid composed of Fe_3O_4 particles when exposed to a magnetic field in the direction of heat flow. This enhancement was particularly notable at a particle loading of *6.3 vol %*, resulting in a K/K_f value of *4.0* and a maximum enhancement of *300%*. They attribute this increase in thermal conductivity to the formation of a chainlike structure, which

facilitates efficient heat conduction when the dipolar interaction energy exceeds thermal energy. These results align with recent theoretical predictions about enhanced thermal conductivity under aggregation phenomena, rather than the previously hypothesized micro convection mechanism [35].

Gavili et al. involved the use of simulations to investigate thermomagnetic convection in a square enclosure that was differentially heated and exposed to a two-dimensional magnetic field generated by Helmholtz coils. The primary aim of the study was to examine how the strength of the magnetic field gradient affects the heat transfer of magnetic fluids within the enclosure. Through their observations, they have discovered that when the direction of the magnetic field strength and temperature gradient are in the same direction, the velocities of magnetic field drift and natural convection work together to enhance heat transfer of magnetic fluids. In contrast, when the direction of the magnetic field strength and temperature gradient are opposite, the heat transfer of magnetic fluids decreases. Interestingly, when the magnetic field gradient is zero at the center of the coils, the temperature profiles within the enclosure are similar to those produced by free convection induced by buoyancy. These findings suggest that the interaction between magnetic fields and natural convection can significantly impact the heat transfer of magnetic fluids, and the strength and direction of the magnetic field gradient play a crucial role in this phenomenon [27].

Mei et al. experimentally investigated the effect of a parallel magnetic field on the thermo-hydraulic performance of Fe_3O_4-H_2O nanofluids in a circular tube. The study found that the Nusselt number was positively related to the nanoparticle mass fraction, but inversely related to the magnetic induction intensity. The resistance coefficient was also found to increase with the nanoparticle mass fraction and was further increased by the magnetic field. Compared to water, the resistance coefficient of the nanofluids could be increased by up to *11.5%*. The experimental data was compared with computational methods and good agreement was found. The comprehensive evaluation index showed that the highest value was found at the critical Reynolds number of *8000*. In addition, the exergy efficiency plot was used to evaluate the flow and heat transfer performance of the nanofluids, which showed that the working points were in Region I and Region II, indicating good heat transfer performance. The results suggest that the addition of

Fe_3O_4 nanoparticles to water can enhance the heat transfer performance of the fluid, but this enhancement is influenced by the nanoparticle mass fraction and magnetic field intensity [36].

Gavili et al. have prepared manuscript reports on an experimental investigation of the thermal conductivity of ferronanofluids containing Fe_3O_4 nanoparticles suspended in de-ionized water under the influence of a magnetic field. The magnetic field was generated using Helmholtz coils, and its intensity was controlled by the electric current. The saturation time and reversibility of the thermal conductivity were also studied after the magnetic field was switched off. Moreover, the effect of temperature on the thermal conductivity was analyzed. The results indicate that a ferronanofluid with *5.0%* volume fraction of nanoparticles with an average diameter of *10 nm* exhibited a maximum thermal conductivity enhancement of more than *200%*. Specifically, the presence of a magnetic field led to an increase in the thermal conductivity of the ferronanofluids, with the maximum enhancement observed at higher magnetic field intensities and with shorter saturation times. However, after the magnetic field was turned off, the thermal conductivity did not immediately return to its initial value but followed an exponential decay. Ultrasonication was necessary to restore the initial thermal conductivity. In addition, the thermal conductivity of the ferronanofluids decreased significantly with increasing temperature in the presence of a magnetic field, which was not proportional to the magnetization of the ferronanofluid sample and did not correspond to the initial temperature at which the thermal conductivity reached its maximum value [26].

There are numerous numbers of scientists and researchers who have tried increasing the efficiency of the nanofluids by dispersing two or more nanoparticles into the base fluids which has been called the hybrid nanofluids.

Suresh et al. were one of the pioneer researchers who added a mix of Aluminum oxide and copper to the distilled water. Their study investigates the convective heat transfer and pressure drop characteristics of a uniformly heated circular tube using a hybrid nanofluid made from Al_2O_3–*Cu/water*. The nanofluid was prepared by synthesizing Al_2O_3–*Cu* nanocomposite powder using a thermos chemical route and dispersing it in deionized water to form a stable hybrid nanofluid with a *0.1%* volume concentration.

The study found that hybrid nanofluid enhances the convective heat transfer performance, with an average increase in Nusselt number of *10.94%* compared to pure water. The convective heat transfer coefficient was found to increase with an increase in Reynolds number, with a maximum enhancement of *13.56%* at a Reynolds number of *1730* compared to pure water. The study also found that the hybrid nanofluid causes a slightly higher friction factor than pure water, with an average increase of *16.97%* compared to water. This implies that the use of dilute Al_2O_3–*Cu/water* hybrid nanofluids will result in extra pumping power compared to Al_2O_3*/water* nanofluid. The experimental data were used to propose empirical correlations for Nusselt number and friction factor, which were found to be in good agreement with the experimental results. These findings have important implications for the development of nanofluids for various heat transfer applications and contribute to a better understanding of the fundamentals of heat transfer and wall friction [37].

Sheikholeslami et al. their study investigates the behavior of a magnetizable hybrid nanofluid of *MWCNT-* Fe_3O_4/H_2O within a circular enclosure featuring two circular heaters. The heaters contain a wire carrying an electric current that generates magnetic fields of different strengths. Key parameters examined include the Rayleigh number ($Ra=104 – 106$), the angle of the heaters $\alpha=0–\pi/2$, the ratio of magnetic strengths, the magnetic number, the Hartmann number, and the concentration of nanocomposite particles. The results indicate that incorporating hybrid nanoparticles into the host fluid enhances convective heat transfer. The study employs finite element methods and a homogeneous model for hybrid nanofluid. The findings reveal that increasing the angle of the heaters results in a thicker temperature boundary layer around them, and adding *MWCNT-* Fe_3O_4 hybrid nanoparticles to the host fluid increases the Nusselt number. The research concludes that natural convection of the hybrid nanofluid in the presence of two magnetic sources has been successfully presented [38].

Tekir et al. studied the hybrid nanofluid and the objective of this experimental study is to investigate the convective heat transfer of Fe_3O_4*-Cu/Water* hybrid nanofluid flow and determine the optimum mixing ratio of the hybrid nanofluid in a straight pipe under the influence of a constant magnetic field perpendicular to the flow direction. A test rig was designed and constructed for rigorous testing under various parameters such as flow rate

and nanoparticle volume concentration. The experimental data reveals that the addition of Fe_3O_4 and *Cu* nanoparticles into distilled water enhances convective heat transfer inside the pipe. The constant magnetic field improves convective heat transfer by up to *14%,* and the Fe_3O_4*-Cu/Water* hybrid nanofluid performs best under the effect of the constant magnetic field. The study highlights the significance of the constant magnetic field in enhancing convective heat transfer. The research also identifies other factors that influence the heat transfer rate, such as Reynolds number and Darcy friction factor. Overall, the study provides valuable insights into the use of hybrid nanofluids for heat transfer applications [39].

Gürdal et. al shredded light on the design of more effective thermal energy storage systems Their study introduces a novel hybrid approach integrating active and passive heat recovery techniques by investigating the combined effects of ferro-nanofluid flow, dimpled tube geometry, and an external magnetic field. Through numerical simulations, key parameters including dimple geometry, Hartmann number, and nanoparticle volume fraction are explored. Notably, the study identifies the dimpled tube geometry of P/d = 7.50 as most efficient for both ferro-nanofluid and distilled water flow, while φ = 2.5 vol% nanoparticle volume fraction yields the highest Nusselt number. The introduction of the magnetic field significantly enhances average Nusselt numbers, particularly at Ha = 75. This investigation culminates in the identification of the most efficient parameter combination for enhanced heat transfer: NPVF of φ = 2.5 vol%, dimpled tube with P/d = 7.50, and MF intensity of Ha = 75 [40].

Aim of the study: This work reports a numerical investigation of water based ferronanofluid (water and Fe_3O_4) flowing through a pipe under laminar regime and the ferronanofluid is influenced by a magnetic field. The magnetic field spatially changing as well as the intensity of the magnetic field. The study also observes the behavior of the ferronanofluid to determine the optimum location of the magnetic field and the intensity of the MF taking into the consideration different physical and thermal properties e.g., the Reynolds number, Nusselt number, heat transfer enhancement, and the pressure drop. As a result, the best and most practical magnetic field location, magnetic field intensity, and *NPVF* selection have been determined to give the best thermal efficiency. The study determines the average convective heat transfer coefficient (*h*), average

Nusselt number (*Nu*), Reynolds number (*Re*), and the average Darcy friction factor (*f*) of the ferronanofluid flowing through the smooth pipe. The Performance Evaluation Criteria (*PEC*) has also been used to measure the efficiency of the using ferronanofluid and MF in the system.

To date, no extant scholarly investigations have been undertaken to ascertain the ramifications of subjecting ferronanofluids to distinct magnetic field intensities at varying spatial coordinates within a smooth conduit operating under laminar flow conditions, particularly concerning diverse nanoparticle volume fractions, with the overarching objective of identifying optimal thermal efficiency.

PART 3: METHODOLOGY

Ansys 2020 R2 has been utilized to undertake a numerical inquiry into the influence of a magnetic field on ferronanofluid with varying nanoparticle volume fractions (NPVF). In this study, ferronanofluid flows under a laminar regime through a seamless aluminum pipe. The investigation involves altering the magnetic field's positioning to three distinct locations, accompanied by variations in the magnetic field's intensity. Figure 3.1 shows the study flowchart to reduce the complexity of the study and to easily track the process of this research.

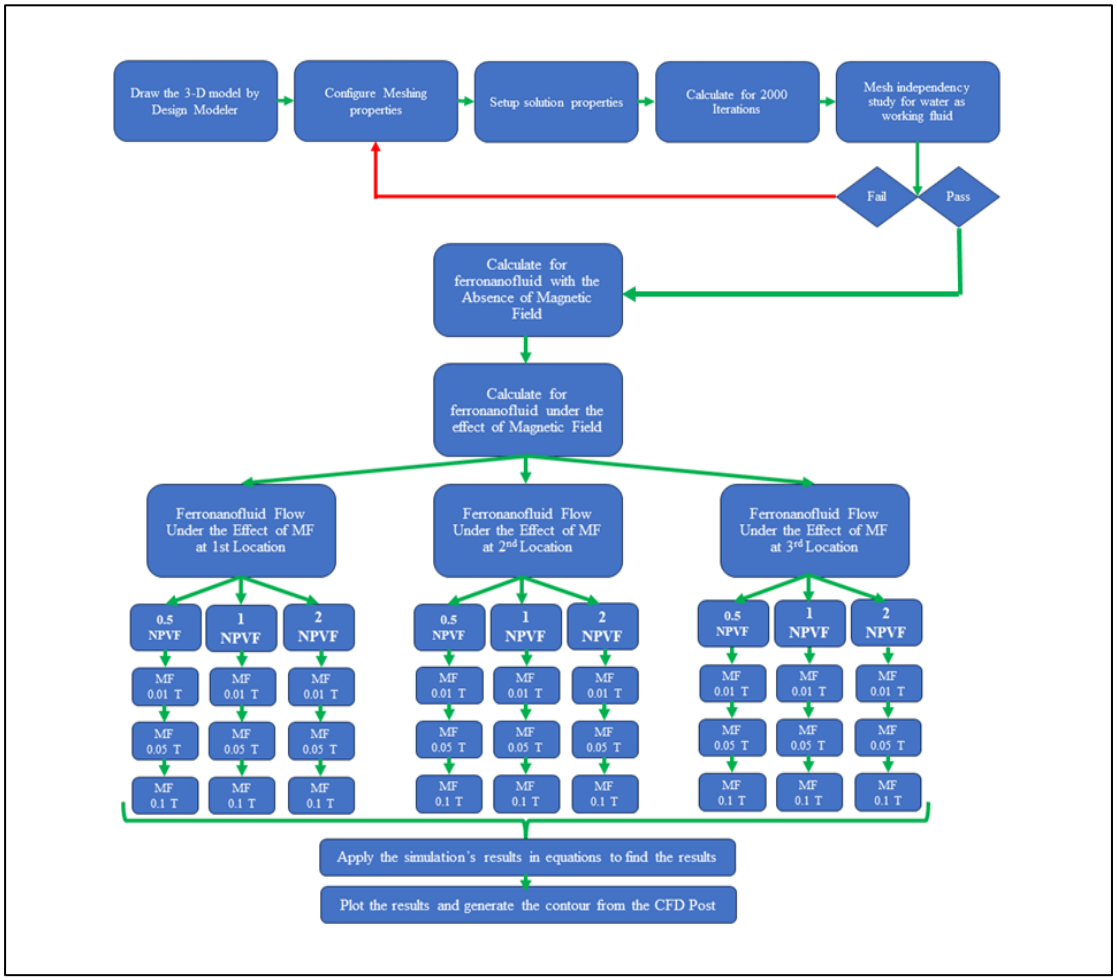

Figure 3. 1: The Study flow chart

The thermophysical properties of the nanofluids were determined based on the properties of the distilled water and nanoparticles at the average temperature of the working fluid [41–44].Table 3.1. shows the thermophysical properties of the water and the ferronanofluid Fe_3O_4/water for different nanoparticles volume fraction. The magnetic permeability is constant with a value of *25000 siemens/m* and the electrical conductivity is constant as well with value of *0.0000088 h/m.*

Table 3. 1 Termophysical properties of the water and Fe_3O_4/water

Ferronanofluids NPVF %	***Reynolds***	***Density kg/m^3***	***Specific heat J/Kg.K***	***Thermal conductivity W/m.K***	***Viscosity Pa.s***
Water	*1000*	*998*	*4182*	*0.598*	*0.001003*
	1250	*998*	*4182*	*0.598*	*0.001003*
	1500	*998*	*4182*	*0.598*	*0.001003*
	1750	*998*	*4182*	*0.598*	*0.001003*
	2000	*998*	*4182*	*0.598*	*0.001003*
0.5	*1000*	*1018.91*	*4092.73*	*0.6068*	*0.001042*
	1250	*1018.91*	*4092.73*	*0.6068*	*0.001042*
	1500	*1018.91*	*4092.73*	*0.6068*	*0.001042*
	1750	*1018.91*	*4092.73*	*0.6068*	*0.001042*
	2000	*1018.91*	*4092.73*	*0.6068*	*0.001042*
1	*1000*	*1039.82*	*4007.45*	*0.6157*	*0.001088*
	1250	*1039.82*	*4007.45*	*0.6157*	*0.001088*
	1500	*1039.82*	*4007.45*	*0.6157*	*0.001088*
	1750	*1039.82*	*4007.45*	*0.6157*	*0.001088*
	2000	*1039.82*	*4007.45*	*0.6157*	*0.001088*
1.5	*1000*	*1060.73*	*3924.74*	*0.6247*	*0.00114*
	1250	*1060.73*	*3924.74*	*0.6247*	*0.00114*
	1500	*1060.73*	*3924.74*	*0.6247*	*0.00114*
	1750	*1060.73*	*3924.74*	*0.6247*	*0.00114*
	2000	*1060.73*	*3924.74*	*0.6247*	*0.00114*
2	*1000*	*1081.64*	*3845.61*	*0.6337*	*0.001198*
	1250	*1081.64*	*3845.61*	*0.6337*	*0.001198*
	1500	*1081.64*	*3845.61*	*0.6337*	*0.001198*
	1750	*1081.64*	*3845.61*	*0.6337*	*0.001198*
	2000	*1081.64*	*3845.61*	*0.6337*	*0.001198*
2.5	*1000*	*1102.55*	*3769.49*	*0.6429*	*0.001263*
	1250	*1102.55*	*3769.49*	*0.6429*	*0.001263*
	1500	*1102.55*	*3769.49*	*0.6429*	*0.001263*
	1750	*1102.55*	*3769.49*	*0.6429*	*0.001263*
	2000	*1102.55*	*3769.49*	*0.6429*	*0.001263*

"Table 3.2 displays the thermophysical properties of aluminum since the pipe is made of aluminum."

Table 3. 2 Thermophysical properties of Aluminum.

Density Kg/M^3	*Specific heat J/Kg.K*	*Thermal conductivity W/m.K*	*Electrical conductivity Siemens/m*	*Magnetic permeability h/m*
2719	*871*	*2.02E+02*	*3.54E+07*	*1.26E-06*

3.1. PHYSICAL MODEL

The idea being explored in this research involves the investigation of the convective heat transfer characteristics of ferronanofluids flowing through a smooth pipe under the influence of an external magnetic field. The pipe has a length of *1500 mm* and a diameter of *16 mm*. The study was conducted numerically under laminar flow regime at different Reynolds numbers ranging from *1000≤Re≤2000*. The effect of the magnetic field intensity was investigated by varying the intensity from *B=0.01 to 0.1 T*. Additionally, the location of the magnetic field was changed to three positions along the length of the pipe at distances of *300, 700,* and *1200 mm* from the inlet. The ferronanofluid used in this study is composed of magnetic nanoparticles (Fe_3O_4) dispersed in a base fluid. The heat flux applied on the surface of the pipe was *6700 W/m^2*. In the first part of the study, the ferronanofluids flow through the pipe has been studied to determine the flow and heat transfer characteristics of the ferronanofluid flowing at the condition of absence of the magnetic field. Figure 3.2 shows a detailed perspective of the computational domain and its dimensions, *L mm* represents the length of the smooth pipe, *D mm* is the diameter of the pipe, and the red arrows represent the heat flux.

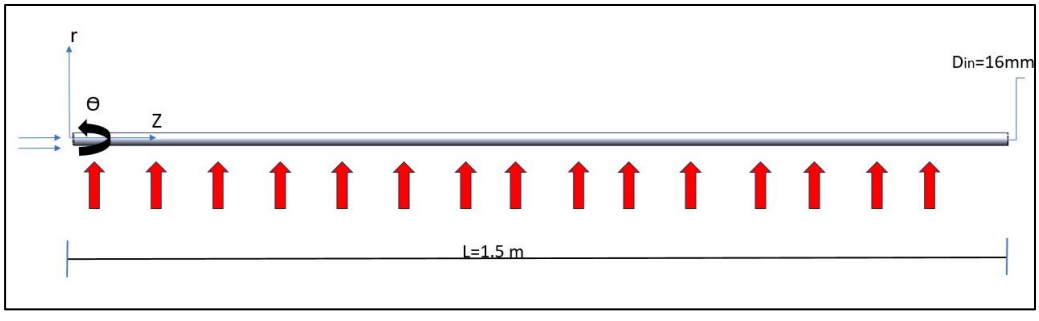

Figure 3. 2: Front view of the smooth pipe under heat flux.

In the subsequent phase of the research, the utilization of a smooth pipe geometry offered a controlled and well-defined environment conducive to the meticulous examination of the intricate flow patterns and velocity distributions exhibited by the ferronanofluids. In order to comprehensively investigate the influence of these variations on fluid flow, distinct magnetic sources were applied at three precise locations along the length of the pipe. In this research investigation, the convective heat transfer characteristics of ferronanofluid flow were studied varying the intensity of the magnetic field. The magnetic intensity was adjusted to different values ranging from *B=0.01, 0.05 to 0.1 T*. The analysis commenced by examining the ferronanofluids in the absence of DC magnetic field. Subsequently, a magnetic field was applied to the ferronanofluids using a magnetic field, with variations in the intensity. The initial magnetic intensity was set at *0.01 T*, followed by an increase to *0.05 T*, and finally reaching the highest intensity of *0.1 T*. By systematically altering the magnetic field intensity, the aim was to investigate the resultant effect on the convective heat transfer characteristics of the ferronanofluid flow. With a total pipe length of *1500 mm*, the first magnetic field was strategically positioned *300 mm* away from the inlet. Subsequently, the second location was identified at a distance of *750 mm* from the inlet, while the third location was established at *1200 mm* from the inlet. It is important to note that the length of the magnetic field remained constant at *100 mm* throughout the numerical process. Based on these specifications, it can be deduced that the magnetic field at the first location spanned a distance of *300 mm to 400 mm* along the pipe as given in Figure 3.3 where the simulation has been repeated three times at different intensities of the magnetic field.

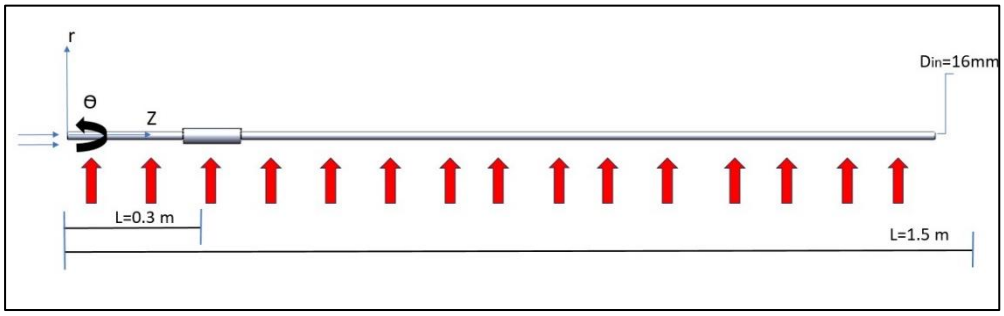

Figure 3. 3: Front view of the smooth pipe with magnetic field at 1st location.

Similarly, the magnetic field at the second location encompassed a range from *750 mm to 850 mm* as given in Figure 3.4, and also the simulation has been generated three times and the results noted down for the comparison and discussion.

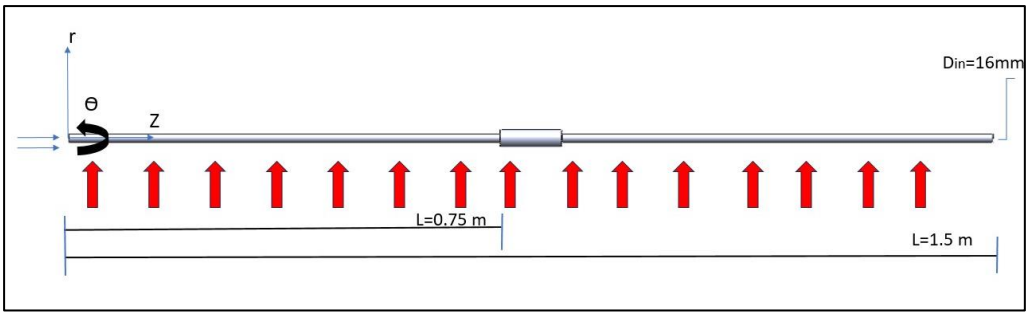

Figure 3. 4: Front view of the smooth pipe with magnetic field 2nd location.

While the third magnetic field extended from *1200 mm to 1300 mm* along the pipe as given in Figure 3.5 and again, the same procedure repeated to investigate all the scenarios in order to conclude the best location for the magnetic field with respect to its intensity.

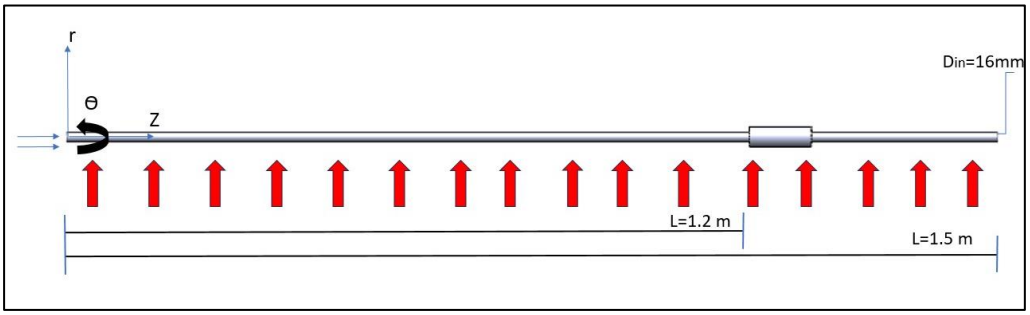

Figure 3. 5: Front view of the smooth pipe with magnetic field 3rd location.

This precise selection of magnetic field locations and intensities within the pipe facilitated a comprehensive assessment of their respective impacts on the flow and heat transfer behavior of the ferronanofluids. By incorporating these specific parameters into the numerical simulations, a detailed understanding of the flow characteristics and their variations in response to the manipulated magnetic field configurations was achieved.

3.2. GOVERNING EQUATIONS

Conservation of Mass, Conservation of Momentum, and Conservation of Energy equations has been solved numerically in this study for laminar flow. This section presents the Governing Equations (1) – (3) employed in the calculations.

Conservation of Mass:

$$\frac{\partial p}{\partial t} + \frac{\partial (p u_i)}{dx} = 0 \tag{3.1}$$

Conservation of Momentum:

$$\frac{\partial (p u_i)}{dt} + \frac{\partial (p u_i u_j)}{dx_j} = -\frac{\partial p}{\partial x_i} + \frac{\partial}{\partial x_j}\left[\mu\left(\frac{\partial u_i}{\partial u_j} + \frac{\partial u_j}{\partial x_i} - \frac{2}{3}\delta_{ij}\frac{\partial u_i}{\partial x_j}\right)\right] + i\frac{\partial}{\partial x_j}(-p\grave{u}_i\grave{u}_j) \tag{3.2}$$

Where u_i and u_j are the time-averaged velocity for i and j directions and $-p\grave{u}_i\grave{u}_j$ are presenting the Reynolds stresses.

Conservation of Energy:

$$\frac{\partial}{\partial \mathrm{t}}(\rho \mathrm{E}) + \frac{\partial}{\partial \mathrm{x_i}}\lfloor \mathrm{u_i}(\rho \mathrm{E} + \mathrm{pr})\rfloor = \frac{\partial}{\partial \mathrm{t}}\left[\left(\frac{\mathrm{cu_i}}{\mathrm{pr_t}}\right)\right]\frac{\partial \mathrm{T}}{\partial \mathrm{x_j}} + \mu_\mathrm{i}(\tau_\mathrm{ij})_\mathrm{eff} \tag{3.3}$$

Where ρ is density, $(\tau_{ij})_{eff}$ is the deviatoric stress tensor.

The study under the magnetic field effect hence the Magnetohydrodynamics equation can be presented by using Ohm's law and Maxwell's formulation in the following equations:

$$(\vec{\mathrm{V}}.\nabla)\vec{\mathrm{B}} = \frac{1}{\mu_0 \sigma}\nabla^2\vec{\mathrm{B}} + (\vec{\mathrm{B}}.\nabla)\vec{\mathrm{V}} \tag{3.4}$$

where the medium's magnetic permeability and electrical conductivity are denoted as μ0 and σ, respectively.

The established boundary conditions for resolving the governing equation encompass a fixed inlet temperature of *25°C* coupled with a consistent velocity. Additionally, the outlet boundary condition was defined as a constant temperature and pressure state. The wall boundaries were prescribed with no-slip conditions and a stable heat flux. Moreover, the magnetic field boundary condition was specified as a uniform field at designated positions and magnitudes, while the heat flux remained constant throughout the analysis.

Convective heat transfer refers to the exchange of energy between a solid surface and a neighboring fluid through a combination of conduction and the movement of the fluid. For the current flow conditions, there are some parameters that need to be determined in order to analyze the energy and to have our initial data set for our simulation and also to calculate some values to be referenced and for comparison purposes.

The average convective heat transfer coefficient (*h*) is a measure of the efficiency of heat transfer between a solid surface and a surrounding fluid through convection. It represents the rate of heat transfer per unit area and per unit temperature difference between the solid surface and the fluid. The value of the average convective heat transfer coefficient depends on various factors such as the properties of the fluid, the velocity of the fluid, the temperature difference, and the geometry of the solid surface, and it can be determined as follows:

$$h = \frac{q''}{(T_w - T_b)_{avg}} \tag{3.5}$$

In this context, q'' *[W/m²]* represents the heat flow imposed on the pipe's surface. T_w *[K] and* T_b *[K],* on the other hand, refer to the temperature of the surface and the bulk temperature of the working fluid, respectively. The bulk temperature can be determined by calculating the average temperature of the fluid at both the inlet *(*T_{in}*)* and outlet *(*T_{out}*)* sections of the pipe, as depicted below:

$$T_b = \frac{T_{in} - T_{out}}{2} \tag{3.6}$$

The average Nusselt *(Nu)* number for internal fluid flow conditions can be computed using the average convective heat transfer coefficient *(h)*, pipe diameter *(D)*, and the thermal conductivity of the working fluid *(k)*.

$$Nu = \frac{hD}{k} \tag{3.7}$$

When examining internal fluid flow conditions, the Reynolds number *(Re)* is employed to anticipate flow patterns in various fluid flow scenarios. It is defined as follows:

$$Re = \frac{\rho V D}{\mu} \tag{3.8}$$

In the given equation, ρ *[kg/m^3]* represents the density of the fluid, *V (m/s)* denotes the average velocity of the fluid inside the pipe, and μ *(N.s/m^2)* signifies the dynamic viscosity of the fluid.

The average Darcy friction factor f can be determined using the Darcy-Weisbach equation, which considers the values of inlet pressure *(P_{in})*, outlet pressure *(Pout)*, pipe length *(L)*, pipe diameter *(D)*, fluid density *(ρ)*, and average fluid velocity *(V)*.

$$f = \frac{P_{in} - P_{out}}{\left(\frac{L}{D}\right) \cdot \left(\frac{\rho V^2}{2}\right)} \tag{3.9}$$

The Performance Evaluation Criteria *(PEC)* is a coefficient utilized to assess the degree of heat transfer enhancement achieved in comparison to the increase in pumping power in applications where heat enhancement is sought. Higher *PEC* values indicate greater improvements in heat transfer, while lower *PEC* values indicate higher pressure drops within the heat transfer systems. The relation of the *PEC* number is given in Eq. (3.6).

$$PEC = \frac{\left(\frac{Nu_{nf}}{Nu_{bf}}\right)}{\left(\frac{f_{nf}}{f_{bf}}\right)^{1/3}} \tag{3.10}$$

Where, Nu_{nf} represents the Nusselt number pertaining to the ferronanofluid, while Nu_{bf} denotes the Nusselt number characterizing the base fluid. Additionally, f_{nf} denotes the Darcy friction factor associated with the ferronanofluid, and f_{bf} indicates the Darcy friction factor of the base fluid.

Figure 3.6 visually presents a clear representation of the prescribed boundary conditions during the condition.

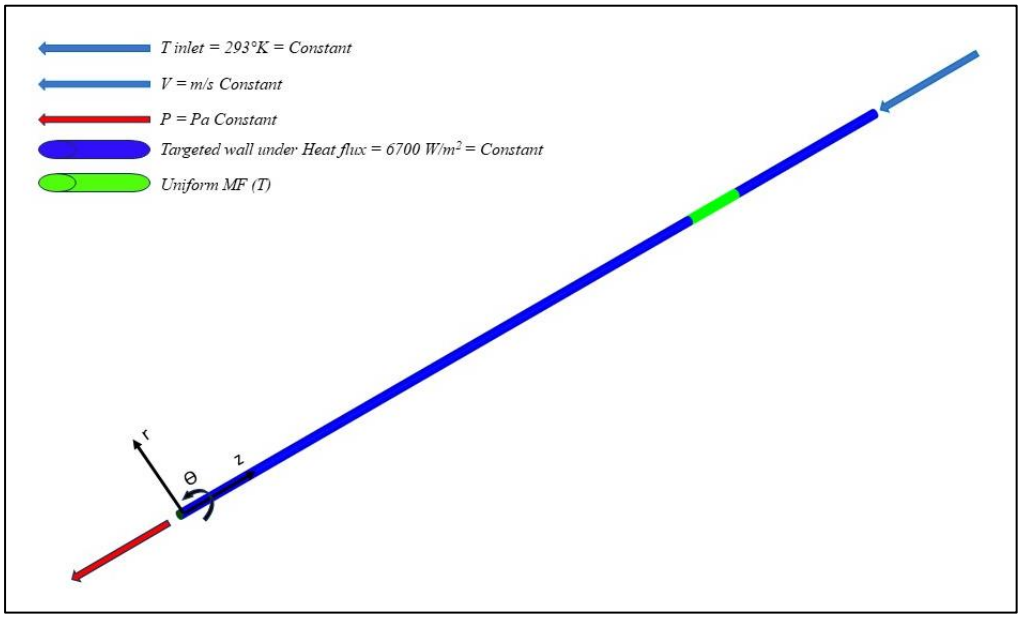

Figure 3. 6: Explanation of computational domain and the boundary conditions

3.3. SOLUTION PROCEDURE

The ANSYS Fluent2020R2 commercial code solver was utilized to conduct the simulation in this study. The pressure-velocity coupling scheme of SIMPLE was employed, along with a second order upwind spatial discretization scheme. To ensure accuracy, the convergence criteria for residual values were set to 10^{-4} for all variables.

The model that has been employed in the simulation is Laminar viscous model, energy on, single-phase approach, and the *MHD* enabled as magnetic induction Figure 3.7. The simulation was initiated with a zero-velocity field and iterated until convergence was achieved for all variables. Convergence was monitored by tracking the residual values of each variable. A total of *195* simulations were carried out, encompassing various Reynolds numbers and magnetic field intensities. Additionally, *10* simulations were performed to identify the optimal magnetic intensity to be used. Furthermore, *17* simulations were conducted to conduct a mesh study and optimize the mesh resolution. Consequently, a total of *222* simulations were generated, providing a comprehensive data set for analysis and further investigation.

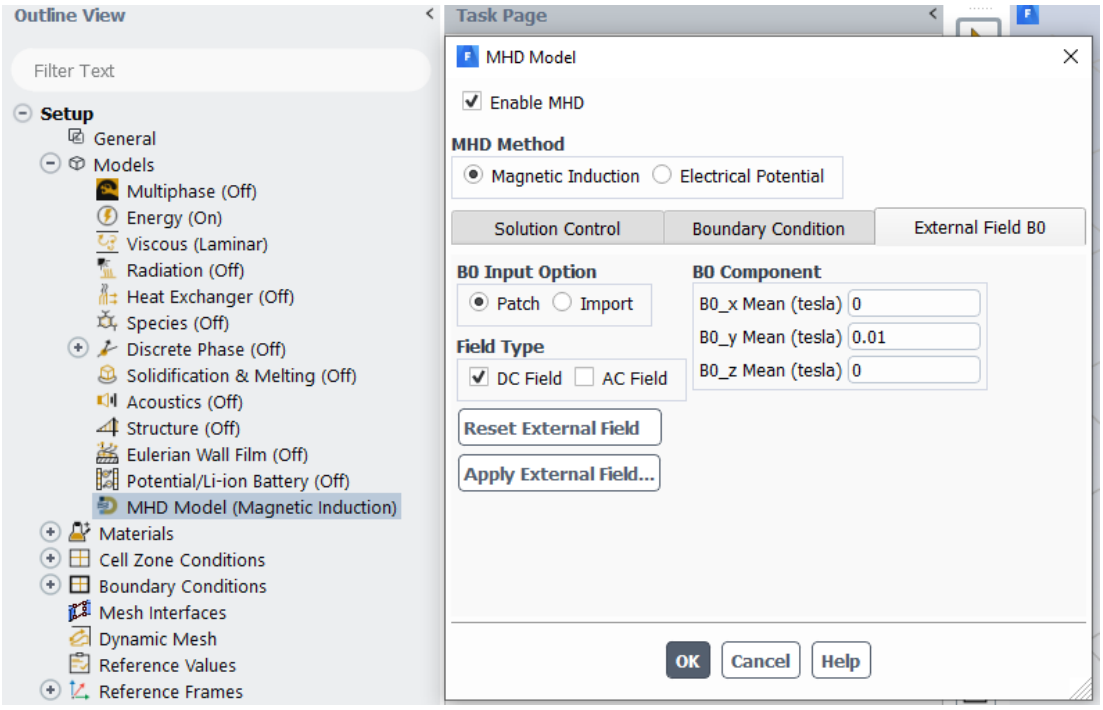

Figure 3. 7: Enableing MHD model.

3.4. MESH INDEPENDENCE STUDY

To guarantee the reliability and accuracy of the analysis, it is imperative to investigate the mesh independence, as it determines whether the results are influenced by changes in the mesh structure. By conducting a mesh independence study, the impact of different mesh resolutions on the analysis outcomes can be assessed. The study involves varying the mesh structure while keeping other parameters constant and analyzing the resulting

changes in the obtained results. Six simulations were performed using different mesh configurations, all-mesh studies have been performed for Reynolds number *1000* ranging from coarse to fine resolutions. The goal is to identify a mesh resolution that yields consistent and reliable results, indicating that further refinement of the mesh does not significantly alter the outcomes. Through this mesh independence study, it can be ensured that the analysis is not overly sensitive to the specific details of the mesh, providing confidence in the validity and robustness of the obtained results. Figure 3.8. shows that there is no significant change in average Nusselt number and average Darcy friction factor after the fifth study of the simulations. Therefore, the fifth mesh structure with an element number of *1455002* was chosen as an optimum mesh structure for this study, this number of elements associated with element size *1.2 mm* and number of divisions *48* for edge sizing.

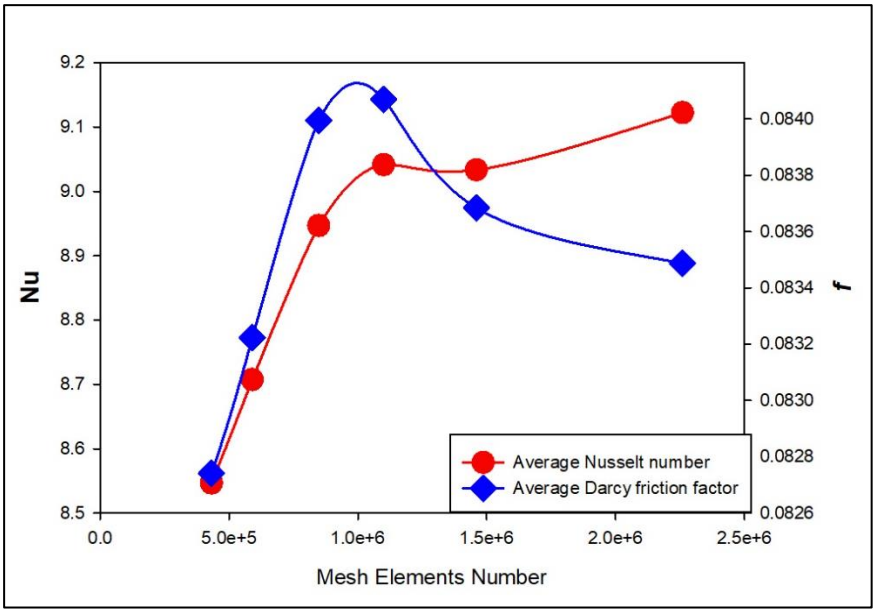

Figure 3. 8: Mesh independence study at Re =1000

Figure 3.9. shows the element metric of the final mesh for *480725* nodes and *1455002* elements where these mesh properties will be used for all the simulations.

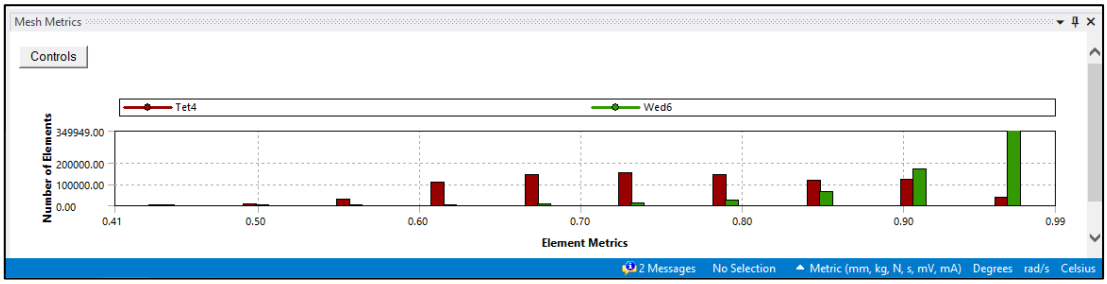

Figure 3. 9: Variation in the number of elements.

Figure 3.10. shows the impact of the inflation as well as the edge sizing where the denser mesh is required on the inlet, outlet, and near the pipe wall because of the fluctuation.

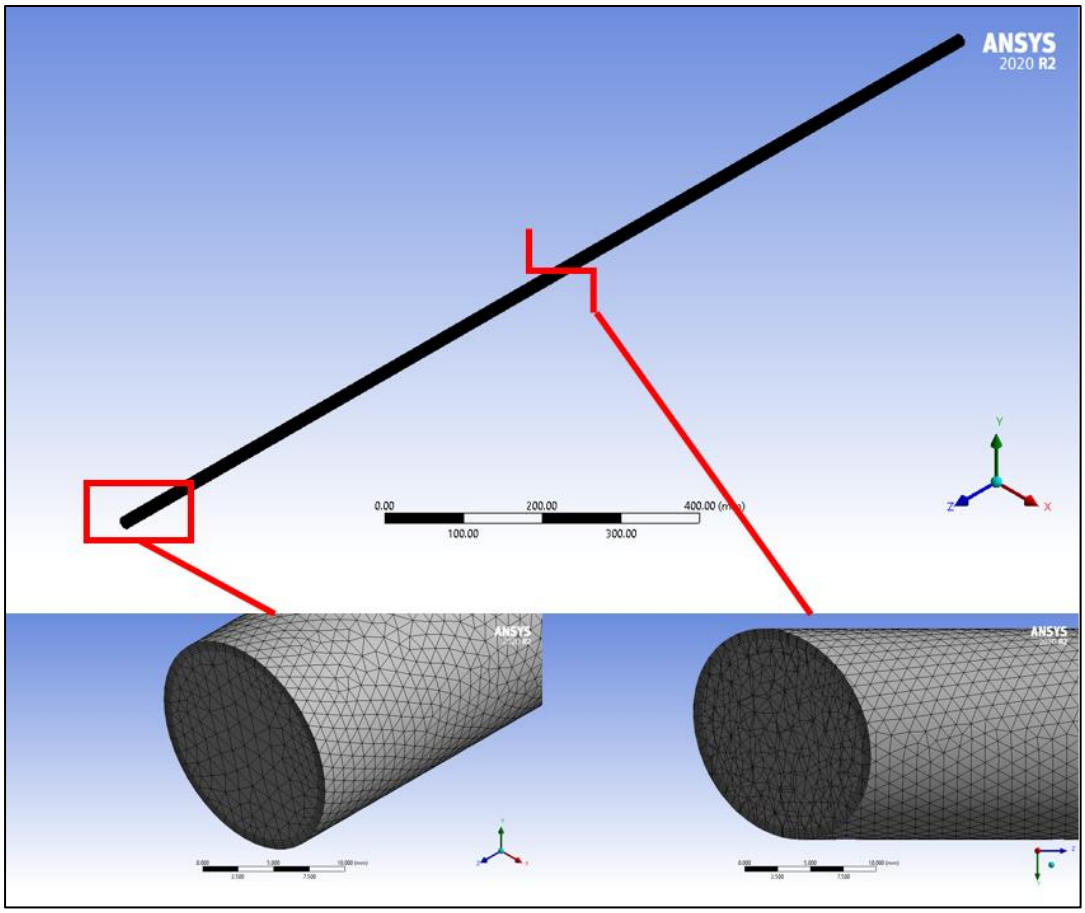

Figure 3. 10: Cross-section view of the meshed pipe.

In the context of our research focus, a more densely refined mesh has been implemented within the region influenced by the magnetic field. This strategic mesh densification serves a dual purpose: firstly, to effectively concentrate our investigative efforts within

this specific area, and secondly, to mitigate potential irregularities or fluctuations. Our pursuit of precision in results necessitates the adoption of an element size of *0.6 mm*, as visually depicted in the accompanying Figure 3.11. This change of mesh in the MF area has reflected on the total number of elements where the total number of elements increased to be *1888285* with *606069* nodes. Additionally, we have vigilantly tracked metrics such as aspect ratio, orthogonal quality, and skewness values throughout each analytical iteration. These metrics collectively serve as indicators of the mesh's structural integrity, thereby contributing to the meticulous assessment of computational accuracy.

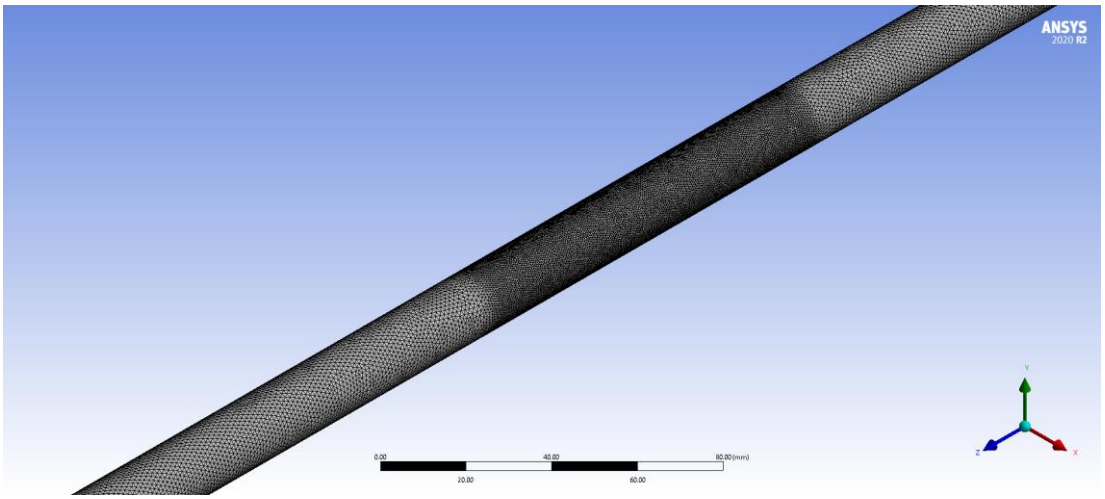

Figure 3. 11: Mesh in the magnetic field area.

PART 4: RESULTS AND DISCUSSION

This numerical investigation focuses on the comprehensive examination and analysis of the thermal characteristics exhibited by ferronanofluids as they flow through a smooth pipe in the presence of an applied magnetic field. Specifically, the study concentrates on the laminar flow regime at various Reynolds numbers. The analysis encompasses the manipulation of magnetic field intensities to further explore the correlation between the magnetic field and the thermal properties. Additionally, the investigation involves altering the position of the magnetic source while maintaining consistent boundary conditions. These conditions include a diameter of *16 mm* and a total pipe length of *1500 mm*. As previously stated, the pipe is subjected to a uniform heat flux with a magnitude of *6700* W/m^2, and the fluid enters the system at a temperature of *293 K*.

To ensure the validity of the results, the study was done by analyzing the flow and heat transfer characteristics of water flowing inside a smooth aluminum pipe, employing five simulations for this purpose. Following the validation stage, the study progressed to investigate the convective heat transfer characteristics of water-based nanofluids with different *NPVF*. These nanofluids consisted of magnetite oxide nanoparticles with the formula Fe_3O_4, and they are referred to as ferronanofluids due to the presence of ferrite particles. For this investigation, a total of *25* numerical calculations were performed. The subsequent stage of the study involves examining the behavior of the ferronanofluid flowing in the smooth pipe under the influence of a magnetic field. Three different magnetic field strengths have been utilized to understand the impact of varying magnetic field intensity on the thermal properties and the hydraulic behavior Furthermore, this procedure was repeated two additional times with changing the location of the magnetic field. This repetition aims to establish the correlation between the location of the magnetic field and the resulting thermal and hydraulic properties. As a result, *165* numerical computations have been conducted in total.

This section presents and discusses the numerical findings for each case, focusing on various aspects including the variations of average convective heat transfer coefficient, average Nusselt number, average Darcy friction factor, and *PEC* with respect to Reynolds number. Additionally, detailed analyses are conducted on surface Nusselt number, velocity, and temperature profiles.

The variations of average convective heat transfer coefficient and average Nusselt number were examined in relation to Reynolds number for each case. This provides insights into the convective heat transfer characteristics and the effectiveness of heat transfer within the system. Similarly, the average Darcy friction factor was analyzed to assess the pressure drop and flow resistance experienced by the fluid. The *PEC*, which serves as an overall performance indicator, was also studied. It takes into account both the convective heat transfer coefficient and the pressure drop, providing a comprehensive evaluation of the system's performance. Furthermore, the surface Nusselt number, temperature distribution, and Darcy friction profiles were analyzed in detail. These analyses provide a more comprehensive understanding of the heat transfer and fluid flow behavior along the pipe surface.

Overall, this section presents a comprehensive analysis of the numerical findings, covering a range of parameters and visualizations to provide a detailed understanding of the heat transfer, fluid flow, and performance characteristics within the system.

4.1. Water Flow in Smooth Pipe

In this particular instance, a comprehensive numerical analysis and thorough discussion have been undertaken to examine the flow of distilled water in a pipe. The investigation commenced by compiling a detailed inventory of the flow and heat transfer characteristics of water flow across various Reynolds numbers (*1000, 1250, 1500, 1750, 2000*). Subsequently, leveraging these properties, calculations were performed to determine the convective heat transfer coefficient, Nusselt number, and Darcy friction. Consequently, a comparative analysis was conducted, comparing the computed results against widely recognized correlations available in the literature. This exercise aimed to validate the accuracy and reliability of the numerical computations. Shah-London [45] correlation utilized for this comparison.

The obtained results are graphically presented in Figure 4.1 to facilitate a comparative analysis for pure water flow in smooth pipe between the numerical findings and the reference results. The plot demonstrates that numerical results exhibit a remarkable proximity to the widely recognized Shah-London correlation [45], with a negligible average error rates along the Reynolds number of *+5%*. Furthermore, Figure 4.2 shows that the mean Darcy friction factor aligns with the well-known Hagen-Poiseuille model [46], exhibiting a deviation within a range of ± 4 %. This convergence in results substantiates the dependability of the numerical dataset.

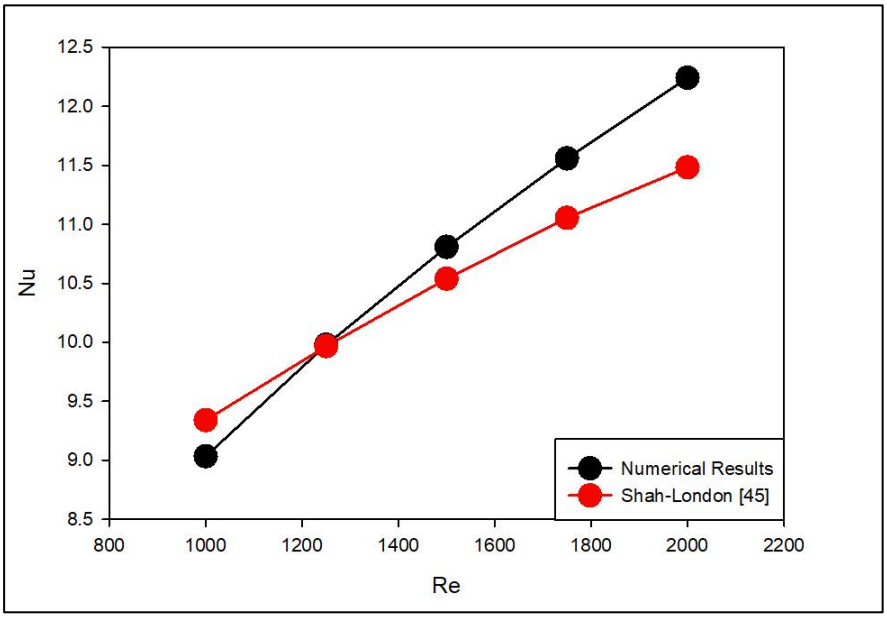

Figure 4.1: Variation of Nu number with Re number for pure water [45].

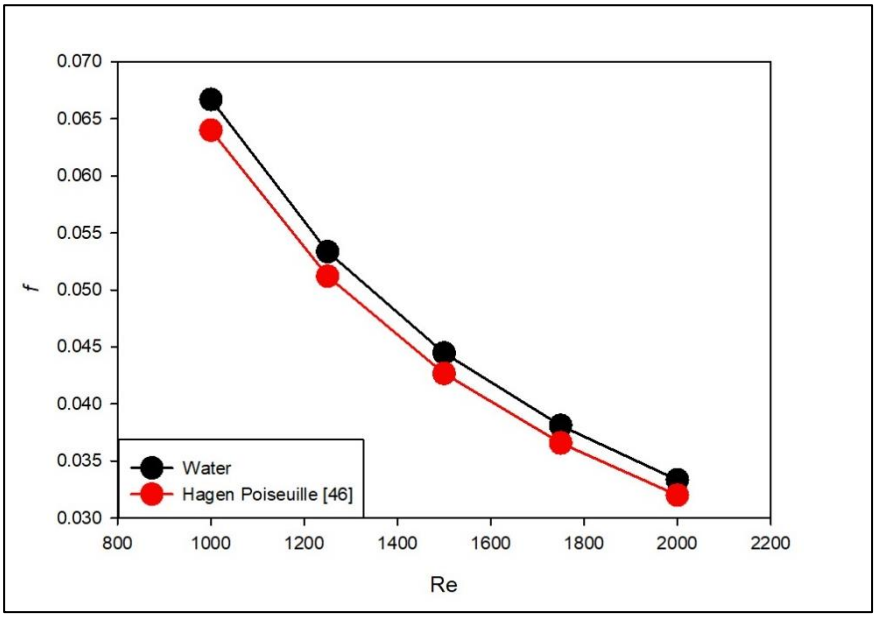

Figure 4. 2: Variation of Darcy friction factor with Re number for pure water [46].

Figure 4.3 presents the spatial distribution of the Nusselt number on the surface of the pipe for the given case, considering a *Re=2000*. The Nusselt number exhibits a higher magnitude at the inlet section of the pipe, gradually decreasing along the length until reaching the minimum value at the outlet section.

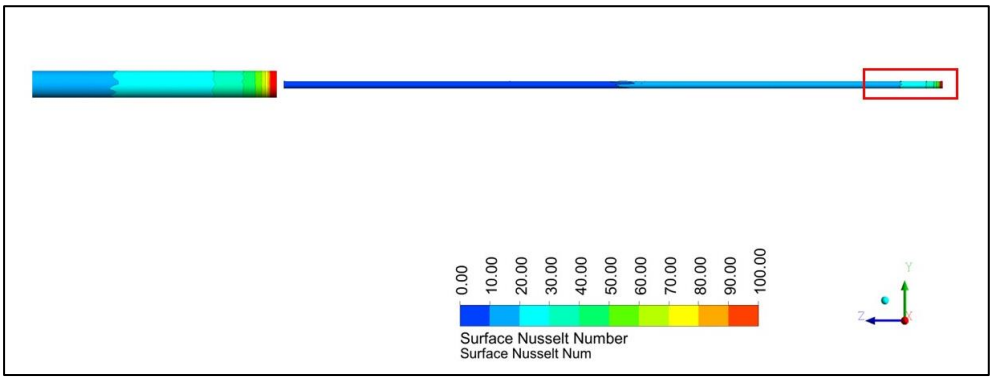

Figure 4.3: Surface Nusselt number distribution for water.

Figure 4.4 depicts the temperature profile observed in the context of the flow of pure water within a smooth pipe at a Reynolds number of 2000. This presentation highlights

the highest temperature manifestation at the exit point of the pipe, concurrently providing insight into the velocity distribution inherent to the water flow phenomenon.

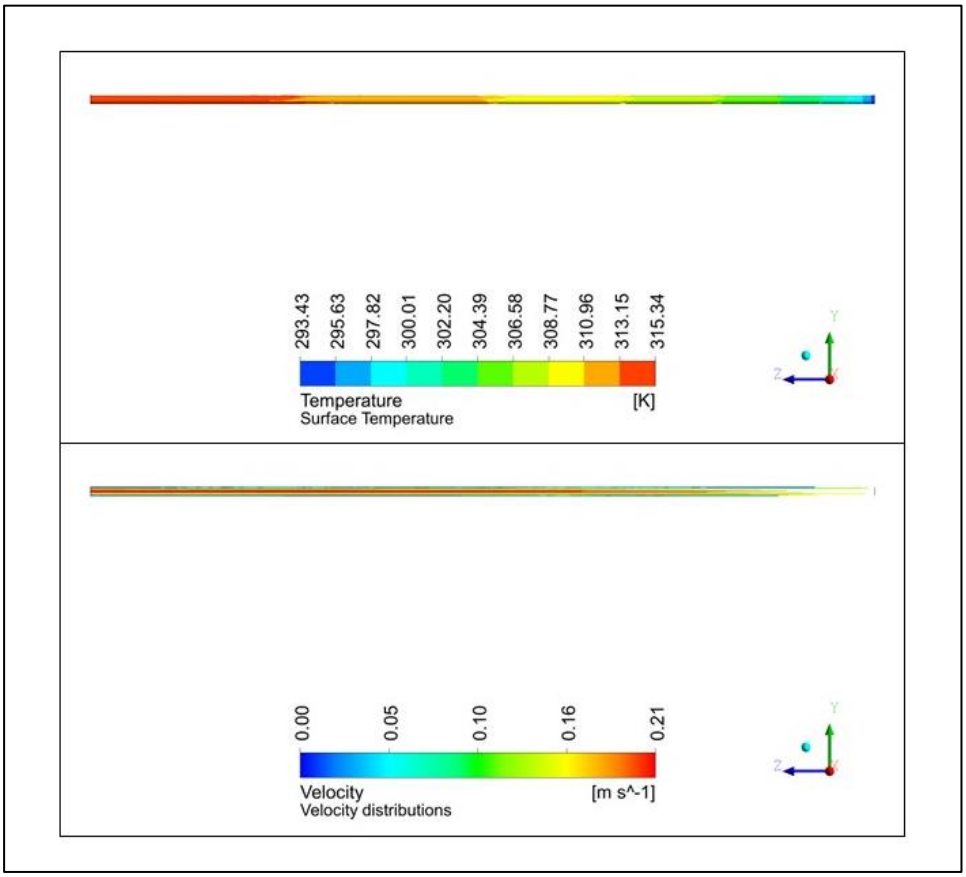

Figure 4. 4: Surface temperature and velocity distribution for water.

Based on the aforementioned observation, the numerical code and process have been successfully validated. This validation enables us to proceed with the subsequent calculations required for the study.

4.2. Ferronanofluid Flow in Smooth Pipe with the Absence of Magnetic Field

The present case focuses on studying the flow of ferronanofluid within a smooth aluminum pipe without magnetic field effect, while maintaining the same boundary conditions as in the previous scenario. The objective is to identify any changes or enhancements in system efficiency and the flow and heat transfer characteristics of the ferronanofluid flow. To determine the most efficient thermal system, different *NPVF* have been selected for this study. *NPVF* represents the ratio of the volume occupied by nanoparticles to the total volume of the dispersion medium or mixture. It serves as a

measure of nanoparticle concentration within the given volume and is typically expressed as a decimal or percentage value [47]. In this study, *NPVF* values ranging from *0.5 to 2.5* have been chosen, specifically (*0.5, 1, 1.5, 2, 2.5*). Each *NPVF* value has been thoroughly examined across various Reynolds numbers.

In this case, the ferronanofluid flows inside a smooth pipe with no magnetic field applied, under laminar flow regime at different Reynolds numbers has been investigated and discussed thoroughly. The aim here is to monitor the changes convection heat transfer coefficient, Nusselt number, Darcy friction, and the *PEC*.

4.2.1. Convection heat transfer coefficient

Figure 4.5 shows the convection heat transfer coefficient changes for different *NPVF* with Reynolds number. It was determined that convection heat transfer coefficient increases proportionally with Reynolds number, and the more increasing the *NPVF* the more higher heat transfer coefficient can be obtained, which's normal behavior because the convection heat transfer coefficient is influenced by factors such as the shape, characteristics of the fluid, movement, and occasionally temperature variations as per Newton's law of cooling and in this case the geometry of the particles is changing, means getting bigger [48].

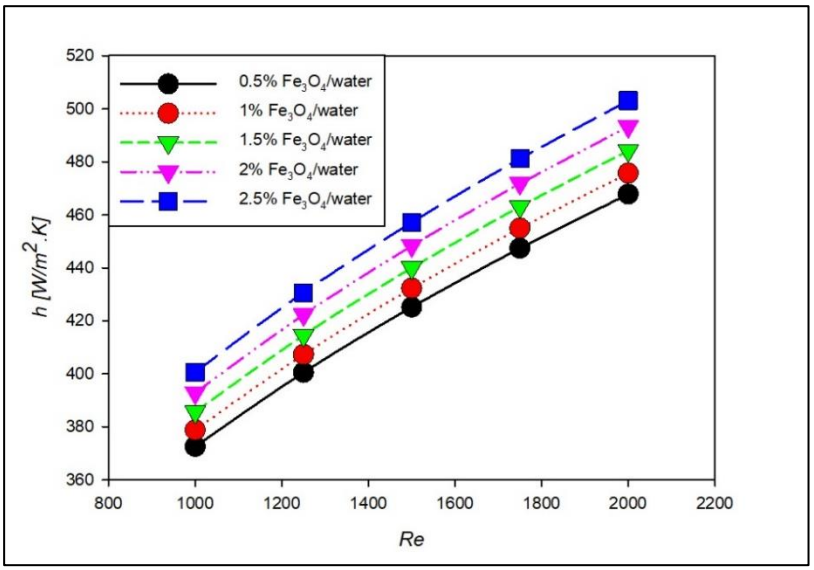

Figure 4.5: Variation of convection heat transfer with Reynolds number for different NPVF.

4.2.2. Nusselt number

Figure 4.6 presents the relation between Nusselt number at different *NPVF* and Reynolds number where the Nu number increases with the increase of Re number. Moreover, it's obvious from the figure, the increase in the *NPVF* drives to increments in the Nusselt number.

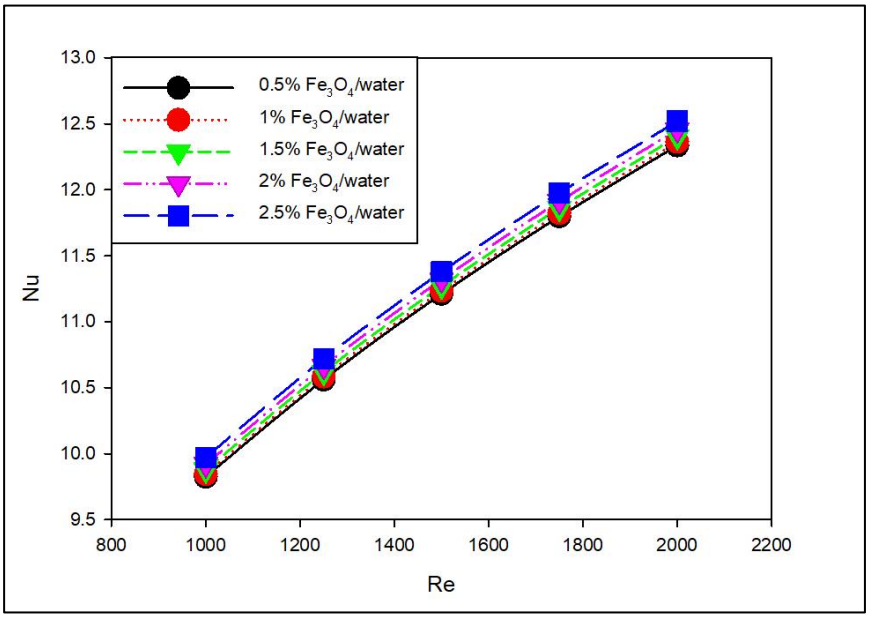

Figure 4. 6 Variation of Nusselt number with Reynolds number for different NPVF.

This increase might seem to be a positive sign where it should be as what is the limitation to increase the *NPVF* and enhance the Nusselt number, hence increase the efficiency of the thermal system, but the limitation will be related to agglomeration and sedimentation, increased viscosity, pressure drop, and in addition to that cost limitations. Therefore, while increasing the *NPVF* initially enhances convective heat transfer, these limitations should be carefully considered to determine the optimal nanoparticle concentration for a given system [49].

4.2.3. Darcy friction factor

The Darcy-Weisbach equation is an empirical equation used to calculate the pressure drop or head loss in a pipe or duct due to fluid flow. It relates the pressure drop to various factors such as the flow rate, pipe characteristics, and fluid properties. Figure 4.7 depicts the variation between the Darcy friction factor (*f*) and Reynolds number for various nanoparticle volume fractions (*NPVF*). The plot demonstrates that the Darcy friction factor experiences a significant decrease as the Reynolds number increases, indicating a non-proportional relationship. This behavior can be attributed to the changes in velocity associated with each Reynolds number. Furthermore, the Darcy friction factor is not affected by variations in the *NPVF*.

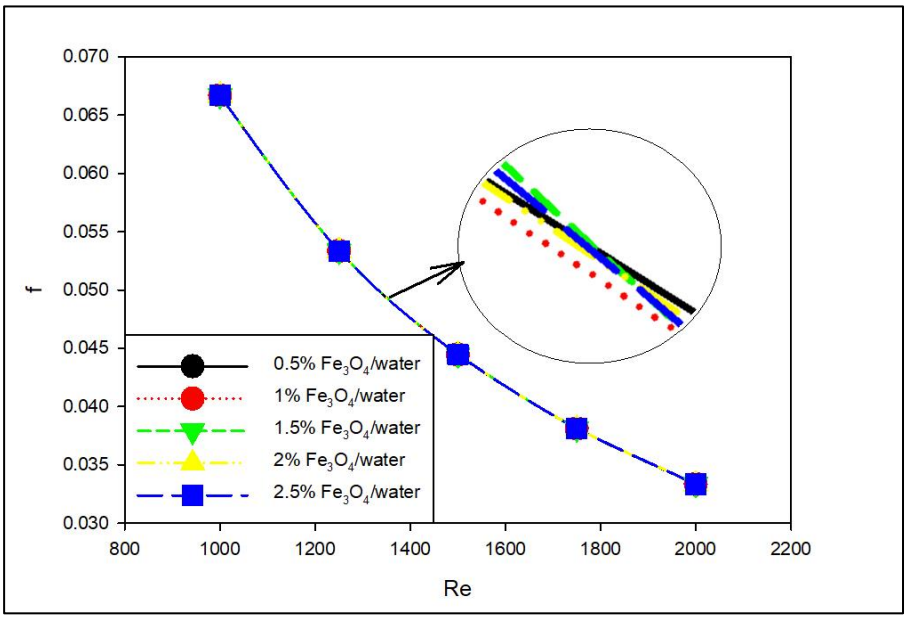

Figure 4. 7 Variation of Darcy friction factor with Re for different NPVF.

4.2.4. Performance evaluation criteria

PEC, or Performance Evaluation Criteria, is a coefficient used to evaluate the effectiveness and efficiency of heat transfer enhancement in systems. It compares the increase in heat transfer achieved to the associated increase in pumping power. *PEC* is particularly relevant in applications involving nanofluids, which are fluids containing nanoparticles. A higher *PEC* value indicates a greater improvement in heat transfer

performance relative to the increase in pumping power. This suggests that the system achieves enhanced heat transfer efficiency with minimal additional energy consumption. Conversely, a lower *PEC* value signifies a higher pressure drop in the heat transfer system, indicating that more energy is required to achieve the desired heat transfer enhancement. *PEC* serves as a quantitative measure to compare different nanofluids or heat transfer systems. By calculating and comparing *PEC* values, researchers and engineers can determine the most efficient and effective nanofluid or heat transfer system for a given application. It's important to note that *PEC* is not a standardized metric, and its calculation may vary depending on the specific application and parameters considered. Therefore, the specific formula or methodology used to calculate *PEC* should be defined within the context of its application. The change of *PEC* with Reynolds number doesn't have specific trend where it varies as every Re number represents a different pressure drop. Figure 4.8. shows the relation between *PEC* and Reynolds number for different concentration of *NPVF Φ (0.5, 1, 1.5, 2, and 2.5) %* respectively.

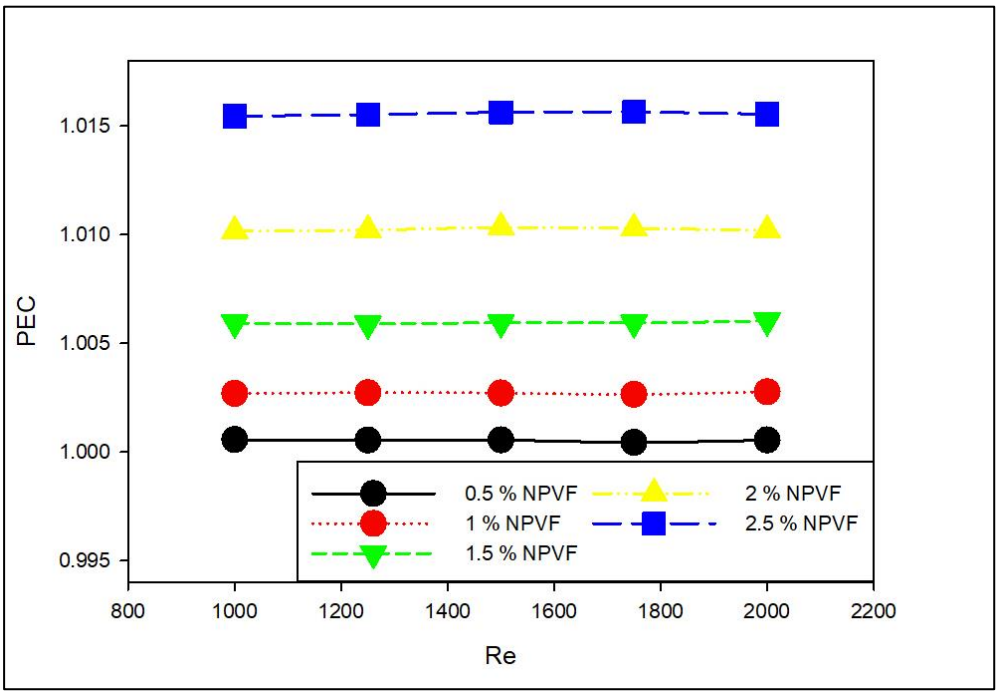

Figure 4. 8 Variation of PEC with Re for different NPVF.

Since the *PEC* value varies for each *NPVF* concentration in a very limited range, Figure 4.8 can't represent the *PEC* curve for each *NPVF Φ*, but it's obvious that the *PEC* has

marked the highest for *2.5 % NPVF*. Hence, Figure 4.9. showing the change in *PEC* against Reynolds number for ferronanofluid with *2.5 NPVF*, where we can see that the relation is nonlinear between the *PEC* and *Re* and that proving the challenge to predict *PEC* trend as the highest *PEC = 1.0156* fall at *Re 1750* for *NPVF Φ 2.5 %.*

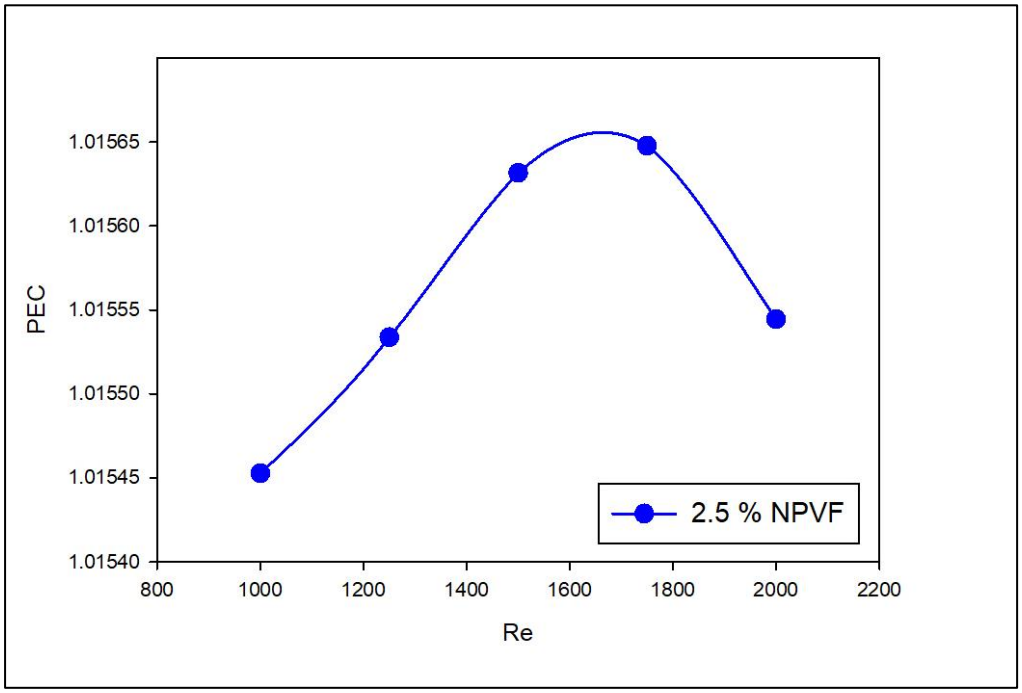

Figure 4. 9 Variation of PEC with Re for 2.5 % NPVF.

Having the above said, will lead to the point of finding the best-case scenario in terms of *NPVF* percentage and for that sake, the highest *PEC* for all *NPVF* s will be compared together and from this point we know that the highest *PEC* value has been indicated at *NPVF Φ 2.5 %* for Reynolds number *1750* in the absence of the magnetic field.

Figure 4.10 shows the surface Nusselt number distribution for ferronanofluid at Reynolds number *2000* and at *5* different *NPVF 0.5, 1, 1.5, 2,* and *2.5* with the absence of the magnetic field.

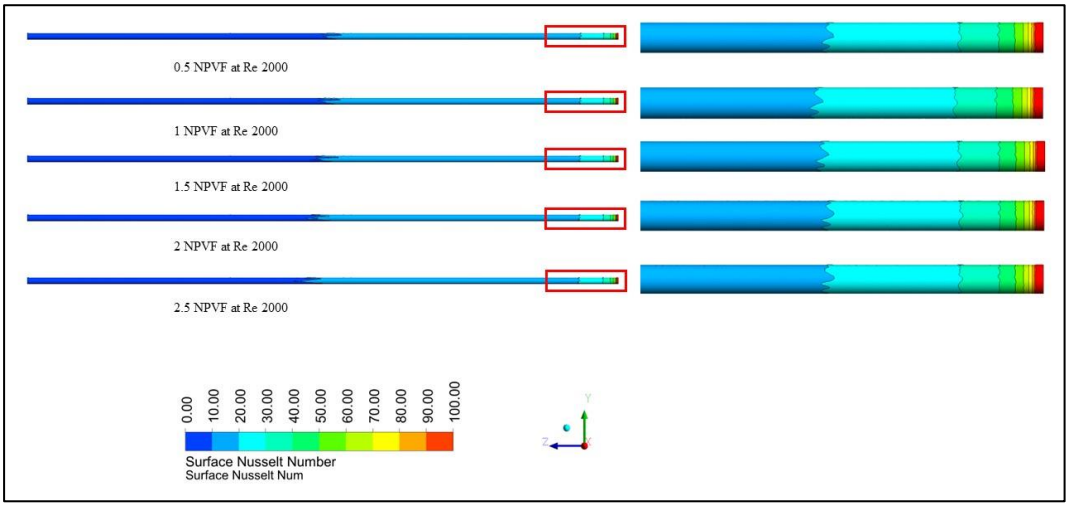

Figure 4. 10. Surface Nusselt number distribution for different NPVF.

The contour of temperature distribution generated for ferronanofluid flow at Reynolds number *2000* for different *NPVF 0.5*, *1*, *1.5*, *2*, and *2.5* with the absence of the magnetic field as illustrated in Figure 4.11.

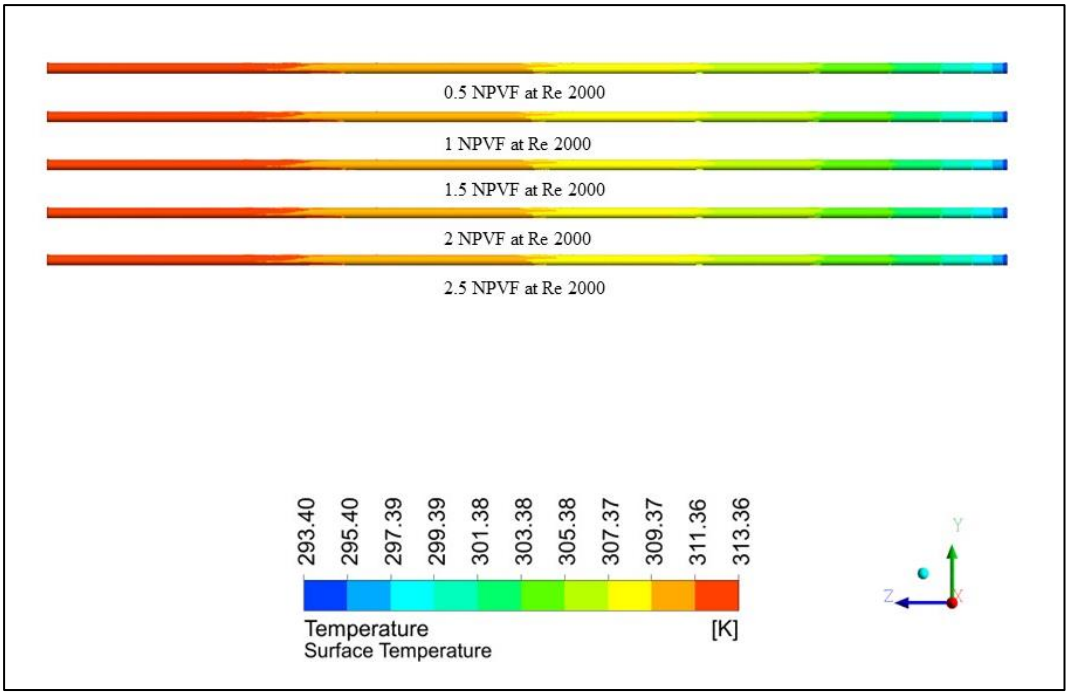

Figure 4. 11. Surface temperature distribution for different NPVF.

The Velocity distribution streamline given in Figure 4.12 for ferronanofluid flow through a pipe at Reynolds number *2000* for different *NPVF 0.5*, *1*, *1.5*, *2*, and *2.5* without the effect of the magnetic field.

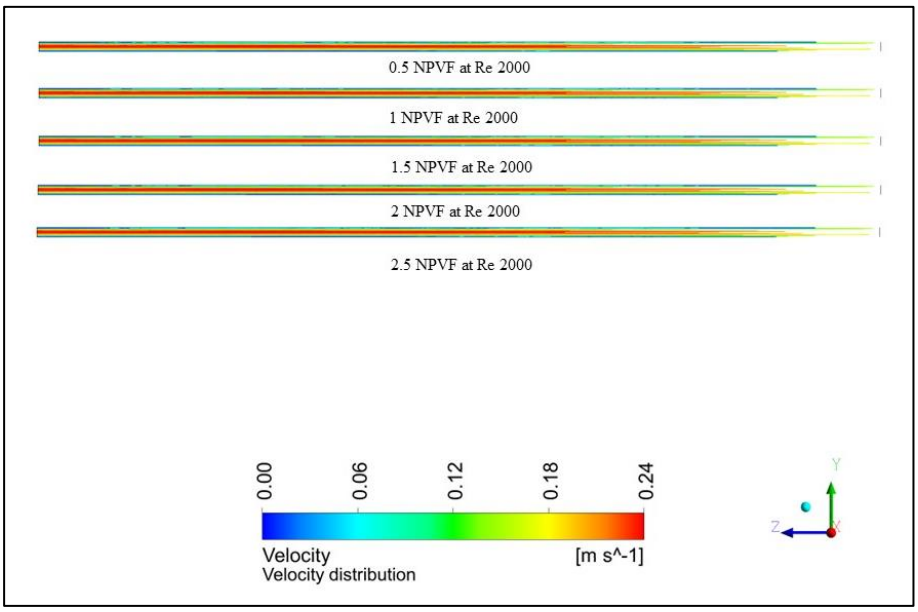

Figure 4. 12. Velocity distribution for different NPVF.

4.3. Ferronanofluid Flow in Smooth Pipe Under the Effect of Magnetic Field

Ferronanofluids possess a notable advantage due to their responsiveness to magnetic fields, which can be attributed to the presence of dispersed ferrite nanoparticles within the base fluid. This characteristic leads to alterations in the thermal properties of the fluids [50]. In this phase of the research, a numerical investigation was focused on the flow of ferronanofluids within a smooth pipe, considering the influence of a magnetic field. The numerical conditions remain consistent with the previous phase, which excludes the presence of a magnetic field. However, to obtain a comprehensive understanding of the behavior of ferronanofluid flow under the influence of a magnetic field, the intensity and location of the magnetic field have been varied throughout the study. The magnitude of the magnetic field intensity has been varied between *0.01* and *0.1 T* to gain a better understanding of the behavior of ferronanofluids under a magnetic field, allowing for a selection of the most suitable scenario. Specifically, magnetic field intensities of *0.01 T, 0.05 T*, and *0.1* T have been chosen. The position of the magnetic

field has been altered in three distinct locations: *300-400 mm, 700-800 mm,* and *1200-1300 mm,* respectively. For each location, simulations have been performed for three different intensities of the magnetic field. The selection of these locations was motivated by their proximity to the inlet, middle, and outlet of the pipe, ensuring comprehensive coverage of the entire pipe in the study. Additionally, the results obtained from the three different magnetic field intensities (*0.01 T, 0.05 T,* and *0.1 T*) at each of the three field locations (*300-400 mm, 700-800 mm*, and *1200-1300 mm*) have been collectively compared and analyzed. This comparative analysis aims to provide valuable insights into the optimal configuration of the magnetic field to enhance heat transfer performance in the system.

To streamline the analysis and improve efficiency, the study initially examined the behavior of the ferronanofluid flow without the presence of a magnetic field using five different nanoparticle volume fractions (*NPVF*). However, for computational time optimization and to avoid excessive data requiring interpretation, the examination of ferronanofluids under the influence of a magnetic field was limited to three selected *NPVF* values: *0.5%, 1%,* and *2%*. This narrowed focus on specific *NPVF* values allows for meaningful and manageable results that can be effectively analyzed and interpreted.

The primary objective of this phase is to assess the same properties as in the previous study in order to determine the extent of thermal system enhancement. Specifically, the focus is on investigating the convection heat transfer coefficient, Nusselt number, Darcy friction factor, and performance evaluation criteria. These parameters provide insights into the effectiveness and efficiency of the heat transfer process in the presence of ferronanofluid flow subjected to a magnetic field. In order to enhance clarity and facilitate the organization of this phase of the study, it was divided into nine distinct cases. Firstly, an examination is conducted on the behavior of ferronanofluid flow in the smooth pipe at the initial location of the magnetic field. This investigation involves studying the thermal properties of the ferronanofluid flow for three different nanoparticle volume fractions (*NPVF*), while also comparing the results across three different magnetic field intensities and a control case without a magnetic field.
Subsequently, the focus shifts to the second location of the magnetic field. Here, the flow of ferronanofluids under the influence of a magnetic field are analyzed for three

different *NPVF* values. Similar to the previous case, comparisons are made among three different magnetic field intensities, as well as a case without a magnetic field.

Finally, the magnetic field is relocated to the third specified location, and investigations continue for three different *NPVF* values. The behavior of ferronanofluid flow under the magnetic field is assessed for each *NPVF*, considering three different magnetic field intensities, along with a control case without a magnetic field.

By organizing the study in this manner Table 4.1, potential confusion can be minimized, and a systematic approach can be implemented to track and analyze the effects of different variables on the behavior of ferronanofluid flow in the smooth pipe.

Table 4.1. Cases of the study under the magnetic field.

Case	*Magnetic field Location (mm)*	*NPVF (%)*	*MF Intensity (T)*
1	300 - 400	0.5	0, 0.01, 0.05, and 0.1
		1	0, 0.01, 0.05, and 0.1
		2	0, 0.01, 0.05, and 0.1
2	700 - 800	0.5	0, 0.01, 0.05, and 0.1
		1	0, 0.01, 0.05, and 0.1
		2	0, 0.01, 0.05, and 0.1
3	1200 - 1300	0.5	0, 0.01, 0.05, and 0.1
		1	0, 0.01, 0.05, and 0.1
		2	0, 0.01, 0.05, and 0.1

4.3.1. Ferronanofluid Flow Under the Effect of MF at Location 1 (300 – 400) mm

In this scenario, the ferronanofluid is directed through an aluminum smooth pipe while being subjected to a magnetic field. The magnetic field is positioned in close proximity to the pipe inlet, specifically within the range of *300-400 mm*. As the ferronanofluid flows inside the pipe, it experiences heating from a heat flux with a magnitude of *6700*

W/m^2. It is noteworthy that aluminum was chosen as the pipe material to facilitate the propagation of the magnetic field through the pipe and attract the ferronanofluids. During the experimentation, measurements were taken to determine the thermal properties of the ferronanofluids, along with recording the outlet temperature. It is important to mention that the inlet temperature was maintained at a constant value of *293 K*.

Case 1 with 0.5% NPVF

In this particular scenario, a computational analysis has been conducted to examine the behavior of ferronanofluid flowing through a uniformly heated pipe. The obtained results have been extensively examined and analyzed in order to establish a basis for comparison with similar cases.

In this instance, it is evident that the Nusselt number exhibits a direct correlation with the intensity of the magnetic field. As illustrated in Figure 4.13, the relationship between the Nusselt number and Reynolds number demonstrates that the curve for the *0 T* magnetic field is nearly identical to that of the *0.01 T* magnetic field. The Nusselt number rises as a result of the greater impact exerted by the *0.1 T* magnetic field on the particles.

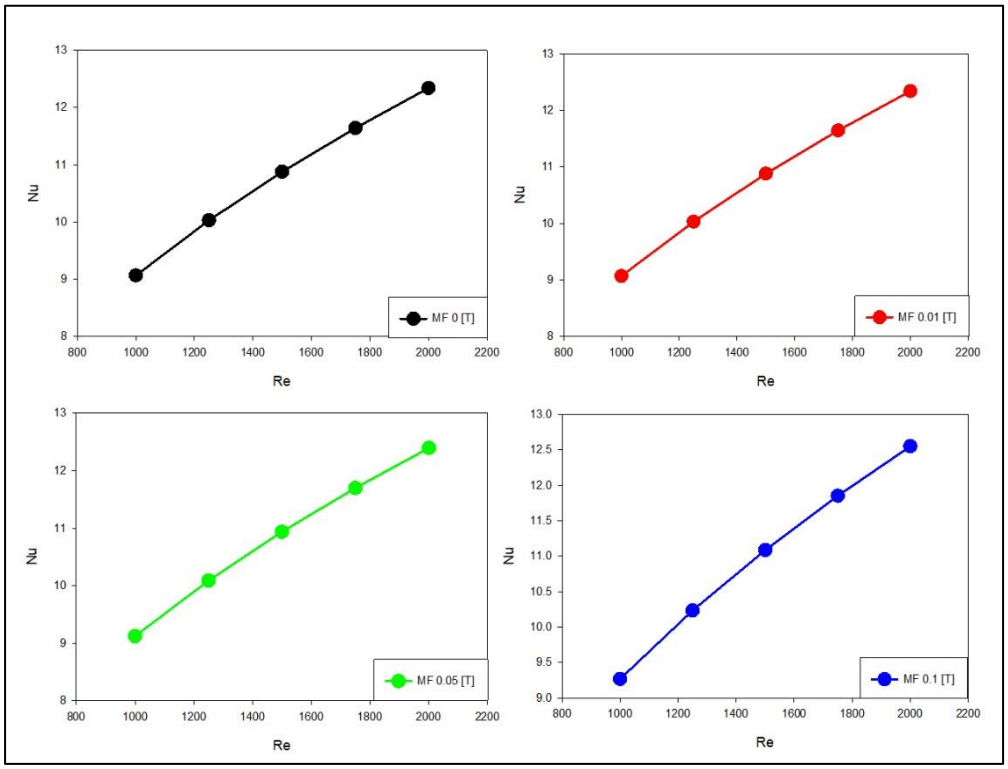

Figure 4.13. Variation of Nu number with Re number for different MF intensities.

In this particular case, the relationship between pressure drop and Reynolds number exhibited a typical pattern when influenced by the magnetic field. It was found that as the intensity of the magnetic field increases, there is a corresponding rise in the pressure drop. This phenomenon can be attributed to the aggregation of nanoparticles within the ferronanofluid, which occurs due to the influence of the magnetic field (Figure 4.14). When the magnetic field intensity is increased, it induces stronger magnetic forces on the nanoparticles in the ferronanofluid. Consequently, the nanoparticles tend to aggregate and form larger clusters or chains due to their magnetic interactions. This aggregation leads to increased resistance to flow, resulting in a higher pressure drop within the system.

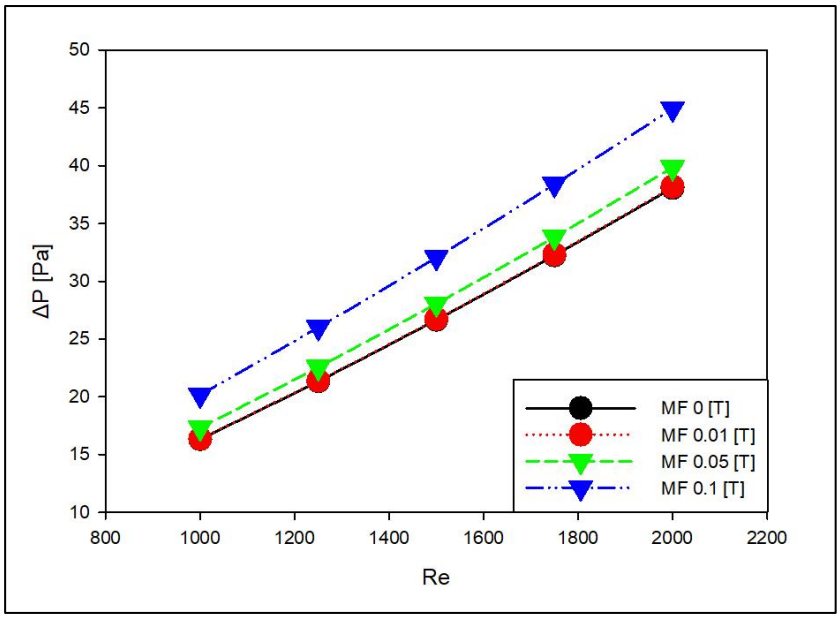

Figure 4. 14 Variation of Pressure drop with Re number for different MF intensities.

Figure 4.15 displays the graphical representation of the relationship between the Darcy friction factor and Reynolds number for various magnetic field intensities. The figure clearly demonstrates the significant influence of magnetic field intensity on the Darcy friction factor. As the intensity of the magnetic field increases, the Darcy friction factor

also increases. This observation aligns with expectations, as the corresponding increase in the magnetic field intensity leads to a rise in the pressure drop (ΔP) within the system. Consequently, the Darcy friction factor, which quantifies the resistance to flow, exhibits an upward trend.

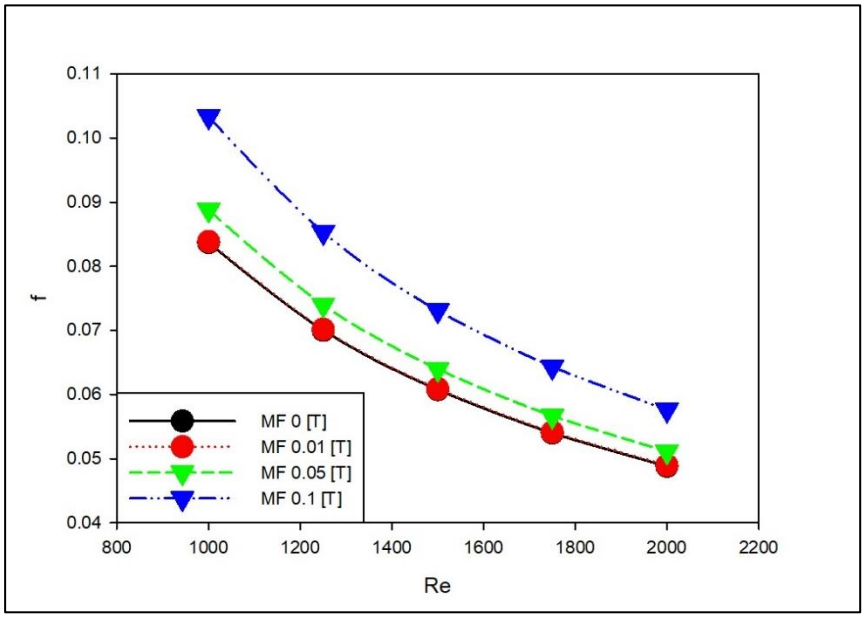

Figure 4. 15 Variation of Darcy Friction with Re number for different MF intensities.

In this scenario, the *PEC* has been established by plotting the Reynolds number against the magnetic field strength for a working fluid consisting of *0.5% NPVF*. The findings, as illustrated in Figure 4.16, indicate that increasing the magnitude of the magnetic field results in a decrease in the *PEC* value. Therefore, in this particular context, the magnetic field has a negative impact on the *PEC*.

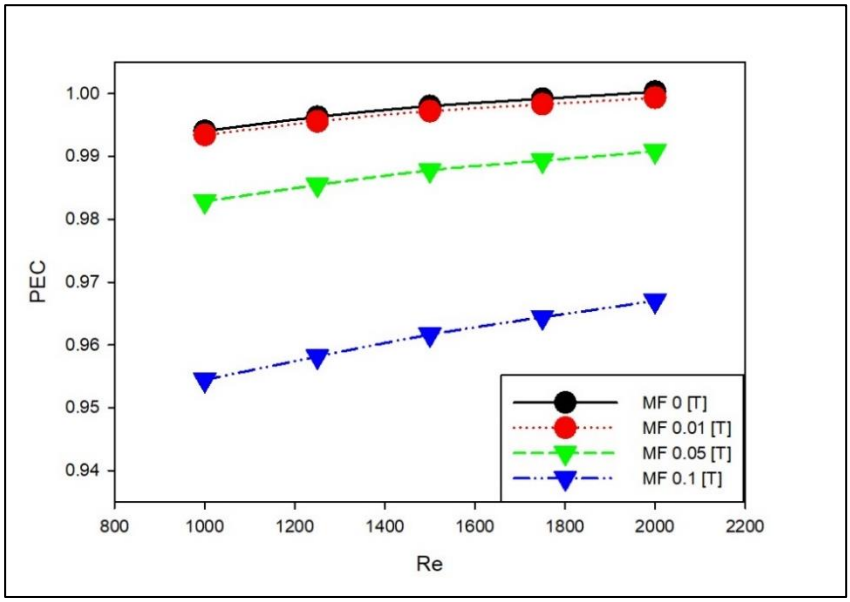

Figure 4. 16 Variation of PEC with Re number for different MF intensities.

Figure 4.17 shows the surface Nusselt number distribution for ferronanofluid with NPVF 0.5 % at Reynolds number 1000 under the effect of Reynolds number, where the Nusselt number is at the maximum at the entrance of the pipe.

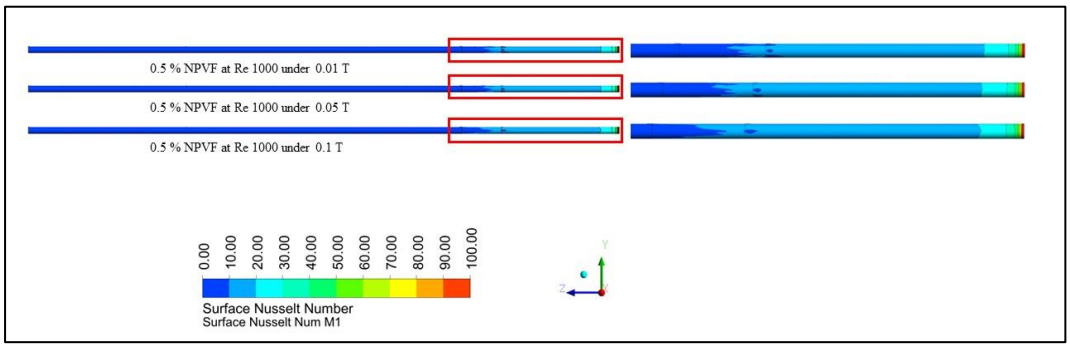

Figure 4. 17. Variation of surface Nusselt number distribution for different MF intensities

The surface temperature distribution contour in Figure 4.18 shows comparison for the impact of the magnetic field with different intensities 0.01, 0.05, and 0.1 T respectively on the ferronanofluid with 0.5 % NPVF at Re 1000.

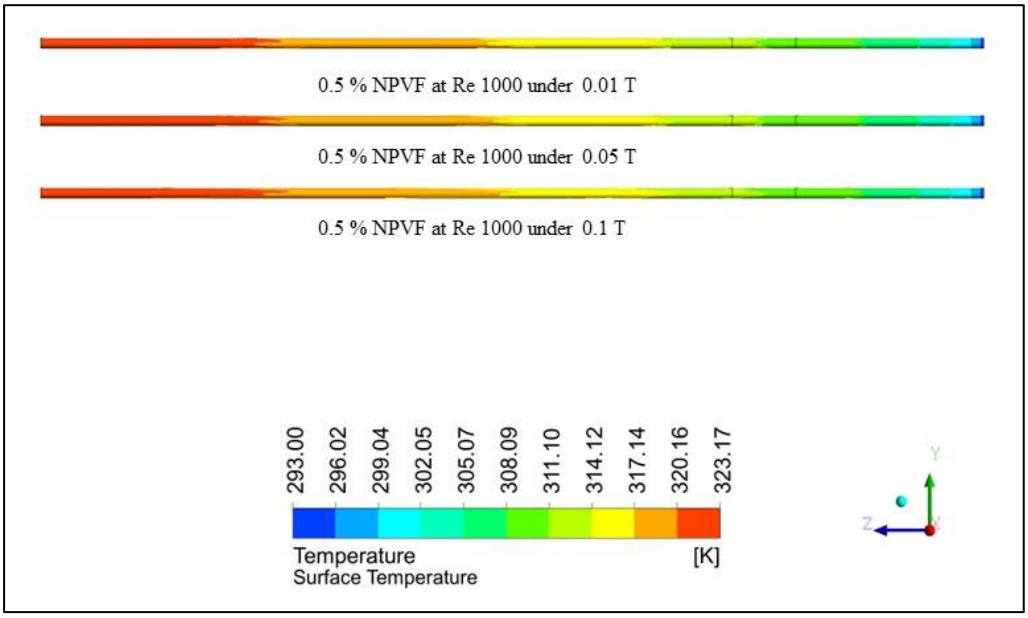

Figure 4. 18. Variation of surface temperature distribution for different MF intensities

The velocity distribution streamline has been generated also to understand the impact of the magnetic field with different intensities 0.01, 0.05, and 0.1 T, on the ferronanofluids with 0.05 % NPVF at Reynolds number 1000 as shown in Figure 4.19.

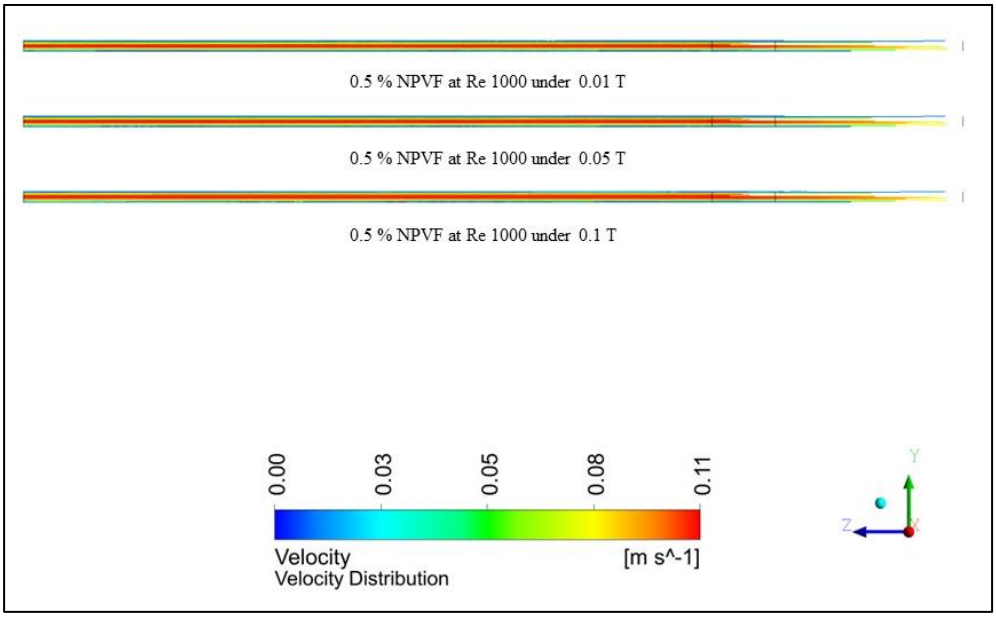

Figure 4. 19 Variation of velocity distribution for different MF intensities

Case 1 with 1.0% NPVF

In this case, a computational analysis has been conducted to examine the behavior of ferronanofluid of *1.0% NPVF* flowing through a uniformly surfaced pipe under the effect of various values of magnetic intensities.

The *NPVF* was increased to *1.0%* in this investigation, as depicted in Figure 4.20. The figure illustrates the variations of the Nusselt number with the Reynolds number for various intensities of the magnetic field. Notably, the Nusselt number demonstrates a proportional relationship with the intensity of the magnet, with the highest Nusselt number observed at an intensity of *0.1 T*.

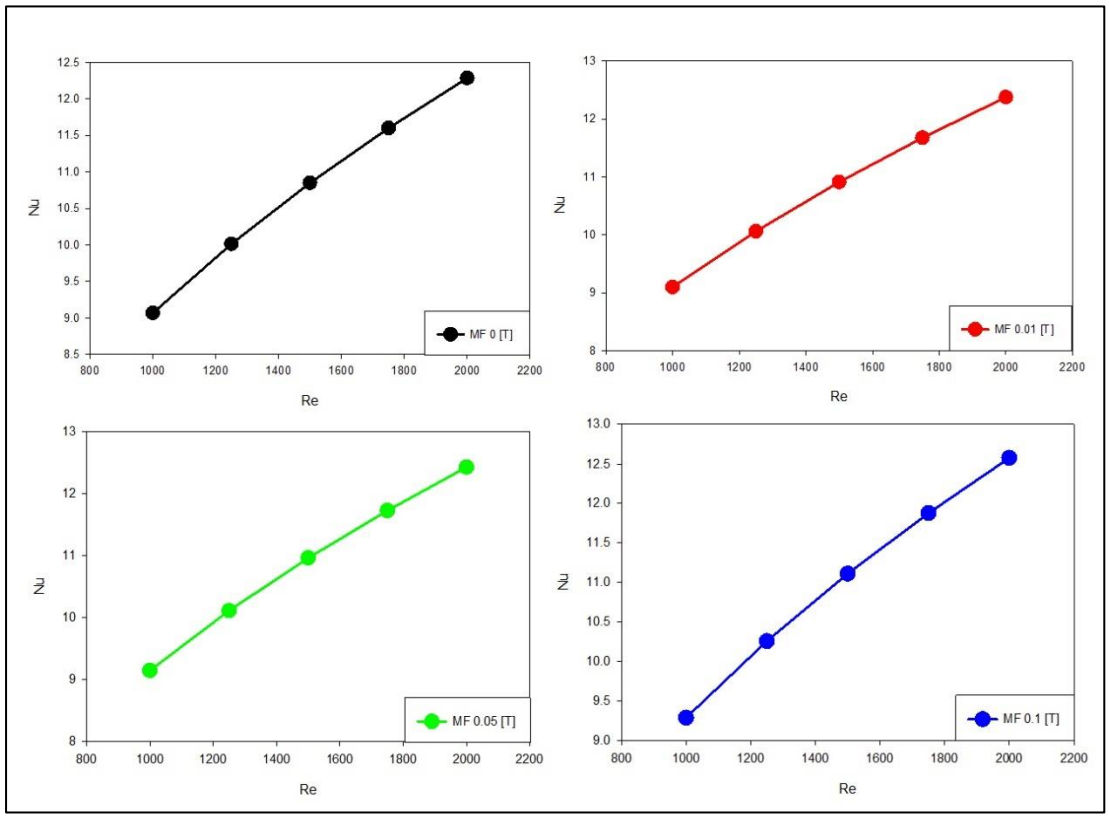

Figure 4. 20 Variation of Nu number with Re number for different MF intensities.

As anticipated, the pressure drop exhibited an increase as the magnetic field intensity was raised. This relationship is demonstrated in Figure 4.21, which illustrates the

correlation between pressure drop and Reynolds number for various intensities of the magnetic fields. Notably, the highest-pressure drop occurred at an intensity of *0.1 T*, specifically at a Reynolds number of *2000*.

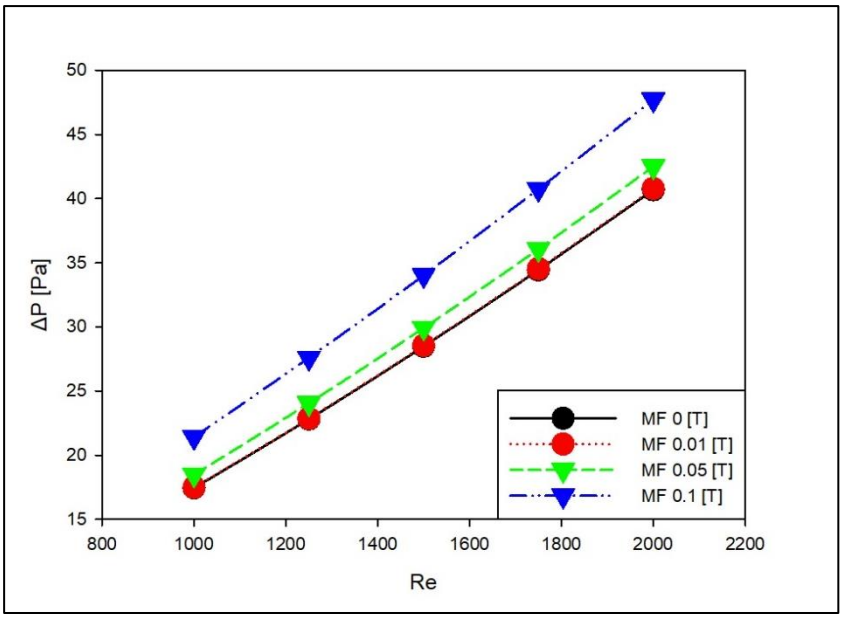

Figure 4. 21 Variation of Pressure Drop with Re number for different MF intensities.

Through careful observation of the pressure drop, it becomes evident that the Darcy friction factor experiences an increase in magnitude as the strength of the magnetic field is augmented Figure 4.22. However, the highest Darcy friction factor is observed at lower Reynolds numbers, and it continues to decrease as the Reynolds number rises.

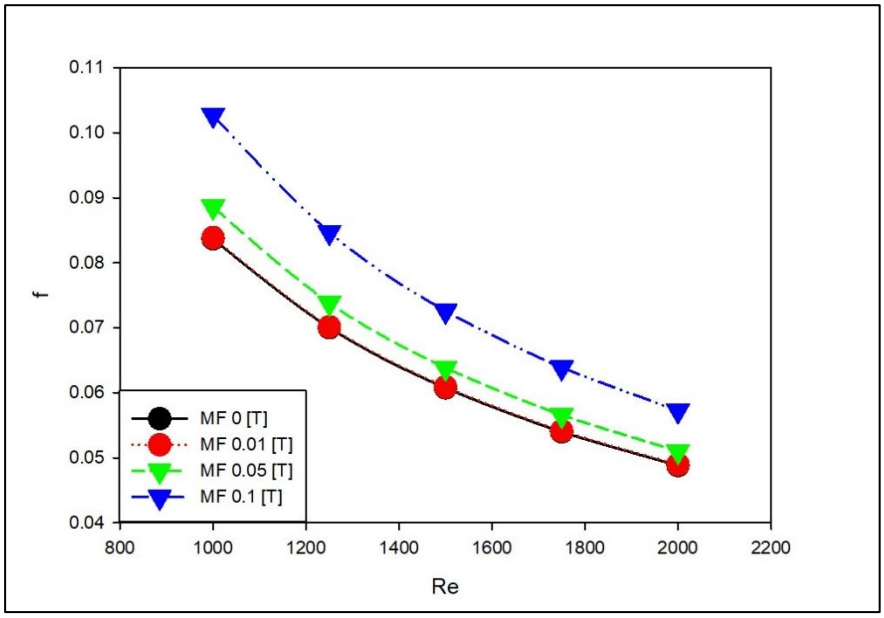

Figure 4. 22 Variation of Darcy friction with Re number for different MF intensities.

Figure 4.23 exhibits a nonproportional relationship between the *PEC* and the magnetic intensity for the case of *NPVF* of *1.0%*. The magnetic field is positioned in close proximity to the inlet of the pipe. Notably, the lower magnitude of magnetic field is observed to correspond to the highest *PEC* value, indicating a lack of significant influence from the magnetic field across the entirety of the pipe.

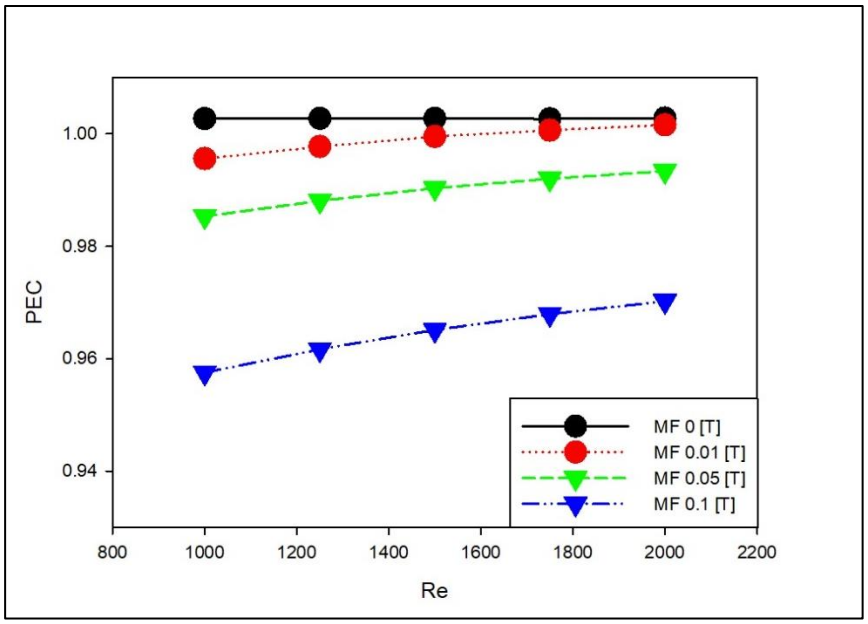

Figure 4. 23 Variation of PEC with Re number for different MF intensities.

Case 1 with 2.0% NPVF

To compare the results with other cases and determine the most efficient one, a simulation was conducted using a concentration of 2.0% *NPVF* at various magnetic field intensities. The simulations were performed at the same location of the magnetic field. By evaluating the outcomes of these simulations, the aim is to identify the case that exhibits the highest efficiency in terms of the desired parameters or performance metrics.

In this particular case, the Nusselt number did not exhibit any discernible variation in its trend compared to other cases involving different *NPVF* s. As depicted in Figure 4.24, the Nusselt number curve displays a proportional relationship with the increase in magnetic field intensity. This behavior is expected and consistent with the anticipated improvement in convection heat transfer due to the presence of nanoparticles, which enhance conduction effects.

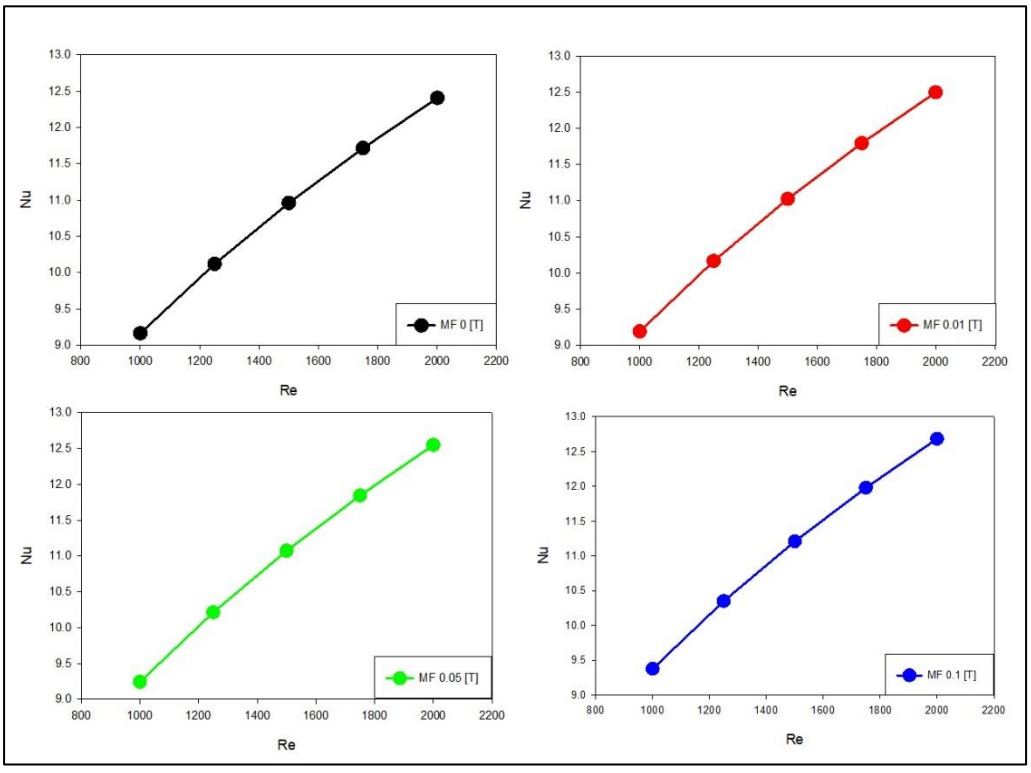

Figure 4. 24 Variation of Nu number with Re number for different MF intensities.

The analysis of pressure drop for a concentration of *2.0% NPVF* indicated that a magnetic field intensity of *0.01 T* did not result in a significant difference in the pressure drop. However, when the magnitude of the magnetic field was increased, there was indeed an observed increase in the pressure drop. This finding is illustrated in Figure 4.25, where the highest pressure drop of *54.9 Pa* was recorded at a Reynolds number of *2000*. Therefore, it can be concluded that an increase in the magnetic field intensity does correspond to an increase in the pressure drop within the system.

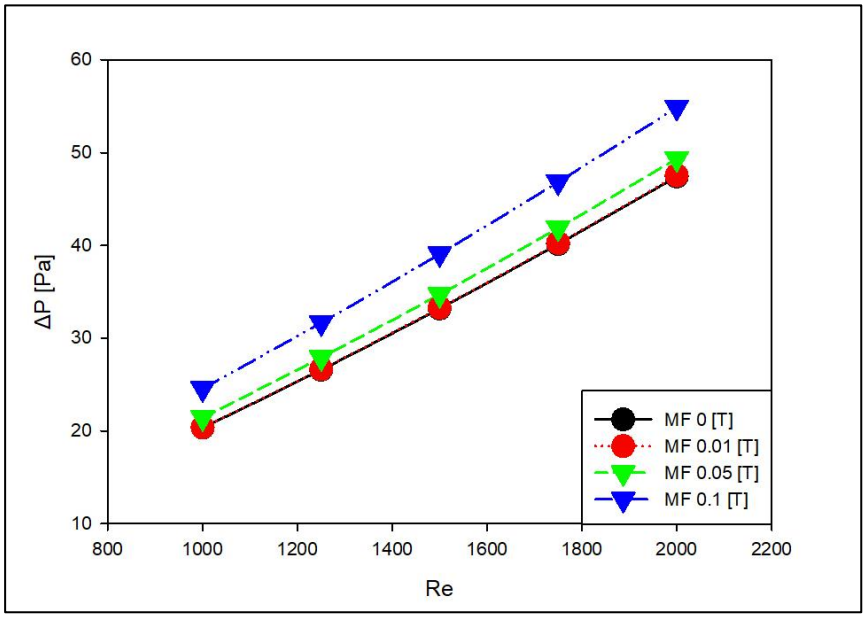

Figure 4. 25 Variation of Pressure drop with Re number for different MF intensities.

In line with previous cases, the Darcy friction factor exhibited a consistent trend. The lowest magnetic field intensity corresponded to the lowest Darcy friction, while an intensity of *0.1 T* displayed the most significant increase in the Darcy friction factor. This trend is depicted in Figure 4.26, which illustrates the variation in Darcy friction with Reynolds number for different magnetic field intensities. The results further affirm that higher magnetic field intensities contribute to an augmented Darcy friction factor, indicating increased resistance to flow within the system.

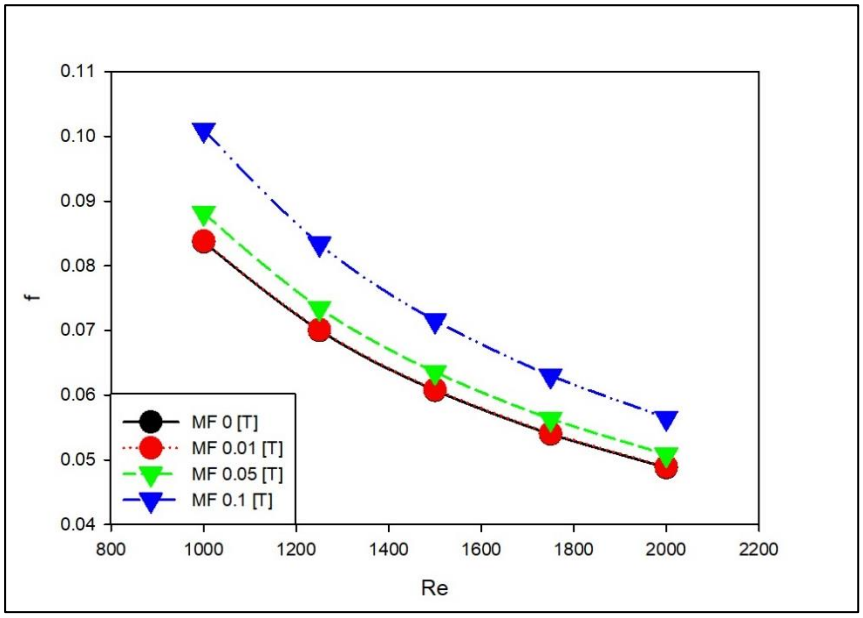

Figure 4. 26 Variation of Darcy friction with Re number for different MF intensities.

The *PEC* were computed for *NPVF* with a concentration of *2.0%* at various Reynolds numbers, considering different magnetic field strengths. Figure 4.27 presents the results, indicating that the *PEC* exhibited lower values for higher magnetic field strengths. These findings suggest that the presence of a strong magnetic field may have a detrimental effect on the *PEC*, while the absence of a magnetic field allows for the maximum *PEC* value to be achieved.

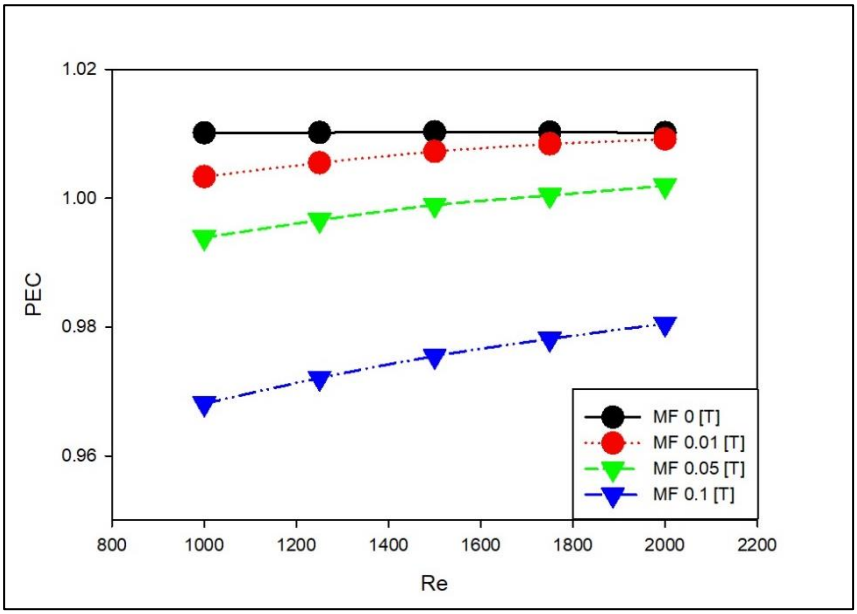

Figure 4. 27 Variation of PEC with Re number for different MF intensities.

4.3.2. Ferronanofluid Flow Under the Effect of MF at Location 2 (700 – 800) mm

In this particular case, the thesis focuses on investigating the behavior of ferronanofluids when directed through an aluminum smooth pipe while subjected to a magnetic field. The magnetic field, which plays a crucial role in influencing the ferronanofluid flow, is positioned within the range of *700 – 800 mm* from the pipe inlet. The experiment aims to analyze the thermal properties of ferronanofluids and record the corresponding outlet temperature. To ensure consistency, the inlet temperature is maintained at a constant value of *293 K*. The choice of aluminum as the pipe material is deliberate, as it facilitates the propagation of the magnetic field through the pipe and enhances the attraction of the ferronanofluids.

Case 2 with 0.5% NPVF

In this particular scenario, a computational analysis has been conducted to examine the behavior of ferronanofluid flowing through a uniformly surfaced pipe. The analysis specifically focuses on a ferronanofluid with a nanoparticle volume fraction *NPVF* of *0.5%*. The obtained results have been extensively examined and analyzed in order to establish a basis for comparison with similar cases.

Figure 4.28 depicts the relationship between the Nusselt and Reynolds number at varying intensities of the magnetic field. It is evident that a marginal enhancement in the Nusselt number value is observed when compared to the first location of the magnetic field. It is notable that the Nusselt number exhibits a higher reading under the magnetic field intensity of *0.01 T* compared to the preceding scenario.

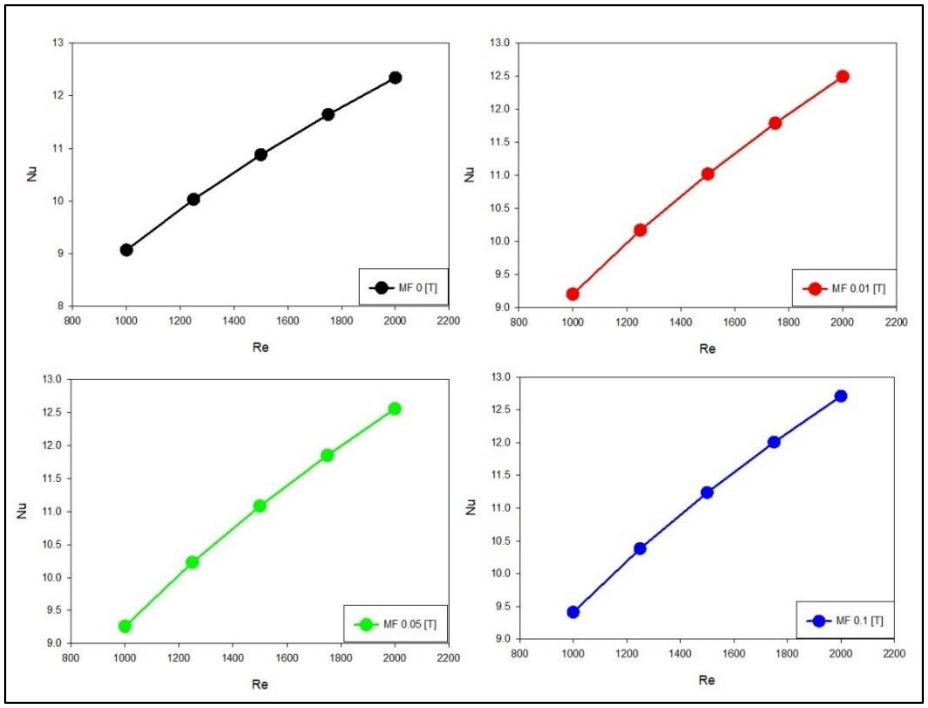

Figure 4. 28 Variation of Nu number with Re number for different MF intensities.

In this specific case, Figure 4.29 represents the relationship between pressure drop and Reynolds number under various magnitudes of the magnetic field. Interestingly, considering the thermal and physical properties of the ferronanofluids, it is observed that there are minimal alterations. However, the pressure drop experiences an increase as the magnetic field strength intensifies. This phenomenon can be attributed to the additional pumping power required by the system to sustain the fluid flow. Where The highest-pressure drop is observed at a magnetic field strength of *0.1 T*.

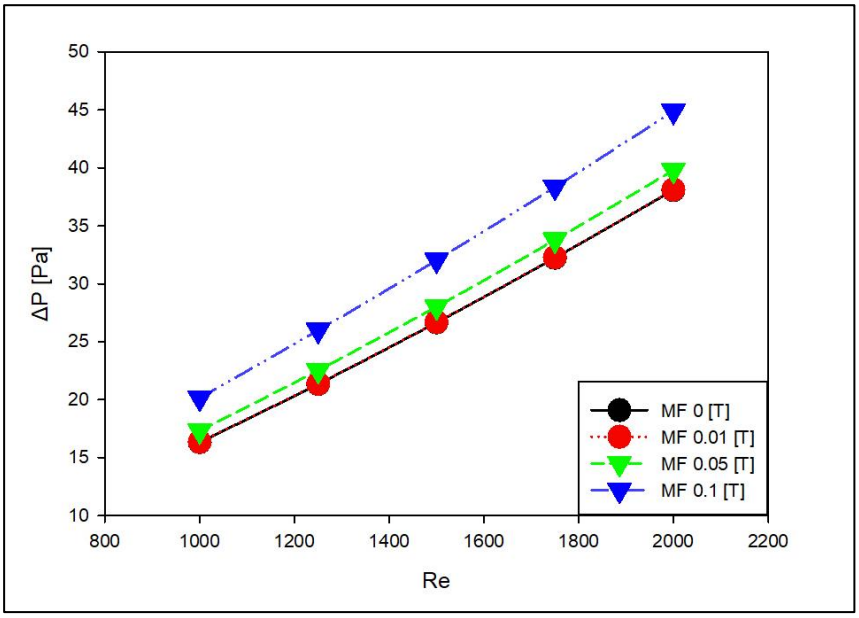

Figure 4. 29 Variation of Pressure drop with Re number for different MF intensities.

According to the findings illustrated in Figure 4.30, the relationship between the Darcy friction factor and Reynolds number is influenced by the presence of a magnetic field. At a magnetic field strength of *0.1 T*, there is a noticeable increase in the Darcy friction factor. This can be attributed to the higher attraction experienced by the ferroparticles, causing them to form chains near the pipe wall. The formation of these chains leads to an elevated friction factor. Conversely, at a magnetic field strength of *0.01 T*, the Darcy friction factor demonstrates a behavior similar to that observed in the absence of a magnetic field.

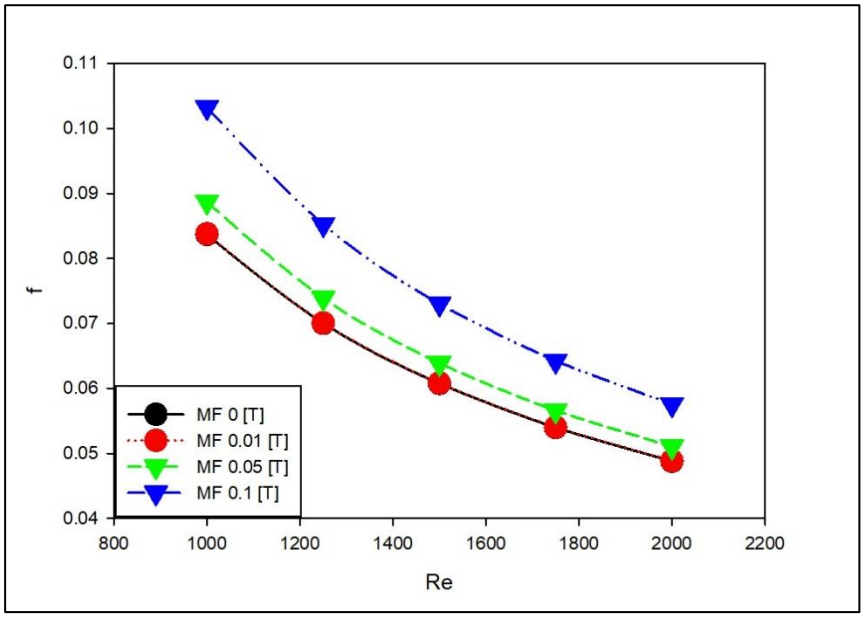

Figure 4. 30 Variation of Darcy friction with Re number for different MF intensities.

In this particular analysis, the *PEC* has been established by plotting the Reynolds number against the magnetic field strength. The working fluid used in the evaluation comprises *0.5% NPVF*. The results, presented in Figure 4.31., indicate that the *PEC* exhibits its lowest value under a magnetic field strength of *0.1 T*. Conversely, the highest *PEC* value is observed under a magnetic field strength of *0.01 T*. Furthermore, a moderate improvement in the *PEC* is noted under a magnetic field strength of *0.05 T*, while the PEC value showed obvious decrease under 0.1 T. Notably, the highest *PEC* value recorded under a magnetic field strength of *0.01 T* is *1.018* for *Re 1000*.

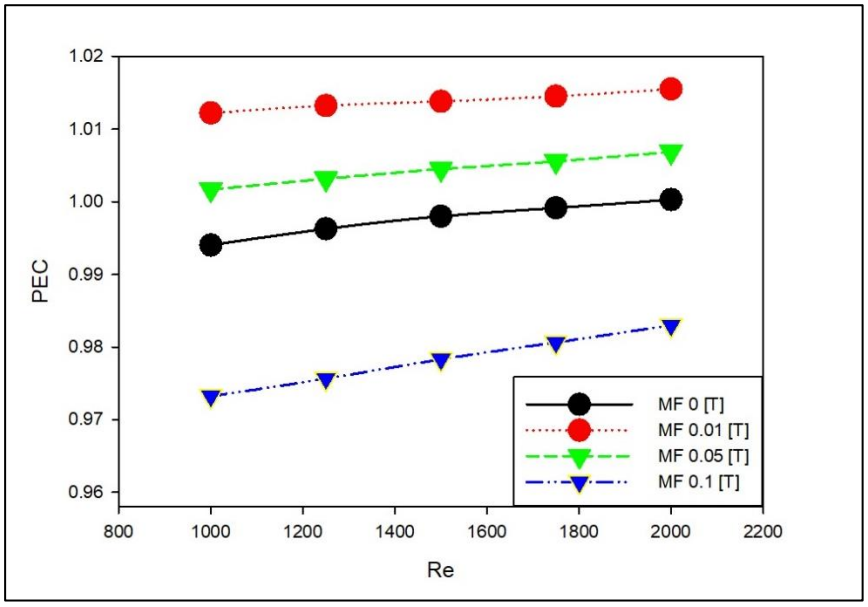

Figure 4. 31 Variation of PEC with Re number for different MF intensities.

Case 2 with 1% NPVF

In this scenario, a computational analysis was undertaken to investigate the behavior of a ferronanofluid consisting of *1% NPVF* (Nanoparticle Volume Fraction) as it flows through a pipe with a uniformly textured surface. The study specifically focused on examining the influence of different magnetic field strengths on the ferronanofluid's characteristics.

In this investigation, the nanoparticle volume fraction (*NPVF*) was raised to *1%*, as indicated in Figure 4.32. The figure demonstrates the changes in the Nusselt number as a function of the Reynolds number for different magnetic field strengths. Unlike the previous scenario at the first location, the Nusselt number exhibited some improvement at magnetic field strengths of *0.01 T* and *0.05 T*. However, the highest value of approximately 12.7 was observed at a magnetic field strength of *0.1 T*.

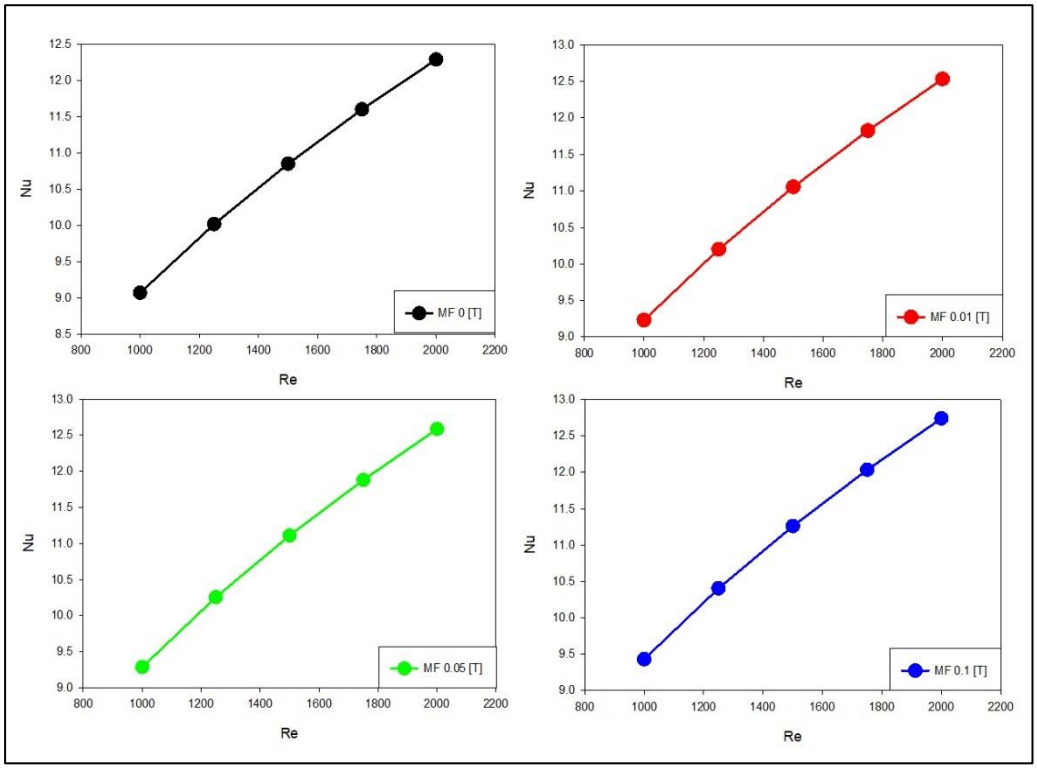

Figure 4. 32 Variation of Nu number with Re number for different MF intensities.

As expected, the increase in magnetic field intensity resulted in a corresponding elevation in the pressure drop. This phenomenon is exemplified in Figure 4.33, which elucidates the correlation between the pressure drop and Reynolds number across varying magnitudes of magnetic field intensities. It is noteworthy that the greatest pressure drop occurred specifically at an intensity of *0.1 T*, specifically at a Reynolds number of *2000*.

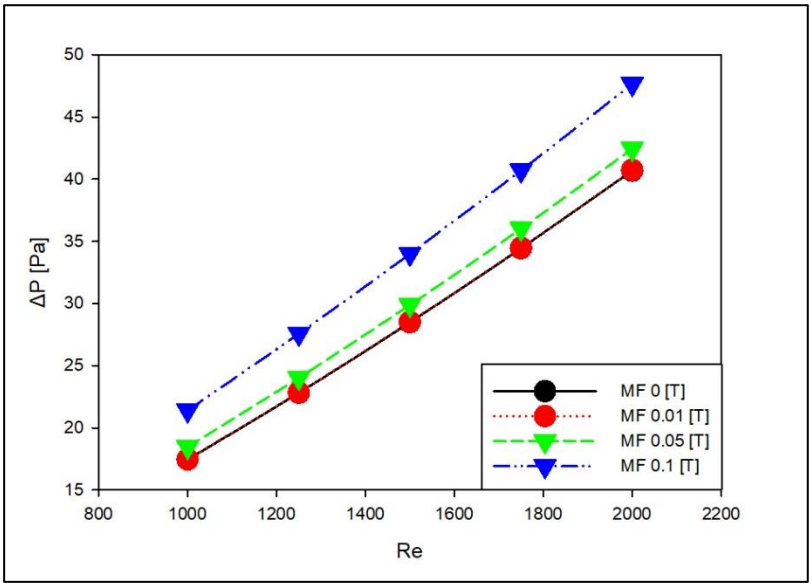

Figure 4. 33 Variation of Pressure drop with Re number for different MF intensities.

Figure 4.34 portrays the association between the Darcy friction factor and Reynolds number for a nanoparticle volume fraction (*NPVF*) of *1%*. The objective is to discern the behavior under different magnetic field strengths. Consistent with prior observations, the Darcy friction factor exhibits a proportional relationship with the magnetic field intensity. Specifically, the lowest value is recorded at a magnetic field strength of *0.01 T*, which is remarkably close to the absence of a magnetic field. Conversely, the highest Darcy friction factor is observed at a MF strength of *0.1 T*.

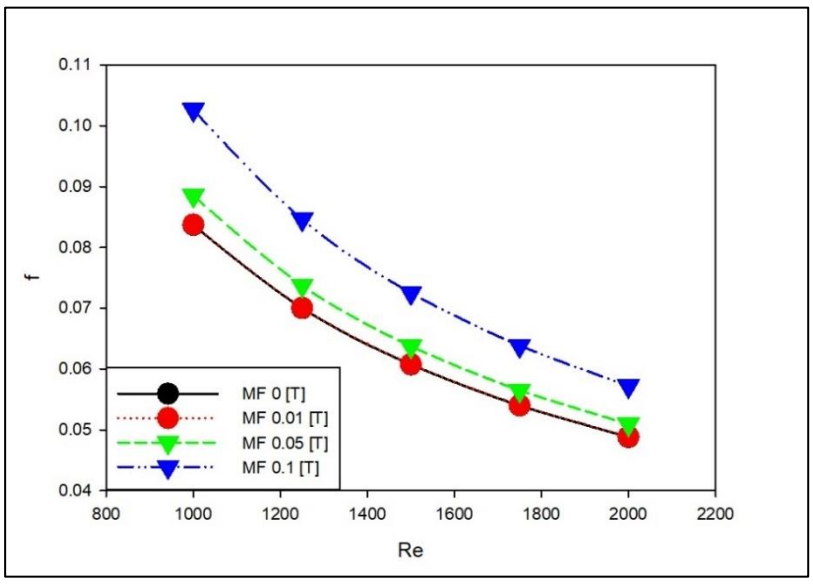

Figure 4. 34 Variation of Darcy friction with Re number for different MF intensities.

Figure 4.35 presents the relationship between the Performance Evaluation Criteria (*PEC*) and Reynolds number under the influence of different magnetic field strengths. It is observed that at a magnetic field strength of *0.1 T*, the *PEC* exhibits the poorest performance. A slight improvement is observed at a magnetic field strength of *0.05*, where the most favorable *PEC* value, reaching approximately *1.015* at Reynolds number *2000*, is achieved at a magnetic field strength of *0.01 T*.

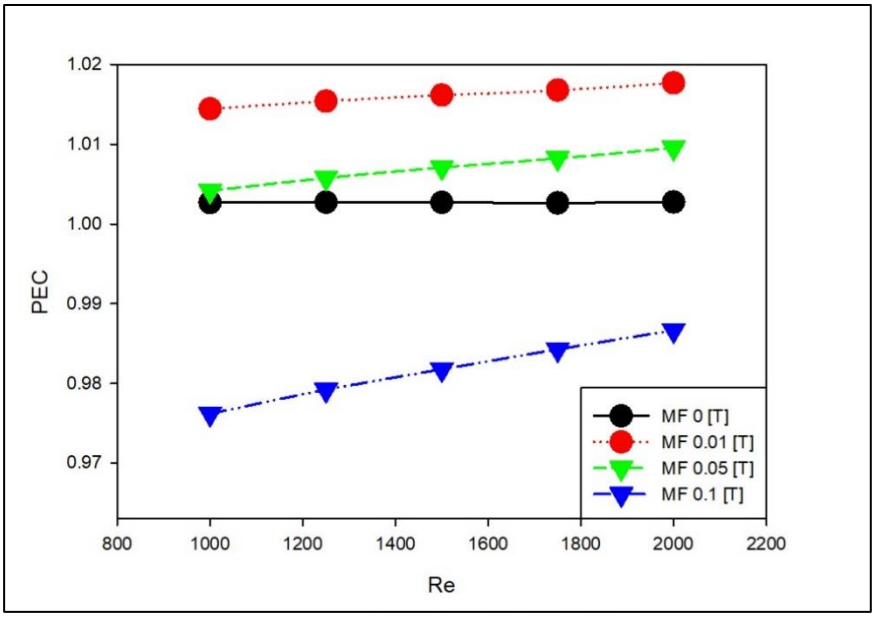

Figure 4. 35 Variation of PEC with Re number for different MF intensities.

Case 2 with 2% NPVF

Currently, we have calculated the thermal characteristics for *NPVF* concentrations of *0.5%*, *1%*, and are now analyzing the remaining *2%* for the second location of the magnetic field. The boundary conditions remain unchanged; however, in this instance, the investigation focuses on the impact of increasing nanoparticle concentration to aid in determining the optimal formula.

Figure 4.36 demonstrates the variation of Nusselt number with respect to Reynolds number, considering different levels of magnetic field intensity. Notably, in this scenario, we observe improvements resulting from alterations in either the source location or the volume fraction of nanoparticles. The Nusselt number values obtained under the influence of the magnetic field surpass those obtained in previous cases, indicating a positive correlation between Nusselt number and magnetic field strength. Additionally, the relationship between Nusselt number and Reynolds number is also proportional in nature. It is worth noting that the highest Nusselt number values are observed at a magnetic field strength of *0.1 T*.

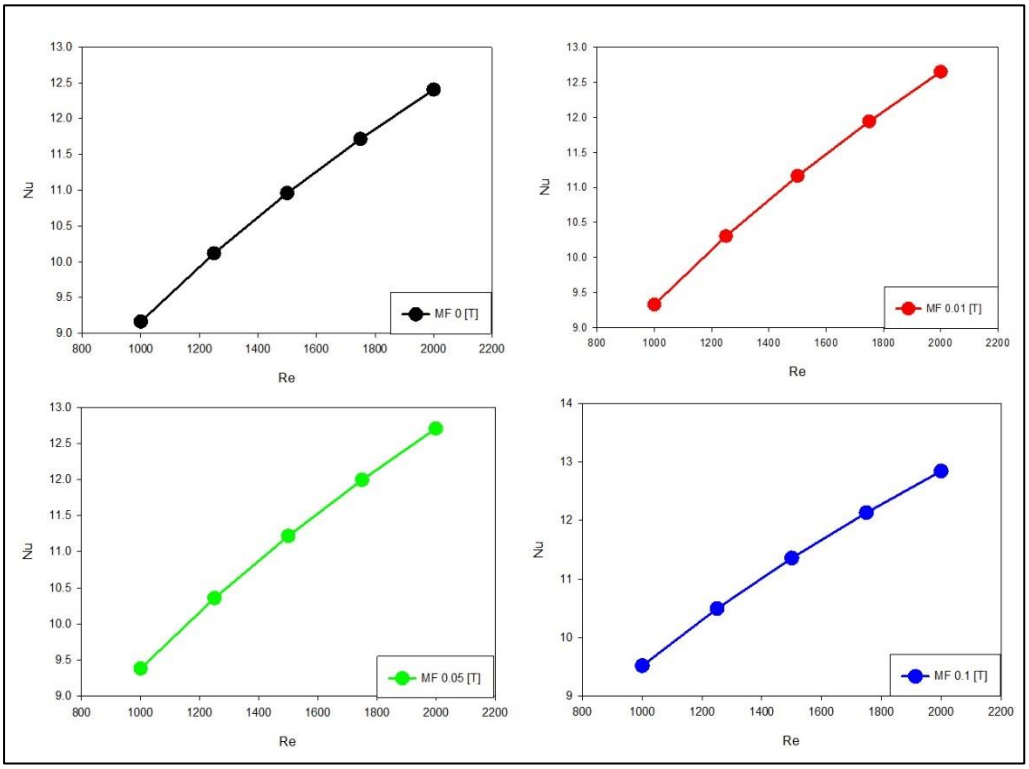

Figure 4. 36 Variation of Nu number with Re number for different MF intensities.

Figure 4.37 presents the outcomes of the pressure drop analysis conducted on a *2% NPVF* concentration. It was found that a magnetic field intensity of *0.01 T* did not yield a noticeable impact on the pressure drop. However, as the magnetic field strength was increased, a corresponding increase in the pressure drop was observed. Remarkably, the highest pressure drop of *55.5 Pa* occurred at a Reynolds number of *2000*. From these

results, it can be inferred that an augmentation in the magnetic field intensity leads to an elevation in the pressure drop experienced within the system.

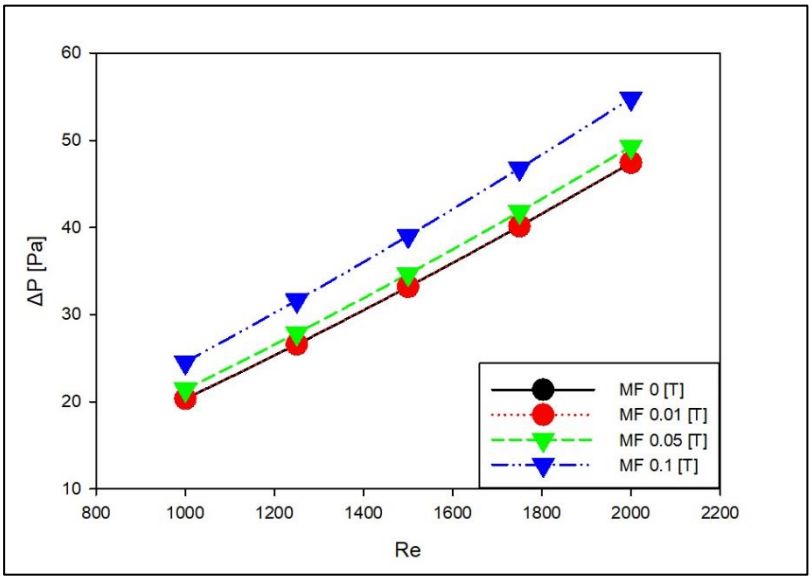

Figure 4. 37 Variation of Pressure drop with Re number for different MF intensities.

Figure 4.38 portrays the relationship between the Darcy friction factor and Reynolds number for different magnetic field intensities. Consistent with previous observations, the Darcy friction factor followed a consistent pattern. The lowest magnetic field intensity resulted in the lowest Darcy friction, while an intensity of *0.1 T* exhibited the most substantial increase in the friction factor. These findings reaffirm the influence of magnetic field intensity on the Darcy friction, with higher intensities leading to an increased resistance to flow within the system.

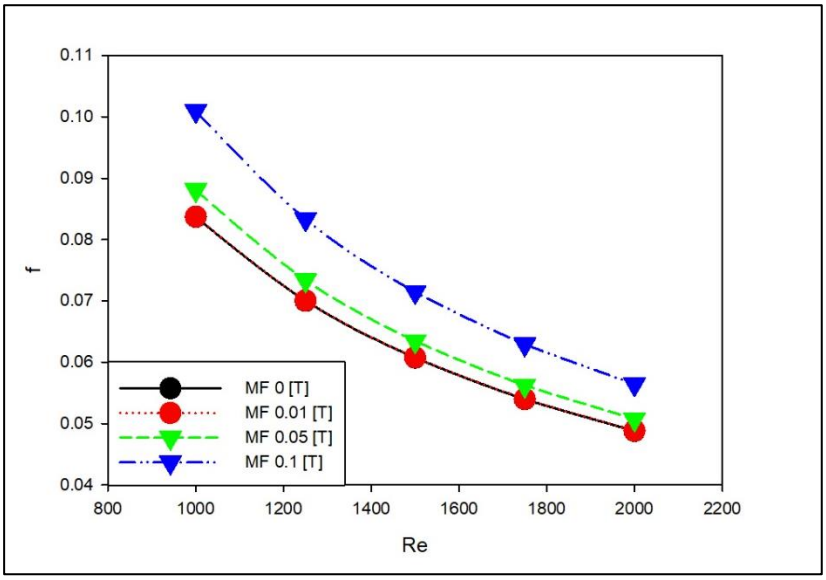

Figure 4. 38 Variation of Darcy friction with Re number for different MF intensities.

In this scenario, the performance evaluation criteria (*PEC*) has been calculated and plotted against the Reynolds number for different magnetic field strengths. Figure 4.39 demonstrates the enhancement in *PEC* compared to previous cases. Notably, the magnetic field with a magnitude of *0.01 T* exhibited the highest *PEC* values, followed by *0.05 T*. Interestingly, *PEC* values show the poorest under magnetic field intensity of *0.1 T*. However, it is worth mentioning that the trend of *PEC* increases with increasing Reynolds number.

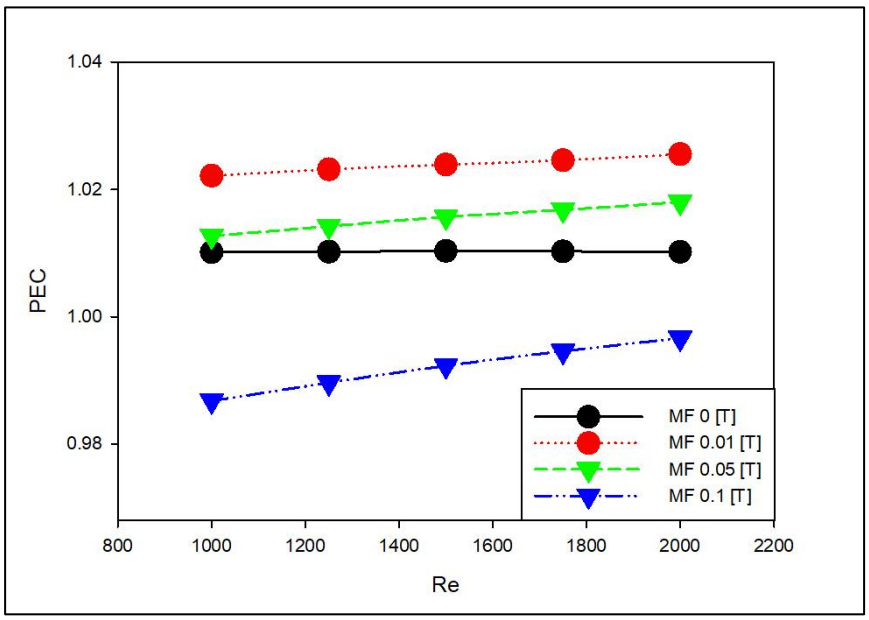

Figure 4. 39 Variation of PEC with Re number for different MF intensities.

The Nusselt number distribution contour has been generated for different NPVF 0.5, 1, and 2 % respectively under the effect of magnetic field of magnitude 0.05 T, at Reynolds number 2000, where figure 4.40 shows that the Nusselt number distribution increases with the increment of NPVF ratio.

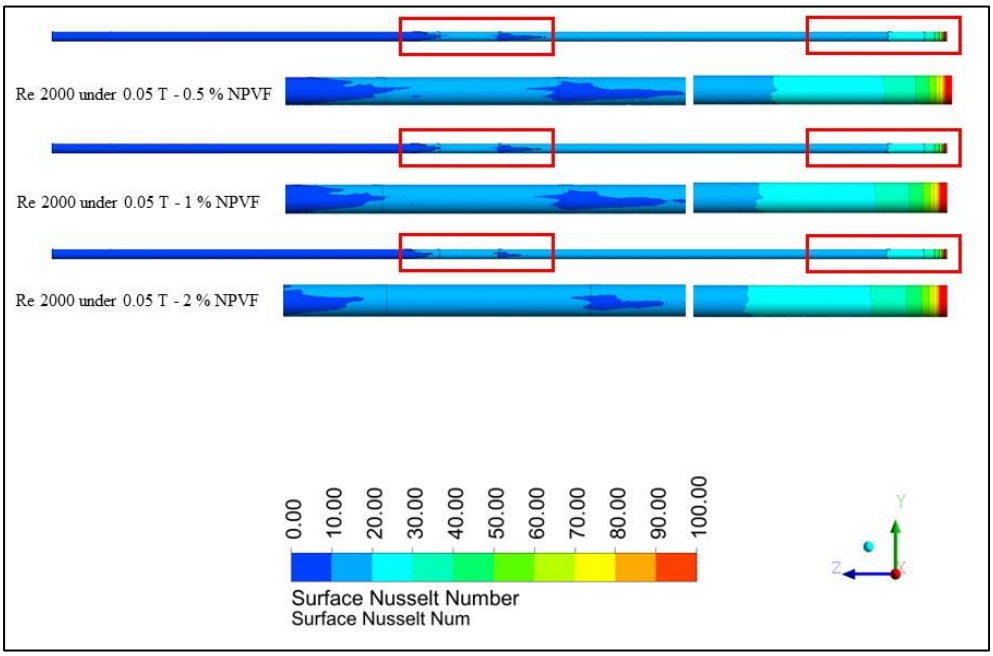

Figure 4. 40. Variation of surface Nusselt number distribution for different NPVF

The surface temperature distribution contour has been granted for different NPVF as illustrated in Figure 4.41.

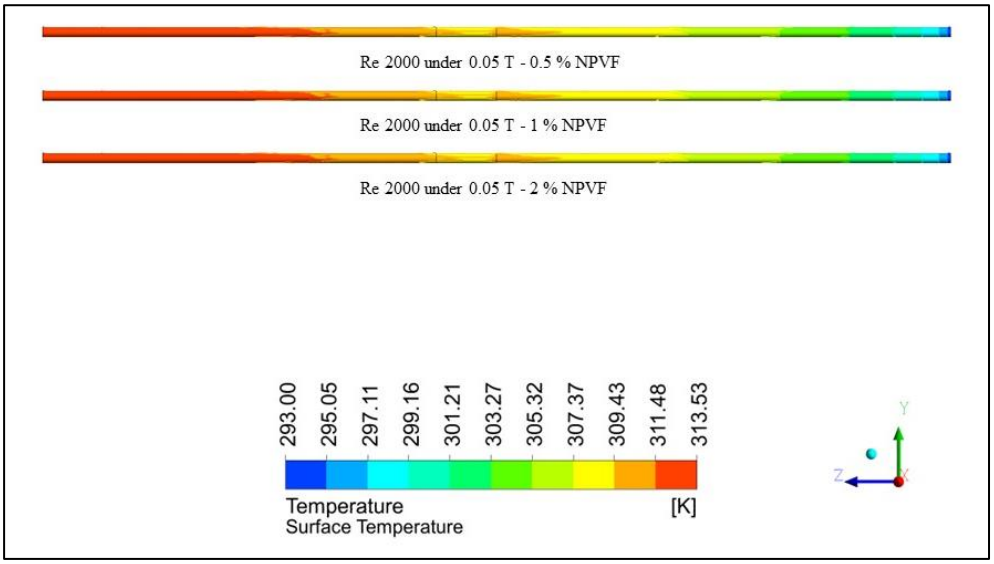

Figure 4. 41. Variation of surface temperature distribution for different NPVF.

Figure 4.42 shows that the Velocity distribution streamline was created to examine the velocity change with changing the NPVF under the effect of magnetic field at Reynolds number 2000.

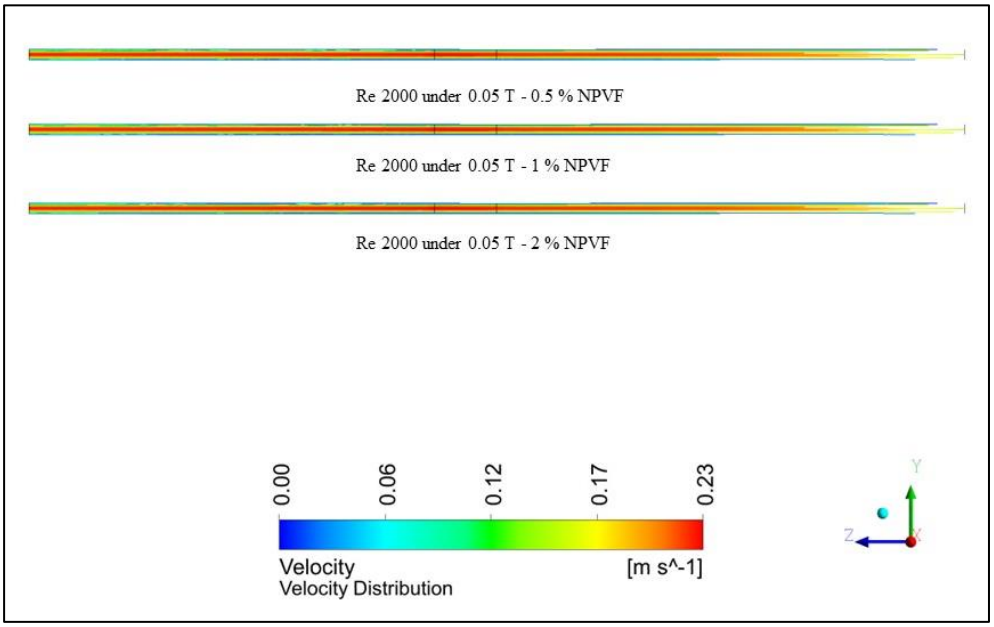

Figure 4. 42. Velocity distribution streamline for different NPVF.

4.3.3 Ferronanofluid Flow Under the Effect of MF at Location 3 (1200 – 1300) mm

The present study focuses on examining the behavior of ferronanofluids when flowing through a smooth aluminum pipe under the influence of a magnetic field. The location of the magnetic field, a significant factor affecting the flow of ferronanofluids, is moved to the third location and adjusted within the range of *1200 – 1300 mm* from the inlet of the pipe. The primary objective of this experiment is to investigate the thermal properties of the ferronanofluids and measure the corresponding outlet temperature. To maintain consistency, the inlet temperature is kept constant at *293 K*. The selection of aluminum as the material for the pipe is intentional, as it facilitates the transmission of the magnetic field through the pipe and enhances the attraction of the ferronanofluids.

Case 3 with 0.5% NPVF

This investigation focuses on numerically studying the flow of a ferronanofluid with a nanoparticle concentration of *0.5%* inside a smooth pipe under the influence of a magnetic field with varying magnitudes. The primary objective is to enhance understanding and identify the optimal conditions by examining different Reynolds numbers.

Figure 4.43 presents a graphical representation illustrating the correlation between the Nusselt number and Reynolds number, taking into account the presence of a magnetic field with varying strengths. The results indicate that the Nusselt number exhibits a modest enhancement when compared to previous cases with the same percentage of non-dimensional parameter of variable fluid properties (*NPVF*) but positioned at different locations within the magnetic field. Notably, the Nusselt number reaches its highest value for magnetic field strengths of *0.1 T*, followed by *0.05 T, 0.01 T*, and absence of magnetic field, respectively. Moreover, a direct proportionality between the Nusselt number and Reynolds number is observed.

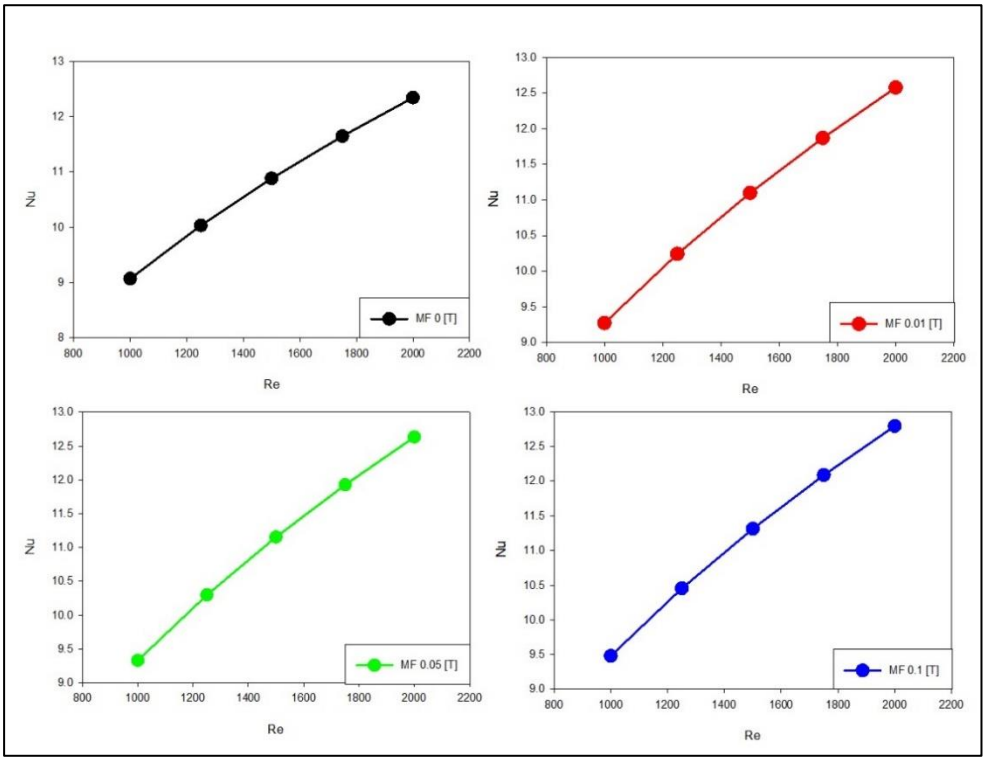

Figure 4. 43 Variation of Nu number with Re number for different MF intensities.

The ferronanofluid with *0.5 % NPVF* under the magnetic field effect at the third location of the magnetic field shows the same behavior for pressure drop, where the pressure drop increases with the increment of the magnetic field strength and in the same time it's proportional with Reynolds number, as the increase in Reynolds number means increase in the velocity therefore reflecting on the pressure drop. Figure 4.44. shows that the pressure drop marked the highest at *45 Pa* for *Re 2000*.

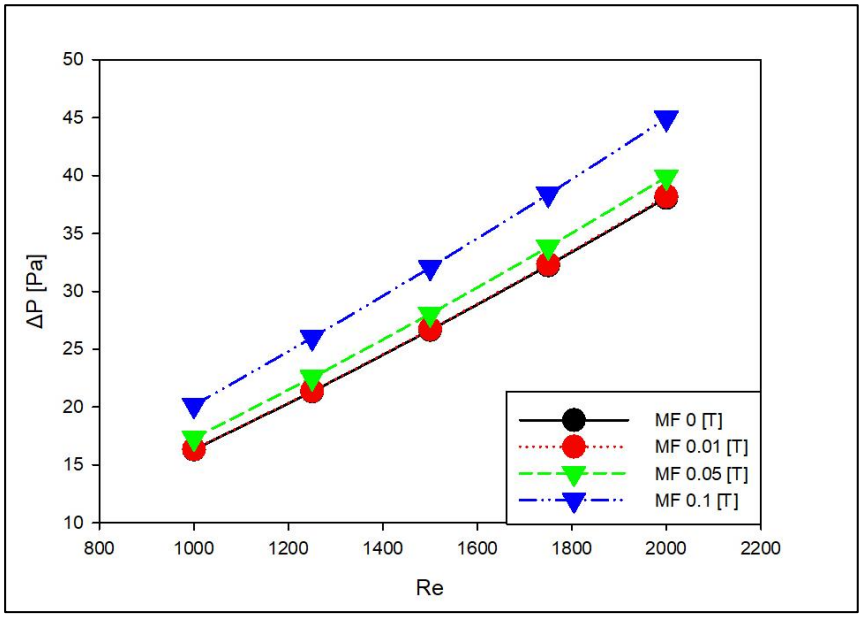

Figure 4. 44 Variation of Pressure drop with Re number for different MF intensities.

Figure 4.45 presents findings regarding the relationship between the Darcy friction factor and Reynolds number in the presence of a magnetic field. The results indicate that the magnetic field has a significant impact on this relationship. At a magnetic field strength of *0.1 T*, a noticeable increase in the Darcy friction factor is observed. This can be attributed to the enhanced attraction experienced by the ferroparticles, causing them to form chains near the inner wall of the pipe. These chains contribute to a higher level of friction, resulting in an elevated Darcy friction factor. Conversely, when the magnetic field strength is reduced to *0.01 T*, the behavior of the Darcy friction factor resembles that observed in the absence of a magnetic field. In this case, the presence of the magnetic field does not significantly alter the frictional characteristics of the system.

These findings highlight the influence of magnetic fields on the flow behavior of ferronanofluid. The formation of chains under higher magnetic field strengths leads to increased friction, while lower magnetic field strengths exhibit behavior similar to non-magnetic systems.

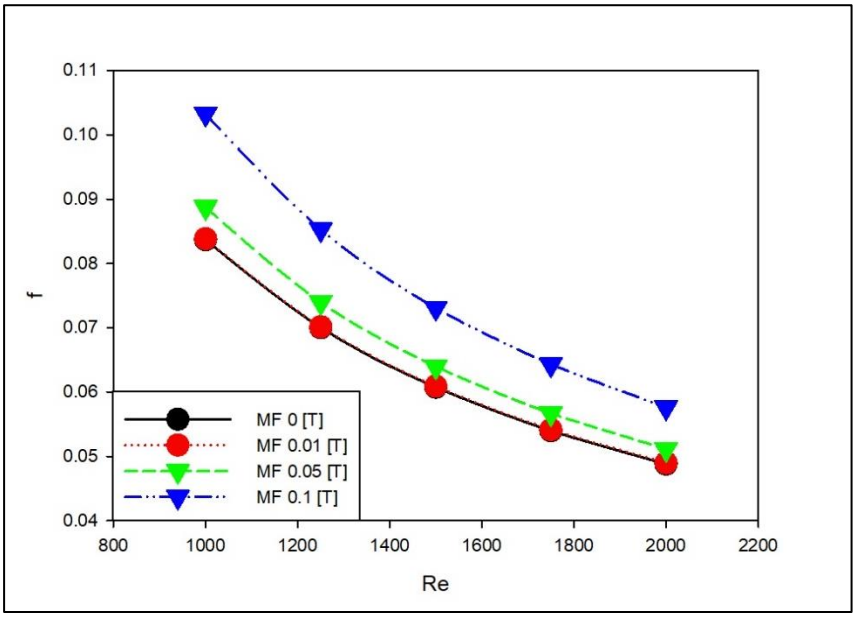

Figure 4. 45 Variation of Darcy friction with Re number for different MF intensities.

Figure 4.46 depicts the alteration of the performance evaluation criteria (*PEC*) as a function of Reynolds number influenced by the presence of a magnetic field. The observed *PEC* values exhibit notable variations when compared to other scenarios. Specifically, the *PEC* values reach their highest levels for the case with a magnetic field strength of *0.01 T*, while the lowest values are recorded for the case with a magnetic field strength of *0.1 T*. Moreover, the *PEC* values for the scenario with a magnetic field strength of *0.05 T* are superior to those for magnetic field 0.1 T. Notably, a negative correlation is observed between Reynolds number and *PEC* for the case with a magnetic field strength of *0.01 T*. while 0.1 T show more stability.

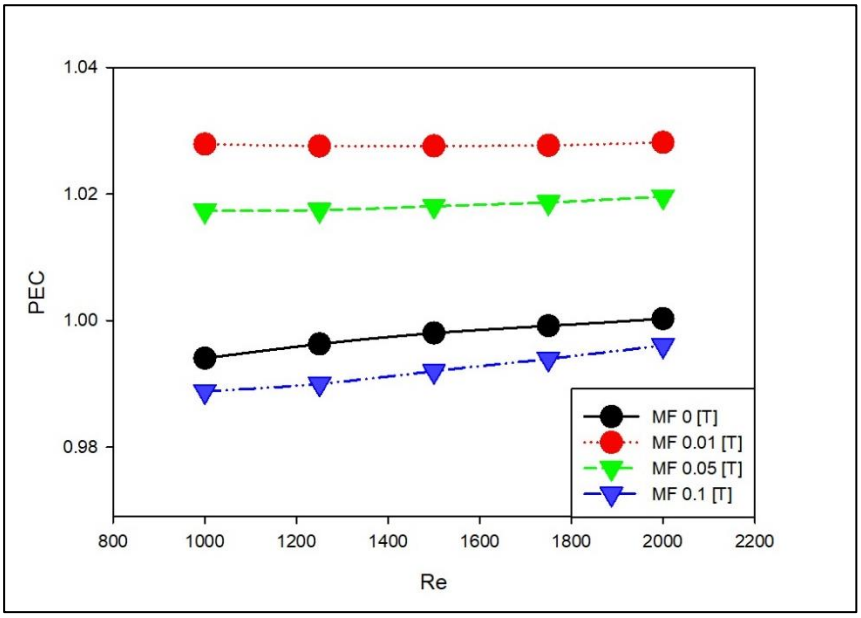

Figure 4. 46 Variation of PEC with Re number for different MF intensities.

Case 3 with 1% NPVF

A computational analysis was performed to investigate the behavior of a ferronanofluid composed of *1% NPVF* Nanoparticle Volume Fraction flowing through a pipe with a uniformly textured surface. The study aimed to examine the influence of different magnetic field strengths on the ferronanofluid's characteristics. In order to assess the impact of the magnetic field's placement, the magnetic field was shifted to the third location along the pipe. This allowed for the examination of the magnetic field's influence on the flow characteristics of the ferronanofluid at a specific location within the system. By studying the behavior of the ferronanofluid under varying magnetic field strengths and at a specific location within the pipe, the analysis sought to provide insights into the dynamic interactions between the magnetic field and the ferronanofluid, shedding light on their combined effect on the fluid flow behavior.

This investigation involved raising the nanoparticle volume fraction (*NPVF*) to *1%*, as depicted in Figure 4.47 the figure illustrates the variations in the Nusselt number as a function of the Reynolds number, considering different magnetic field strengths. The observed behavior of the Nusselt number aligns with the findings from the previous case involving the second magnetic field location. Under a magnetic field strength of *0.01 T*,

the Nusselt number shows improvement, reaching a value close to that obtained for *0.05 T*. However, a significant improvement is observed at a magnetic field strength of *0.1 T*, where the Nusselt number attains its highest value of *12.8* for a Reynolds number of *2000*. Importantly, it is worth noting that the relationship between the Nusselt number and Reynolds number is directly proportional.

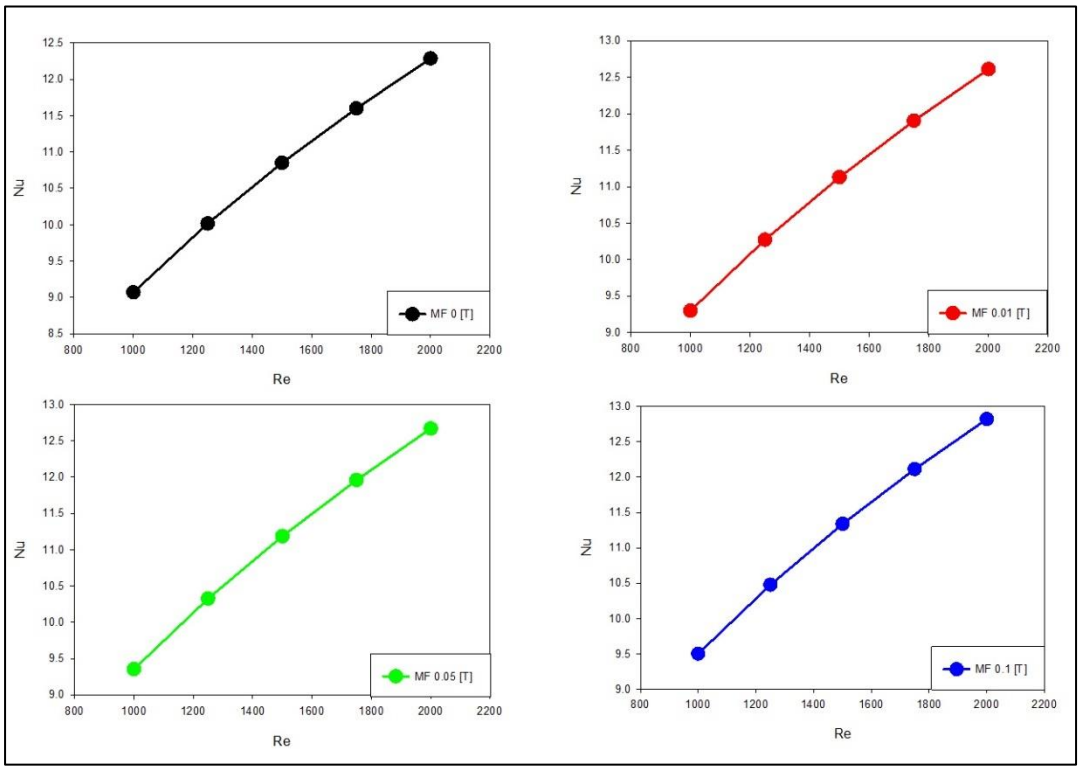

Figure 4. 47 Variation of Nu number with Re number for different MF intensities.

Figure 4.48 illustrates the anticipated relationship between magnetic field intensity and the associated pressure drop. As the magnetic field intensity increases, a corresponding elevation in the pressure drop is observed. Notably, the highest-pressure drop occurs at an intensity of *0.1 T*, specifically at a Reynolds number of *2000*. This finding underscores the influence of magnetic field intensity on the pressure drop phenomenon, with the highest magnitude occurring at the specified conditions.

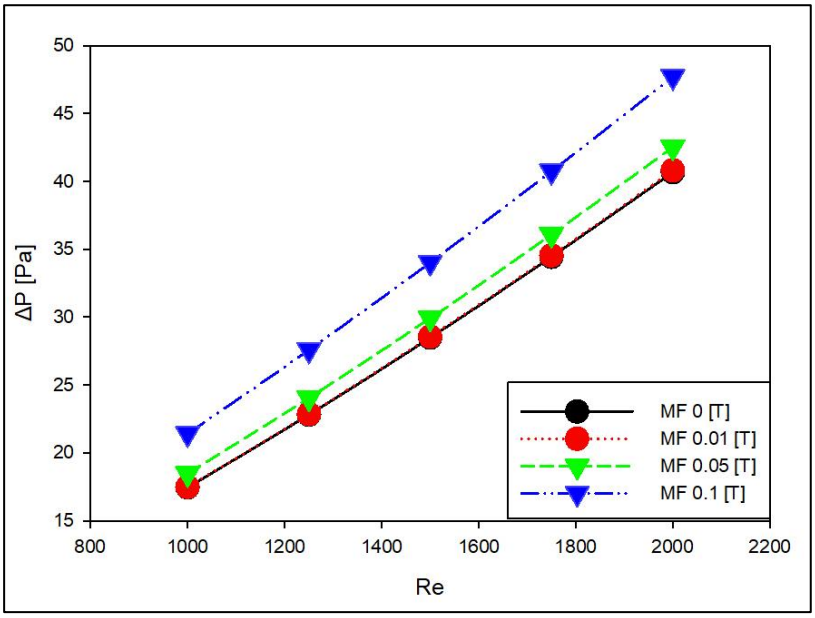

Figure 4. 48 Variation of Pressure drop with Re number for different MF intensities.

The relationship between the Darcy friction factor and Reynolds number is depicted in Figure 4.49, focusing on a nanoparticle volume fraction (*NPVF*) of *1%*. The aim is to examine the behavior under varying magnetic field strengths. Consistent with previous findings, the Darcy friction factor demonstrates a proportional relationship with the intensity of the magnetic field.

Remarkably, the lowest value of the Darcy friction factor is recorded at a magnetic field strength of *0.01 T*, which closely resembles the absence of a magnetic field. This suggests that the presence of a weak magnetic field has minimal influence on the frictional characteristics. In contrast, the highest Darcy friction factor is observed at a magnetic field strength of *0.1 T*, indicating a significant impact on the fluid flow behavior.

These results highlight the significant role played by magnetic field strength in modifying the Darcy friction factor. The data indicate that a higher magnetic field intensity results in an increase in the frictional resistance experienced by the fluid, while lower field strengths have a negligible effect, resembling the behavior observed in the absence of a magnetic field.

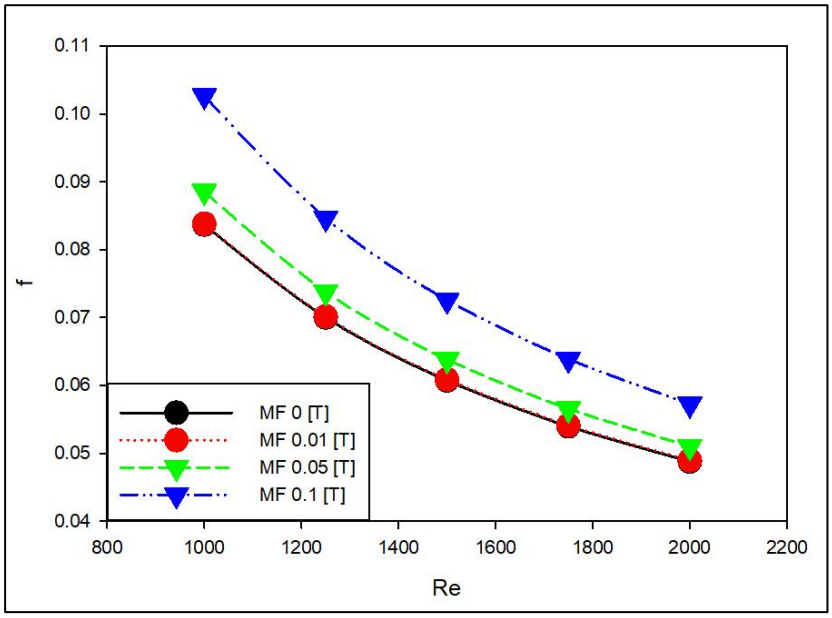

Figure 4. 49 Variation of Darcy friction with Re number for different MF intensities.

The relationship between the Performance Evaluation Criteria (*PEC*) and Reynolds number was investigated, considering various magnetic field strengths, as illustrated in Figure 4.50. Notably, the *PEC* exhibited different performance levels depending on the magnetic field strength. At a magnetic field strength of *0.1 T*, the *PEC* displayed the poorest performance, indicating suboptimal outcomes. Conversely, the absence of a magnetic field resulted in improved performance.

Furthermore, a notable improvement was observed at a magnetic field strength of *0.05 T*; however, this improvement remained inferior to the results obtained at a magnetic field strength of *0.01 T*. The most favorable *PEC* value, approximately *1.03*, was achieved at a Reynolds number of *2000* when the magnetic field strength was *0.01 T*. These findings emphasize the influence of magnetic field strength on the performance of the system, with the magnetic field of *0.01 T* demonstrating the most favorable outcomes in terms of the *PEC*.

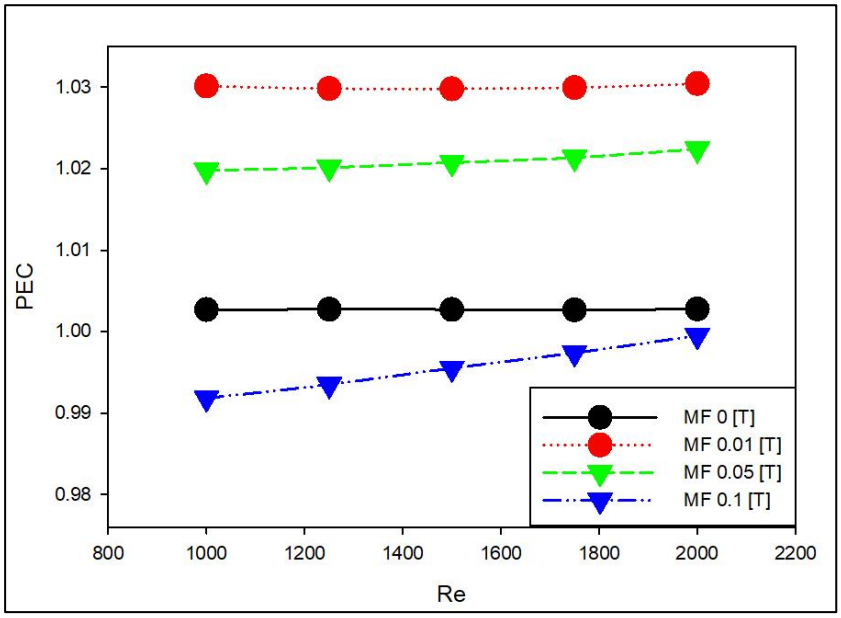

Figure 4. 50 Variation of PEC with Re number for different MF intensities.

Case 3 with 2% NPVF

At the third location of the magnetic field, thermal characteristics were calculated for nanoparticle volume fraction (*NPVF*) concentrations of *2 %*. The boundary conditions employed in this analysis were consistent with previous cases. The primary objective of this phase was to investigate the effects of increasing nanoparticle concentration and determine the optimal formulation for the system under study.

In Figure 4.51, the relationship between the Nusselt number and Reynolds number is presented, taking into account various levels of magnetic field intensity. Notably, in this investigation, modifications in both the source location and the nanoparticle volume fraction contribute to observed improvements. The Nusselt number values obtained under the influence of the magnetic field exceed those obtained in previous cases, indicating a positive correlation between the Nusselt number and the intensity of the magnetic field. Furthermore, the relationship between the Nusselt number and the Reynolds number also demonstrates a proportional nature. It is noteworthy that the highest Nusselt number values, reaching *12.92*, are observed at a magnetic field strength of *0.1 T*.

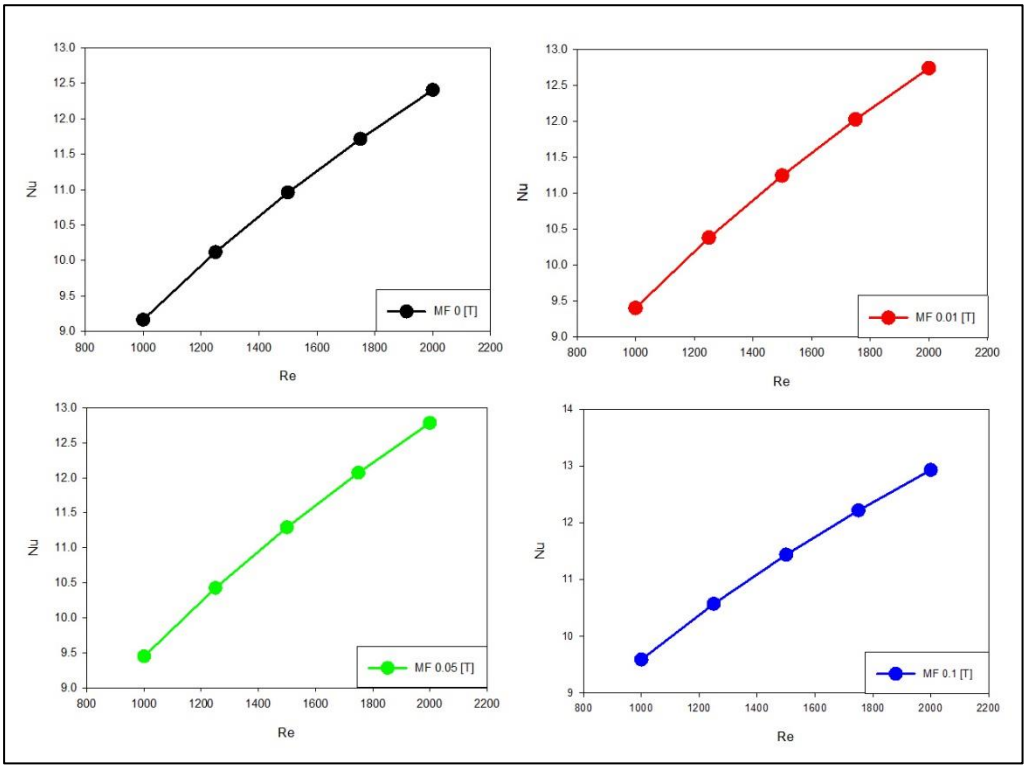

Figure 4. 51 Variation of Nu number with Re number for different MF intensities.

The outcomes of the pressure drop analysis for a *2% NPVF* concentration are depicted in Figure 4.52. Notably, a magnetic field intensity of *0.01 T* exhibited negligible influence on the pressure drop. However, as the magnetic field strength increased, a corresponding increase in the pressure drop was observed. Remarkably, the highest recorded pressure drop of *55.5 Pa* occurred at a Reynolds number of *2000*. These findings suggest that an augmentation in the magnetic field intensity leads to an elevation in the pressure drop experienced within the system.

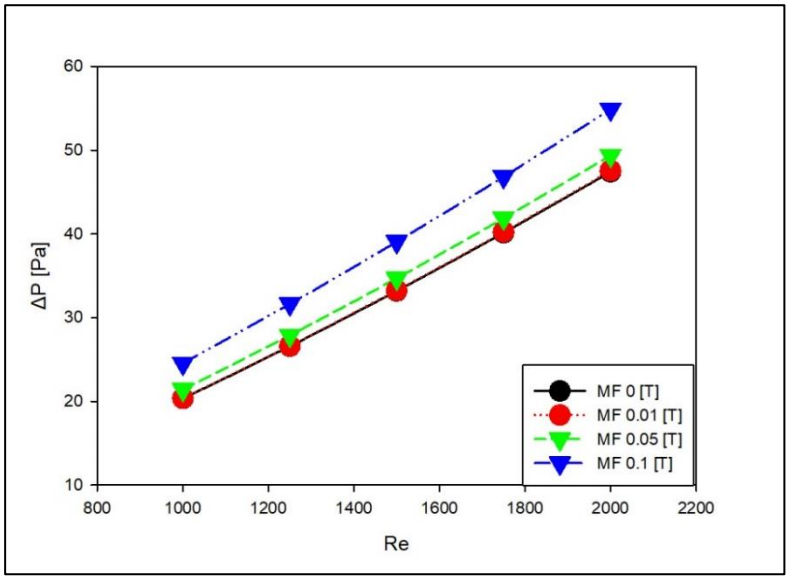

Figure 4. 52 Variation of Pressure drop with Re number for different MF intensities.

In Figure 4.53, the interplay between the Darcy friction factor and Reynolds number is illustrated across various magnetic field intensities. In alignment with earlier findings, the Darcy friction factor demonstrated a consistent trend. The lowest magnetic field intensity corresponded to the lowest Darcy friction, while an intensity of *0.1 T* yielded a significant increase in the friction factor. These observations further establish the direct impact of magnetic field intensity on the Darcy friction, with higher intensities intensifying the flow resistance within the system.

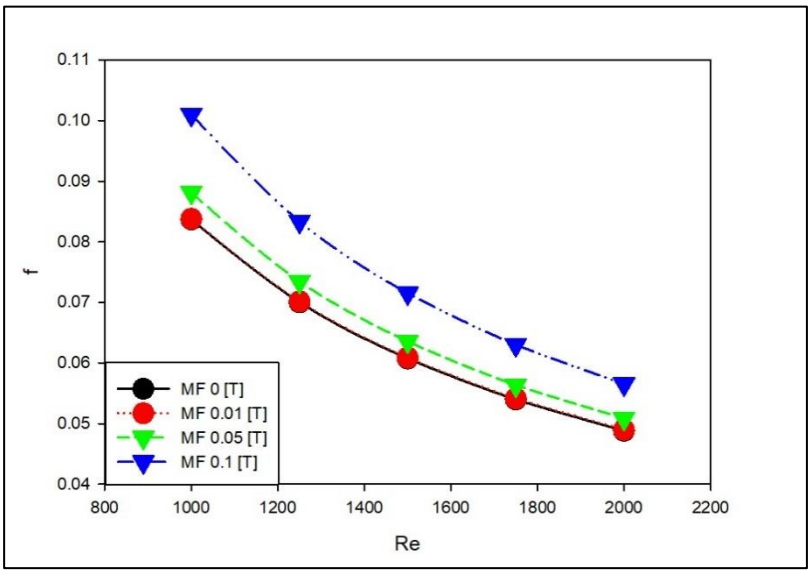

Figure 4. 53 Variation of Darcy friction with Re number for different MF intensities.

The performance evaluation criteria (*PEC*) were assessed in relation to the Reynolds number for different magnetic field strengths. Figure 4.54 presents the findings, highlighting the changes in *PEC* compared to previous cases and the influence of the magnetic field location. Notably, the magnetic field intensity of *0.01 T* exhibited the highest *PEC* values, followed by *0.05 T*. It is important to note that the relationship between *PEC* and Reynolds number is not proportional by looking the trend. These results emphasize the intricate relationship between magnetic field strength, Reynolds number, and the resulting *PEC* values in the evaluated system.

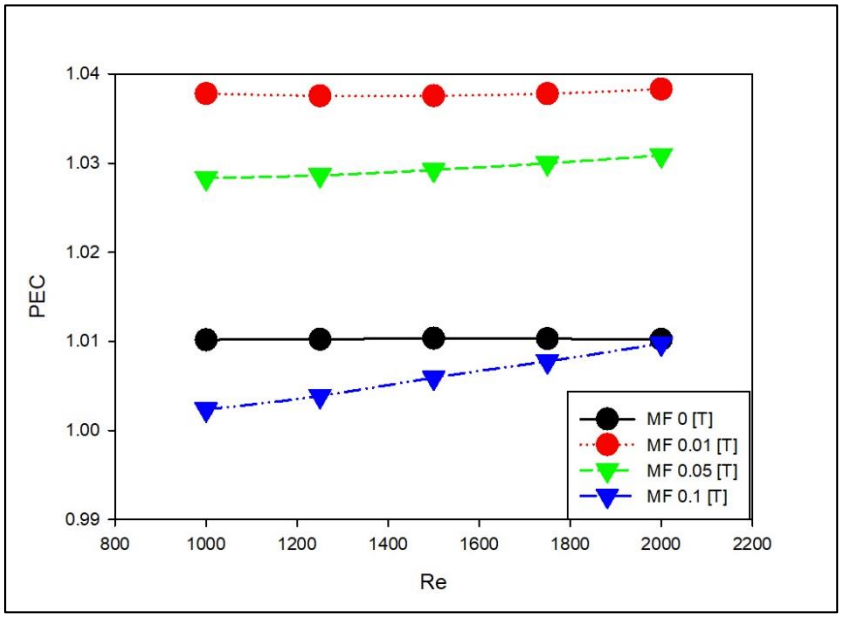

Figure 4. 54 Variation of PEC with Re number for different MF intensities.

The Surface Nusselt number distribution has been generated from ANSYS for 3 different locations,1, 2, and 3 for ferronanofluid with 2 % NPVF at Reynolds number 2000 under the effect magnetic field 0.1 T. The contours compared as illustrated in Figure 4.55.

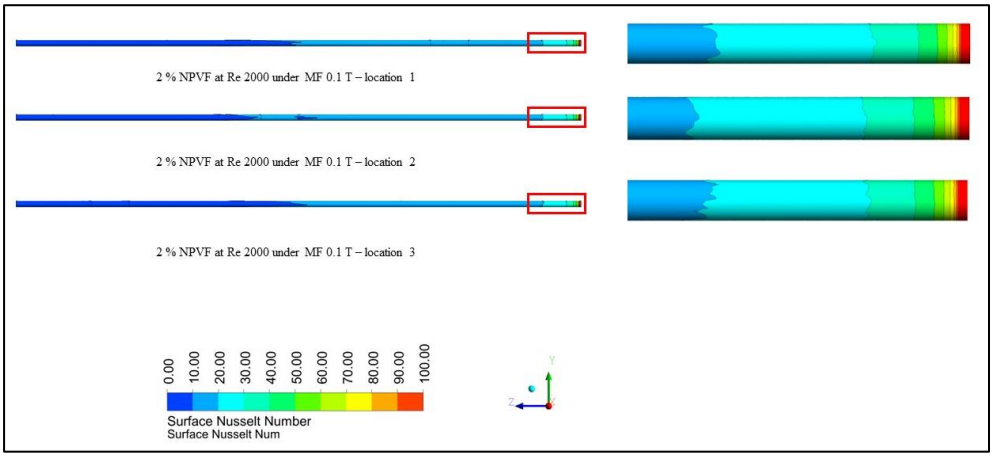

Figure 4. 55. Variation of surface Nusslet number distribution for different locations.

The surface temperature distribution contours have been compared for 3 different locations in Figure 4.56 for the ferronanofluid flow at Reynolds number 2000, with 2 % NPVF, under the impact of magnetic field of magnitude 0.1 T.

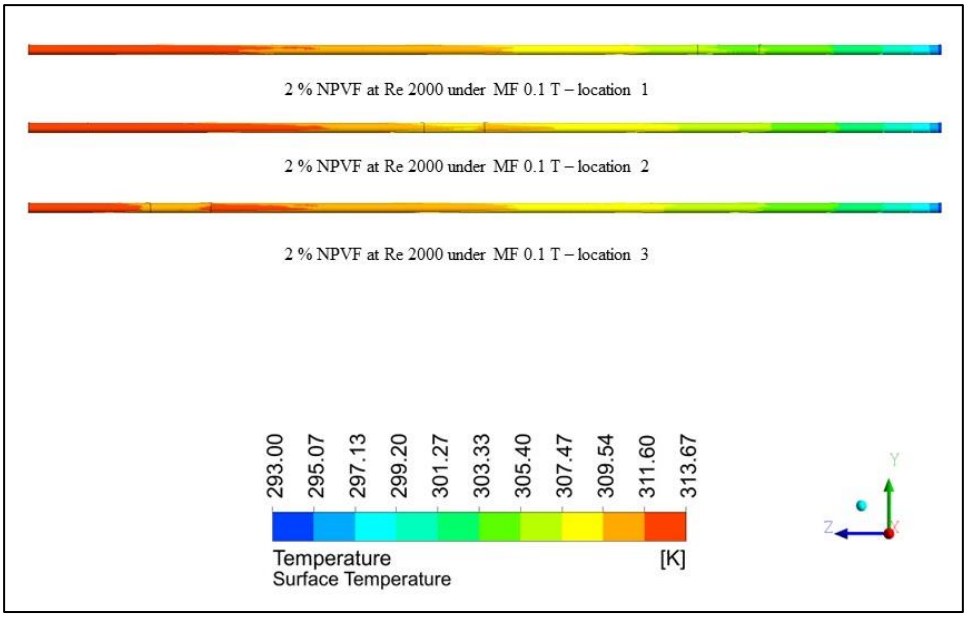

Figure 4. 56 Variation of Surface temperature distribution for different MF locations.

The effect of the magnetic field location on the velocity distribution has also been compared for 3 different locations in Figure 4.57 where the ferronanofluid 2% NPVF flow at 2000 and the magnetic field strength is 0.1 T.

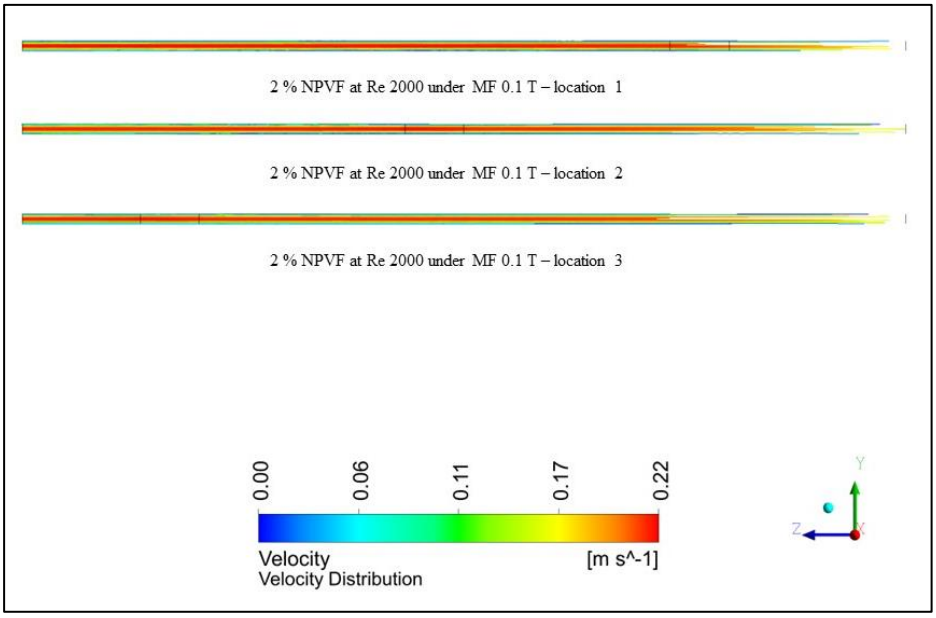

Figure 4. 57 Variation of velocity distribution for different MF locations.

4.4. Comparing the Cases

In the preceding section, a comprehensive analysis was conducted for all three cases, considering various parameters such as the Nusselt number, *PEC*, pressure drop, and Darcy friction factor. Upon examining the results, it becomes evident that the Nusselt number, pressure drop, and Darcy friction factor exhibit consistent trends across all cases, irrespective of differences in *NPVF*, the location of the magnetic field, or variations in magnetic field intensity. Considering the significance of evaluating the efficiency of the thermal system, the *PEC* emerges as the primary parameter for this purpose.

The *PEC* encompasses multiple factors, including heat transfer effectiveness, pressure drop, and energy consumption. Thus, in the overall comparison of the cases, the focus has primarily been on the *PEC* to determine the optimal scenario. By emphasizing the *PEC*, it becomes possible to evaluate and identify the case that achieves the highest level of thermal performance while considering the trade-offs between heat transfer enhancement and the associated pressure drop and energy consumption.

4.4.1. PEC for Different NPVFs at 1st Location

Figure 4.58 presents a graphical representation of the Performance Evaluation Criteria *(PEC)* as a function of Reynolds number for different nanoparticle volume fraction *(NPVF)* values *(0.5%, 1%, and 2%)* under varying magnetic field intensities. Notably, the PEC achieved its highest values for the *2% NPVF* case. Surprisingly, the absence of a magnetic field yielded the highest *PEC* value. This observation can be attributed to several factors, with the location of the magnetic source being the primary determinant. The specific positioning of the magnetic source can influence the flow characteristics and subsequent heat transfer performance, ultimately impacting the overall efficiency of the system.

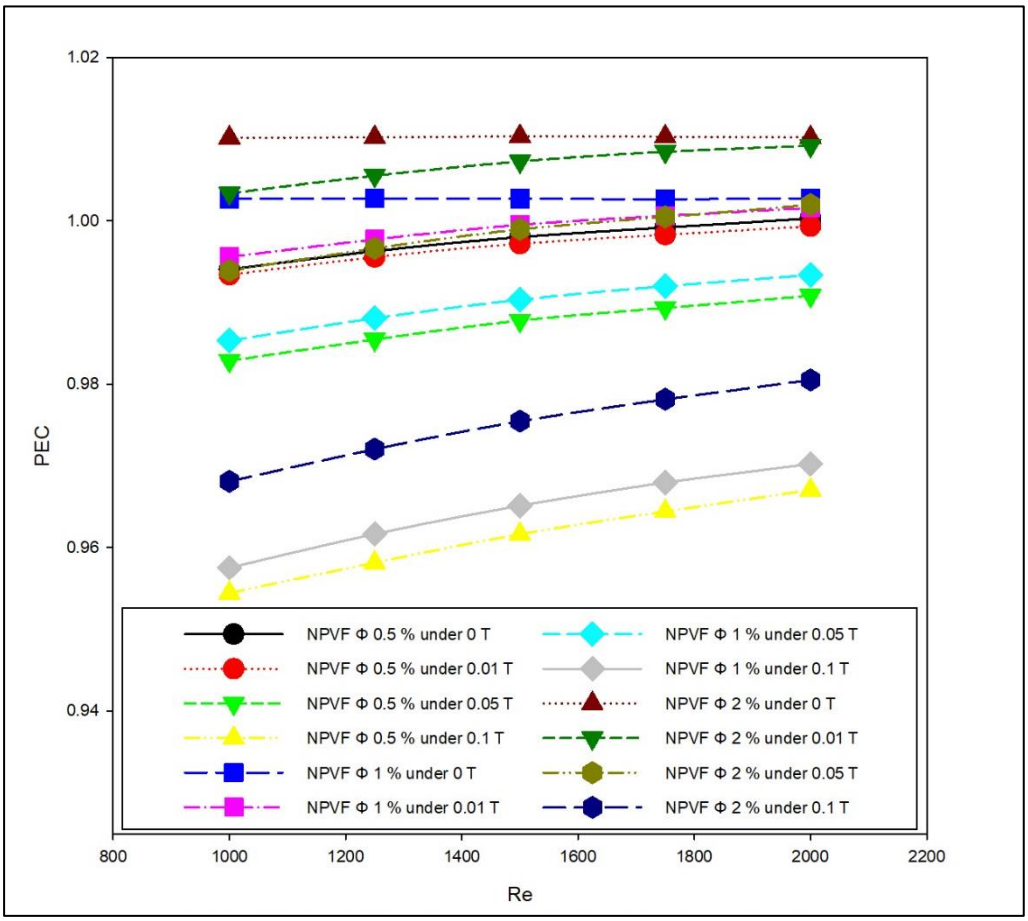

Figure 4.58. Variation of PEC with Re number for various NPVFs.

Table 4.2 provides a comprehensive overview of the Performance Evaluation Criteria *(PEC)* values for different nanoparticle volume fraction *(NPVF)* levels and magnetic field intensities when the magnetic source is positioned in the first location, specifically at coordinates ranging from *300 mm* to *400 mm*. The table highlights the top *5 PEC* values achieved under these conditions, emphasizing the cases that exhibit superior thermal performance, from the table we can notice that the best *PEC* value has been marked for ferronanofluids of *2 % NPVF* under the absence of the magnetic field.

Table 4.2. PEC of various NPVFs and MF intensities at 1st Location.

First Location				
NPVF Φ 0.5%				
Re	*PEC - 0 T*	*PEC - 0.01 T*	*PEC - 0.05 T*	*PEC - 0.1 T*
1000	*0.9940*	*0.9934*	*0.9829*	*0.9544*
1250	*0.9963*	*0.9956*	*0.9855*	*0.9582*
1500	*0.9980*	*0.9972*	*0.9878*	*0.9616*
1750	*0.9992*	*0.9983*	*0.9894*	*0.9644*
2000	*1.0003*	*0.9993*	*0.9908*	*0.9671*
NPVF Φ 1%				
Re	*PEC - 0 T*	*PEC - 0.01 T*	*PEC - 0.05 T*	*PEC - 0.1 T*
1000	*1.0027*	*0.9956*	*0.9853*	*0.9575*
1250	*1.0027*	*0.9977*	*0.9881*	*0.9617*
1500	*1.0027*	*0.9995*	*0.9904*	*0.9651*
1750	*1.0026*	*1.0006*	*0.9920*	*0.9680*
2000	*1.0028*	*1.0016*	*0.9934*	*0.9703*
NPVF Φ 2%				
Re	*PEC - 0 T*	*PEC - 0.01 T*	*PEC - 0.05 T*	*PEC - 0.1 T*
1000	*1.0102*	*1.0034*	*0.9939*	*0.9681*
1250	*1.0102*	*1.0055*	*0.9966*	*0.9721*
1500	*1.0103*	*1.0073*	*0.9990*	*0.9755*
1750	*1.0103*	*1.0085*	*1.0005*	*0.9782*
2000	*1.0102*	*1.0092*	*1.0020*	*0.9805*

4.4.2. PEC for Different NPVFs at 2nd Location

Figure 4.59 displays a visual depiction of the Performance Evaluation Criteria (PEC) plotted against Reynolds number for distinct nanoparticle volume fraction (NPVF) values (0.5%, 1%, and 2%) across a range of magnetic field intensities. Of particular interest is the 2% NPVF case involving Fe_3O_4 nanoparticles in water. This particular case exhibited the highest PEC value, achieving peak performance. Moreover, the optimal PEC value was attained under a magnetic field intensity of 0.01 T. This specific

combination of NPVF and magnetic field intensity yielded significantly superior results compared to the other cases analyzed at the same magnetic source location.

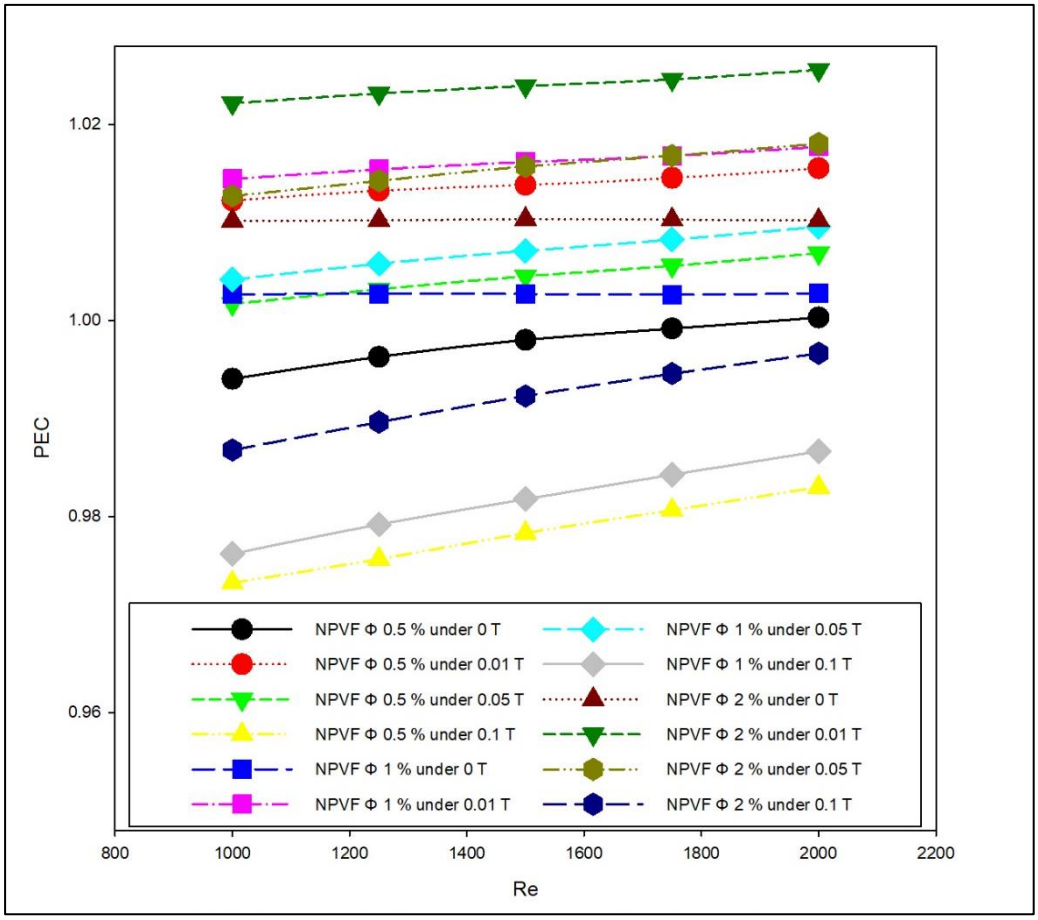

Figure 4. 59 Variation of PEC with Re number for various NPVFs .

Table 4.3 presents a comprehensive summary of the Performance Evaluation Criteria *(PEC)* values corresponding to various levels of nanoparticle volume fraction *(NPVF)* and magnetic field intensities, with the magnetic source positioned in the second location between *750 mm* and *850 mm*. The table showcases the top *5 PEC* values attained under these specific circumstances, drawing attention to the cases that showcase exceptional thermal performance. Notably, upon close examination of the table, it becomes evident that the most favorable *PEC* value is observed for ferronanofluids with a 2% NPVF, specifically under a magnetic field magnitude *0.01 T*. Notably, within the provided table, a *PEC* value of *1.0256* is prominently highlighted in red, corresponding to a Reynolds number of *2000*.

Table 4. 3 PEC of various NPVFs and MF intensities at 2nd Location.

Second Location				
NPVF Φ 0.5%				
Re	*PEC - 0 T*	*PEC - 0.01 T*	*PEC - 0.05 T*	*PEC - 0.1 T*
1000	*0.9940*	*1.0122*	*1.0017*	*0.9732*
1250	*0.9963*	*1.0132*	*1.0032*	*0.9756*
1500	*0.9980*	*1.0138*	*1.0045*	*0.9783*
1750	*0.9992*	*1.0145*	*1.0056*	*0.9806*
2000	*1.0003*	*1.0155*	*1.0069*	*0.9830*
NPVF Φ 1%				
Re	*PEC - 0 T*	*PEC - 0.01 T*	*PEC - 0.05 T*	*PEC - 0.1 T*
1000	*1.0027*	*1.0144*	*1.0042*	*0.9762*
1250	*1.0027*	*1.0154*	*1.0058*	*0.9792*
1500	*1.0027*	*1.0162*	*1.0071*	*0.9818*
1750	*1.0026*	*1.0168*	*1.0083*	*0.9843*
2000	*1.0028*	*1.0177*	*1.0096*	*0.9867*
NPVF Φ 2%				
Re	*PEC - 0 T*	*PEC - 0.01 T*	*PEC - 0.05 T*	*PEC - 0.1 T*
1000	*1.0102*	*1.0222*	*1.0127*	*0.9868*
1250	*1.0102*	*1.0232*	*1.0143*	*0.9896*
1500	*1.0103*	*1.0239*	*1.0157*	*0.9923*
1750	*1.0103*	*1.0246*	*1.0168*	*0.9946*
2000	*1.0102*	*1.0256*	*1.0180*	*0.9967*

4.4.3. PEC for Different NPVFs at 3rd Location

In this particular investigation, the *PEC* has been compared across all cases where the magnetic field is applied from the third location, while keeping all other parameters unchanged from the previous scenario at the second location. It is noteworthy that the highest *PEC* value was once again observed for the *2 % NPVF* case under a magnetic field strength of *0.01 T*, indicating the persistence of its favorable thermal performance. However, it is worth mentioning that the *PEC* value has shown an overall increase compared to the previous scenario. Moreover, the relationship between *PEC* and Reynolds number remains intricate, as observed in Figure 4.60, where the *PEC* value for the *2 % NPVF* case under a magnetic field intensity of *0.01 T* is slightly higher compared to the other cases, thereby providing further evidence to support the findings in this scenario.

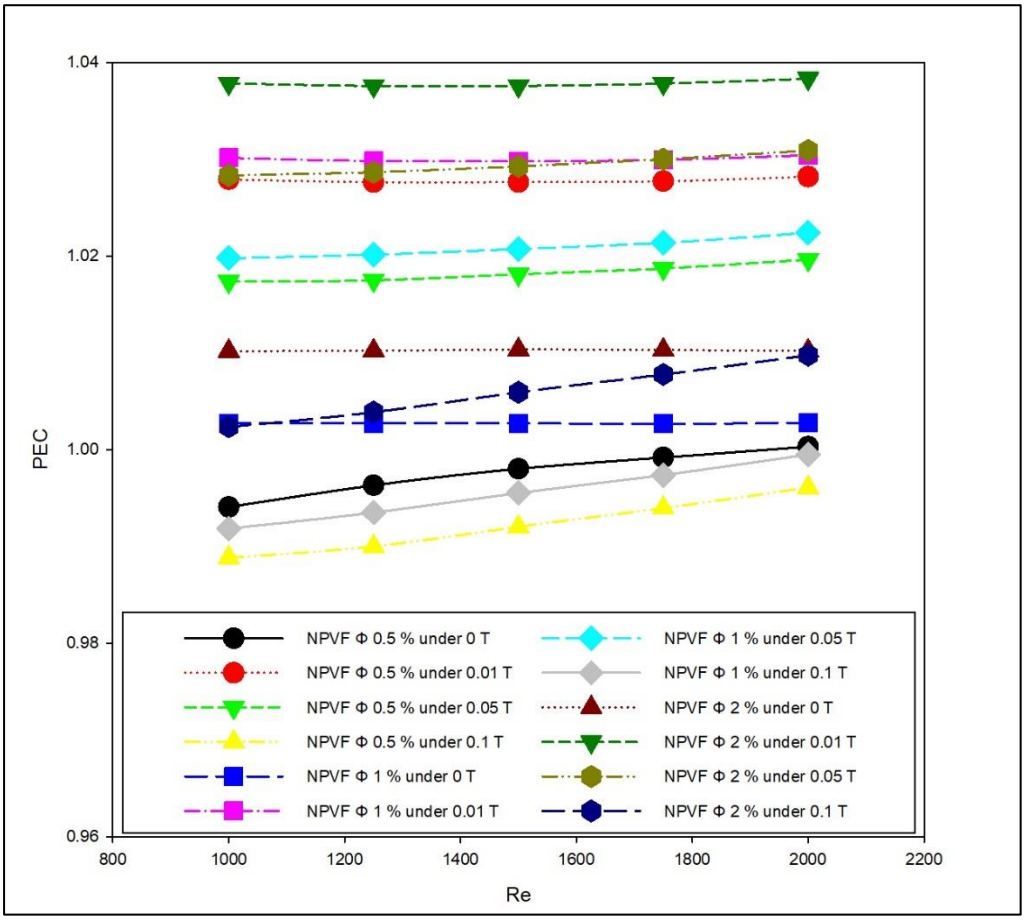

Figure 4. 60 Variation of PEC with Re number for various NPVFs.

Table 4.4 provides a comprehensive overview of the *PEC* values for different *NPVFs* and magnetic field intensities, with the magnetic field positioned in the third location between *1200 mm and 1300 mm*. The table highlights the top *5 PEC* values achieved under these specific conditions, focusing on the cases that exhibit exceptional thermal performance.

A thorough analysis of the table reveals that the most favorable *PEC* value is observed for ferronanofluids with a *2 % NPVF*, particularly when subjected to a magnetic field intensity of *0.01 T*. This finding suggests that the combination of a higher *NPVF* concentration and a moderate magnetic field strength leads to improved thermal performance in the system.

The results underscore the importance of carefully selecting the *NPVF* and magnetic field intensity to optimize the thermal characteristics of the ferronanofluid system.

Table 4. 4 PEC of various NPVFs and MF intensities at 2nd Location.

Third Location				
NPVF Φ 0.5%				
Re	*PEC - 0 T*	*PEC - 0.01 T*	*PEC - 0.05 T*	*PEC - 0.1 T*
1000	*0.9940*	*1.0279*	*1.0174*	*0.9888*
1250	*0.9963*	*1.0276*	*1.0175*	*0.9900*
1500	*0.9980*	*1.0276*	*1.0181*	*0.9920*
1750	*0.9992*	*1.0277*	*1.0187*	*0.9939*
2000	*1.0003*	*1.0282*	*1.0196*	*0.9961*
NPVF Φ 1%				
Re	*PEC - 0 T*	*PEC - 0.01 T*	*PEC - 0.05 T*	*PEC - 0.1 T*
1000	*1.0027*	*1.0301*	*1.0198*	*0.9918*
1250	*1.0027*	*1.0298*	*1.0201*	*0.9935*
1500	*1.0027*	*1.0298*	*1.0207*	*0.9955*
1750	*1.0026*	*1.0299*	*1.0214*	*0.9974*
2000	*1.0028*	*1.0304*	*1.0224*	*0.9995*
NPVF Φ 2%				
Re	*PEC - 0 T*	*PEC - 0.01 T*	*PEC - 0.05 T*	*PEC - 0.1 T*
1000	*1.0102*	*1.0378*	*1.0283*	*1.0023*
1250	*1.0102*	*1.0376*	*1.0287*	*1.0039*
1500	*1.0103*	*1.0376*	*1.0293*	*1.0059*
1750	*1.0103*	*1.0378*	*1.0300*	*1.0078*
2000	*1.0102*	*1.0383*	*1.0309*	*1.0097*

4.5. The best-case scenario of PEC

Figure 4.61 illustrates a comparative analysis of the *PEC* for the optimal case scenarios obtained by positioning the magnetic field at different locations. The graph reveals that the highest *PEC* values can be achieved when the magnetic field is placed in the third location, specifically at *1200 mm – 1300 mm* from the inlet. Notably, this favorable outcome is observed under a magnetic field magnitude of *0.01 T* for ferronanofluids consisting of *2 % Fe_3O_4/water*. Figure 4.62 shows that the peak performance evaluation criteria value coincides with a Reynolds number of *2000*, further emphasizing the significance of this particular configuration in enhancing the overall thermal performance of the system. The findings emphasize the importance of careful selection of the magnetic field location and magnetic field intensity to optimize the thermal characteristics of the ferronanofluid-based system.

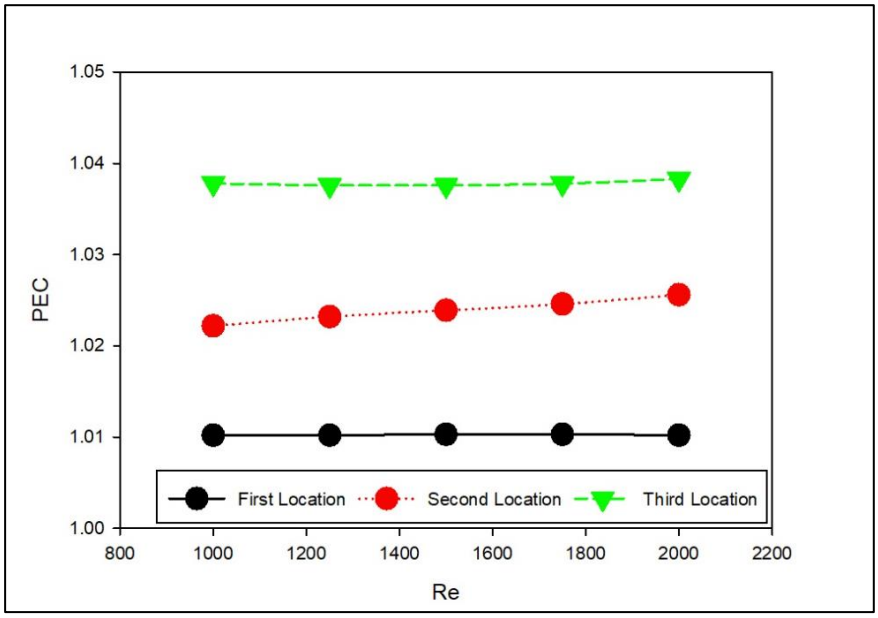

Figure 4. 61 Variation of PEC with Re number for different MF locations.

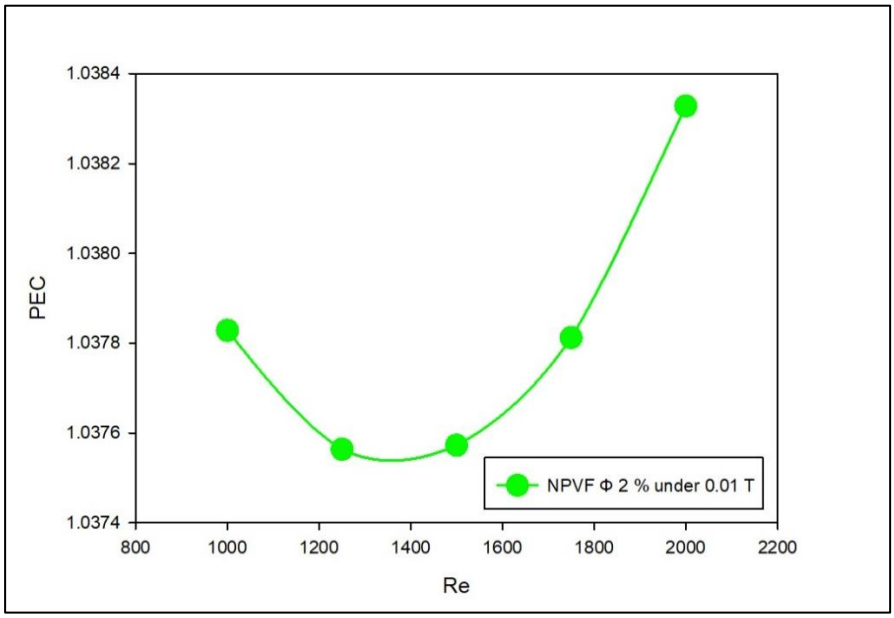

Figure 4. 62 PEC with Re number for 2 % NPVF under 0.01 T MF – 3rd location.

Figure 4.63 shows the surface Nusselt number distribution for the best-case scenario where the ferronanofluid with 2 % NPVF at Reynolds number 2000 and the magnetic field 0.01 T applied at the third location 1300 mm – 1400 mm from the inlet.

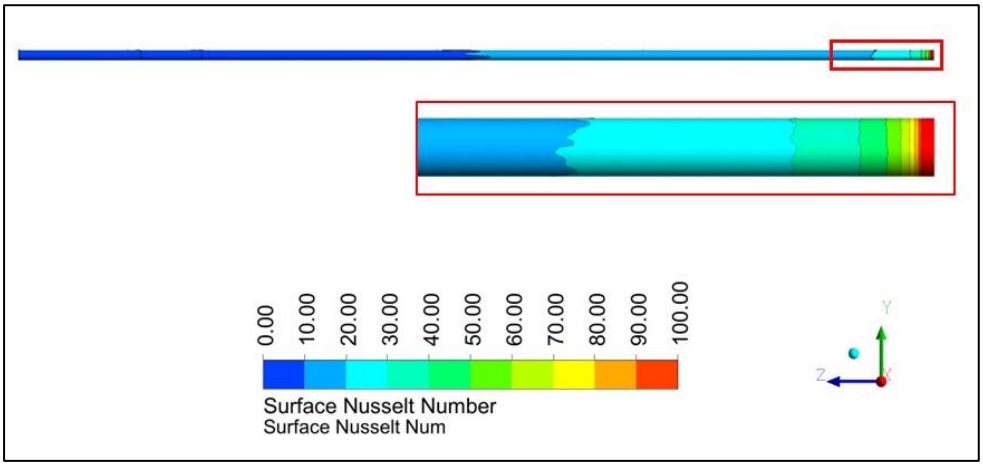

Figure 4. 63 Surface Nusselt number distribution.

The surface temperature distribution contour Figure 4.64 shows the change in the temperature at the location of the magnetic field, where we can see the temperature drop, and Figure 4.65 shows the temperature distribution on the this location of the pipe as well as the outlet.

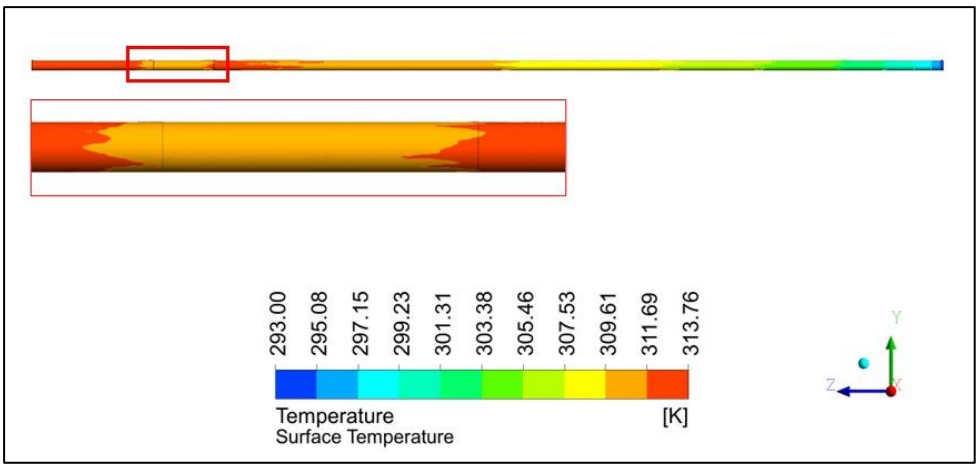

Figure 4. 64 Surface temperature distribution.

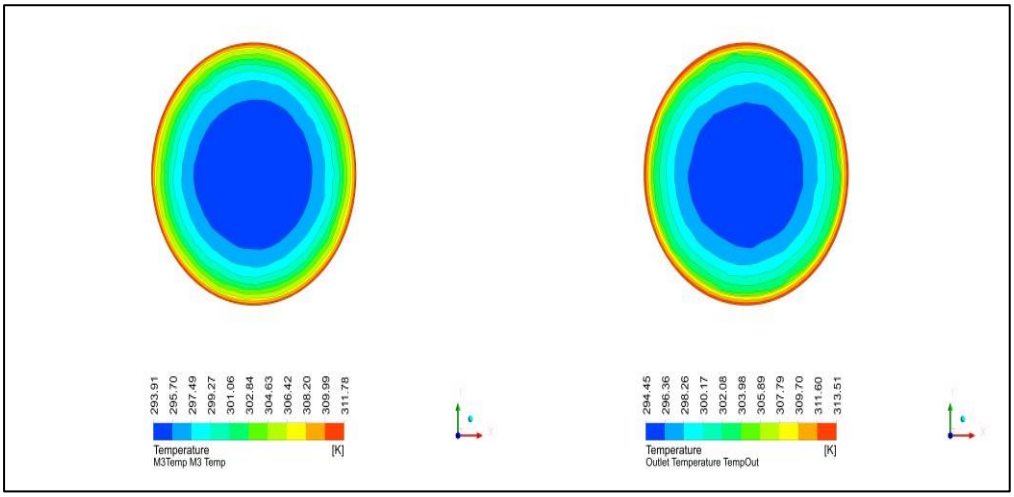

Figure 4. 65 Pipe cross section temperature distribution on the 3rd location and outlet.

The velocity streamline for the ferronanofluid flow has been generated and illustrated in figure 4.66, and Figure 4.67 shows the velocity distribution on the third location and at the outlet.

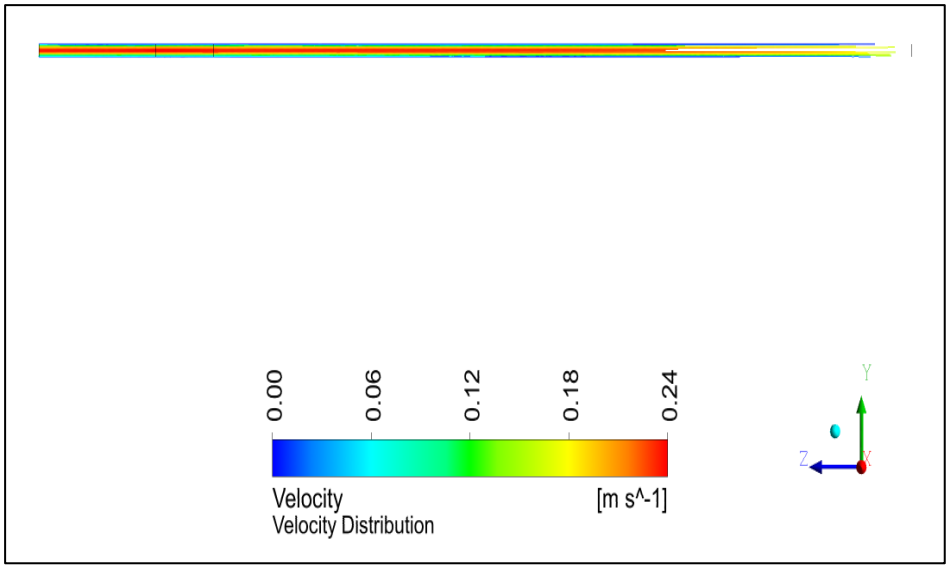

Figure 4. 66 Velocity streamline distribution.

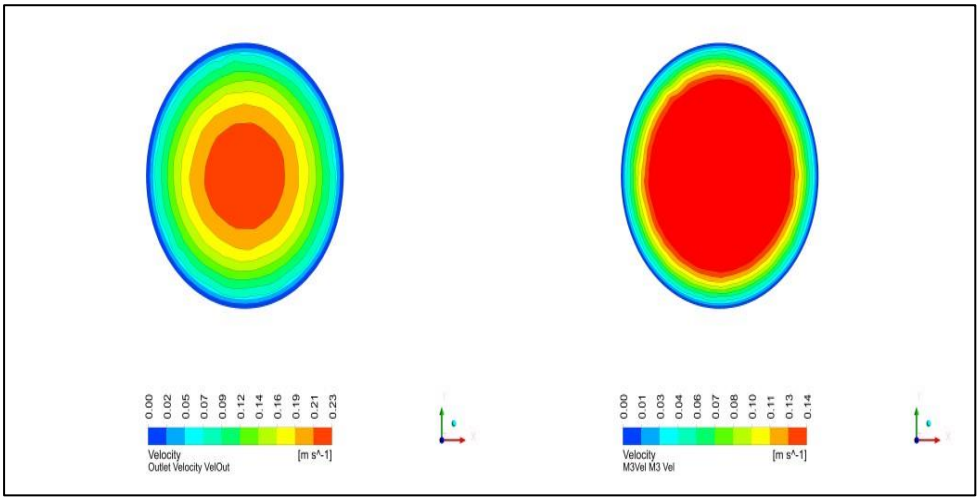

Figure 4. 67 Pipe cross section velocity distribution on the 3rd location and outlet.

PART 5: CONCLUSION

This study aims to conduct a numerical investigation on the flow and heat transfer characteristics of Fe_3O_4/*water* ferronanofluid flow in a smooth pipe, considering different *NPVFs*, magnetic field intensities, and locations on the pipe. The numerical calculations were performed under laminar flow condition, specifically within the Reynolds number range of *1000 to 2000*. The length and diameter of the pipe were kept constant at *1500 mm and 16 mm*, respectively. The *NPVF* values varied from *0.5% to 2.5%*, while the magnetic field intensities of *0.01, 0.05*, and *0.1 T* were thoroughly examined. Through this comprehensive numerical analysis, the objective was to explore the influence of *NPVF*, magnetic field intensity, and location on the pipe on the flow behavior of the ferronanofluid system.

The following are the summarized findings of this study:

- The convective heat transfer coefficient of ferronanofluids exhibits an increasing trend with higher Reynolds numbers, both in the presence and absence of a magnetic field.
- The addition of ferrite particles enhances the Nusselt number of the working fluids, indicating improved heat transfer capabilities.
- Ferronanofluids, particularly when subjected to a magnetic field, experience a significant increase in pressure drop within the thermal system.
- The Darcy friction factor demonstrates a direct relationship with the intensity of the magnetic field.
- The *NPVF* plays a crucial role in the thermal system and has a substantial impact on the PEC, where *Φ 2 %* showed the best performance.
- The positioning of the magnetic field has a notable influence on the *PEC* where the far location from the inlet has shown highest *PEC* value.
- The *PEC* can attain higher values in the absence of a magnetic field.

- *PEC* has marked the highest values in case 3, where the magnetic field located in the third location *(1200 – 1300) mm* and specifically for *2% NPVF* and the peak *PEC* value coincides with a Reynolds number of *2000*.
- Examining the consequences of implementing a magnetic field and its associated energy consumption reveals that incorporating a magnetic field is dispensable when contemplating the overall efficiency.

SUGGESTIONS FOR FUTURE WORK

In this part of the research, I have delineated several potential topics that possess the capacity to enhance the application significantly for future research.

- Consider conducting the study under turbulent flow conditions, as it holds the potential to enhance the Nusselt number and performance evaluation criteria.
- Explore the simultaneous application of a magnetic field in two different locations, which may yield interesting and novel effects on the system.
- Investigate the impact of varying the intensities of an alternating magnetic field, as this could unveil valuable insights into the system's behavior.
- Focus on increasing the *NPVF* of the ferronanofluid, as it could lead to improved heat transfer and enhanced performance.
- Extend the analysis to examine the flow characteristics within a pipe featuring a pattern of regularly spaced dimples, as this unique geometry could potentially offer enhanced heat transfer capabilities.

REFERENCES

1. Mogra, A., Pandey, P. K., and Gupta, K. K., "Enhancement of boiling heat transfer performance using nano coating-a review", ***Journal Of Advanced Research In Fluid Mechanics And Thermal Sciences***, 71 (1): 100–116 (2020).
2. Dewan, A., Mahanta, P., Raju, K. S., and Kumar, P. S., "Review of passive heat transfer augmentation techniques", ***Proceedings Of The Institution Of Mechanical Engineers, Part A: Journal Of Power And Energy***, 218 (7): 509–527 (2004).
3. Internet: Josh Perry, "Industry Developments: Heat Exchangers for Electronics Cooling | Advanced Thermal Solutions", **https://www.qats.com/cms/2017/05/25/industry-developments-heat-exchangers-for-electronics-cooling/** (2023).
4. Bergles, A. E., "Recent developments in enhanced heat transfer", ***Heat And Mass Transfer***, 47 (8): 1001–1008 (2011).
5. Ibrahim, N. I., Al-Sulaiman, F. A., Rahman, S., Yilbas, B. S., and Sahin, A. Z., "Heat transfer enhancement of phase change materials for thermal energy storage applications: A critical review", ***Renewable And Sustainable Energy Reviews***, 74: 26–50 (2017).
6. Lee, S., Choi, S.-S., Li and, S., and Eastman, J. A., "Measuring thermal conductivity of fluids containing oxide nanoparticles", (1999).
7. Saidur, R., Leong, K. Y., and Mohammed, H. A., "A review on applications and challenges of nanofluids", ***Renewable And Sustainable Energy Reviews***, 15 (3): 1646–1668 (2011).
8. Imran, M., Chaudhary, A. A., Ahmed, S., Alam, M. M., Khan, A., Zouli, N., Hakami, J., Rudayni, H. A., and Khan, S.-U.-D., "Iron oxide nanoparticle-based ferro-nanofluids for advanced technological applications", ***Molecules***, 27 (22): 7931 (2022).
9. Wong, K. V and De Leon, O., "Applications of nanofluids: current and future", ***Advances In Mechanical Engineering***, 2: 519659 (2010).

10. Yu, W., France, D. M., Routbort, J. L., and Choi, S. U. S., "Review and comparison of nanofluid thermal conductivity and heat transfer enhancements", ***Heat Transfer Engineering***, 29 (5): 432–460 (2008).
11. Kim, S. J., Bang, I. C., Buongiorno, J., and Hu, L. W., "Study of pool boiling and critical heat flux enhancement in nanofluids", ***Bulletin Of The Polish Academy Of Sciences: Technical Sciences***, 55 (2): (2007).
12. Kim, S. J., Bang, I. C., Buongiorno, J., and Hu, L. W., "Surface wettability change during pool boiling of nanofluids and its effect on critical heat flux", ***International Journal Of Heat And Mass Transfer***, 50 (19–20): 4105–4116 (2007).
13. Donzelli, G., Cerbino, R., and Vailati, A., "Bistable heat transfer in a nanofluid", ***Physical Review Letters***, 102 (10): 104503 (2009).
14. Tester, J. W., Anderson, B. J., Batchelor, A. S., Blackwell, D. D., DiPippo, R., Drake, E. M., Garnish, J., Livesay, B., Moore, M. C., and Nichols, K., "The future of geothermal energy", ***Massachusetts Institute Of Technology***, 358: (2006).
15. Ma, H. B., Wilson, C., Borgmeyer, B., Park, K., Yu, Q., Choi, S. U. S., and Tirumala, M., "Effect of nanofluid on the heat transport capability in an oscillating heat pipe", ***Applied Physics Letters***, 88 (14): 143116 (2006).
16. Vafaei, S., Borca-Tasciuc, T., Podowski, M. Z., Purkayastha, A., Ramanath, G., and Ajayan, P. M., "Effect of nanoparticles on sessile droplet contact angle", ***Nanotechnology***, 17 (10): 2523 (2006).
17. Singh, D., Toutbort, J., and Chen, G., "Heavy vehicle systems optimization merit review and peer evaluation", ***Annual Report, Argonne National Laboratory***, 23: 405–411 (2006).
18. Kao, M. J., Lo, C. H., Tsung, T. T., Wu, Y. Y., Jwo, C. S., and Lin, H. M., "Copper-oxide brake nanofluid manufactured using arc-submerged nanoparticle synthesis system", ***Journal Of Alloys And Compounds***, 434–435 (SPEC. ISS.): 672–674 (2007).
19. Sarkar, J., Ghosh, P., and Adil, A., "A review on hybrid nanofluids: recent research, development and applications", ***Renewable And Sustainable Energy Reviews***, 43: 164–177 (2015).

20. Choi, S. U. S. and Eastman, J. A., "Enhancing thermal conductivity of fluids with nanoparticles", ***Argonne National Lab.(ANL), Argonne, IL (United States)***, (1995).
21. Kumar, D. H., Patel, H. E., Kumar, V. R. R., Sundararajan, T., Pradeep, T., and Das, S. K., "Model for heat conduction in nanofluids", ***Physical Review Letters***, 93 (14): 144301 (2004).
22. Xuan, Y. and Li, Q., "Heat transfer enhancement of nanofluids", ***International Journal Of Heat And Fluid Flow***, 21 (1): 58–64 (2000).
23. Hong, K. S., Hong, T.-K., and Yang, H.-S., "Thermal conductivity of Fe nanofluids depending on the cluster size of nanoparticles", ***Applied Physics Letters***, 88 (3): 031901 (2006).
24. Eastman, J. A., Choi, S. U. S., Li, S., Yu, W., and Thompson, L. J., "Anomalously increased effective thermal conductivities of ethylene glycol-based nanofluids containing copper nanoparticles", ***Applied Physics Letters***, 78 (6): 718–720 (2001).
25. Berger, P., Adelman, N. B., Beckman, K. J., Campbell, D. J., Ellis, A. B., and Lisensky, G. C., "Preparation and Properties of an Aqueous Ferrofluid", ***Journal Of Chemical Education***, 76 (7): 943 (1999).
26. Gavili, A., Zabihi, F., Isfahani, T. D., and Sabbaghzadeh, J., "The thermal conductivity of water base ferrofluids under magnetic field", ***Experimental Thermal And Fluid Science***, 41: 94–98 (2012).
27. Gavili, A., Lajvardi, M., and Sabbaghzadeh, J., "The effect of magnetic field gradient on ferrofluids heat transfer in a two-dimensional enclosure", ***Journal Of Computational And Theoretical Nanoscience***, 7 (8): 1425–1435 (2010).
28. Rosensweig, R. E., "Ferrohydrodynamics", ***Courier Corporation***, (2013).
29. Gubin, S. P., Koksharov, Y. A., Khomutov, G. B., and Yurkov, G. Y., "Magnetic nanoparticles: preparation, structure and properties", ***Russian Chemical Reviews***, 74 (6): 489 (2005).
30. Li, Q., Xuan, Y., and Wang, J., "Experimental investigations on transport properties of magnetic fluids", ***Experimental Thermal And Fluid Science***, 30 (2): 109–116 (2005).

31. Popplewell, J., Al-Qenaie, A., Charles, S. W., Moskowitz, R., and Raj, K., "Thermal conductivity measurements on ferrofluids", ***Colloid And Polymer Science***, 260: 333–338 (1982).
32. Hong, T.-K., Yang, H.-S., and Choi, C. J., "Study of the enhanced thermal conductivity of Fe nanofluids", ***Journal Of Applied Physics***, 97 (6): 064311 (2005).
33. Zhu, H., Zhang, C., Liu, S., Tang, Y., and Yin, Y., "Effects of nanoparticle clustering and alignment on thermal conductivities of Fe 3 O 4 aqueous nanofluids", ***Applied Physics Letters***, 89 (2): 023123 (2006).
34. Abareshi, M., Goharshadi, E. K., Zebarjad, S. M., Fadafan, H. K., and Youssefi, A., "Fabrication, characterization and measurement of thermal conductivity of Fe3O4 nanofluids", ***Journal Of Magnetism And Magnetic Materials***, 322 (24): 3895–3901 (2010).
35. Philip, J., Shima, P. D., and Raj, B., "Enhancement of thermal conductivity in magnetite based nanofluid due to chainlike structures", ***Applied Physics Letters***, 91 (20): 203108 (2007).
36. Mei, S., Qi, C., Liu, M., Fan, F., and Liang, L., "Effects of paralleled magnetic field on thermo-hydraulic performances of Fe3O4-water nanofluids in a circular tube", ***International Journal Of Heat And Mass Transfer***, 134: 707–721 (2019).
37. Suresh, S., Venkitaraj, K. P., Selvakumar, P., and Chandrasekar, M., "Effect of Al2O3–Cu/water hybrid nanofluid in heat transfer", ***Experimental Thermal And Fluid Science***, 38: 54–60 (2012).
38. Sheikholeslami, M., Mehryan, S. A. M., Shafee, A., and Sheremet, M. A., "Variable magnetic forces impact on magnetizable hybrid nanofluid heat transfer through a circular cavity", ***Journal Of Molecular Liquids***, 277: 388–396 (2019).
39. Tekir, M., Taskesen, E., Gedik, E., Arslan, K., and Aksu, B., "Effect of constant magnetic field on Fe3O4-Cu/water hybrid nanofluid flow in a circular pipe", ***Heat And Mass Transfer/Waerme- Und Stoffuebertragung***, 58 (5): 707–717 (2022).
40. Gürdal, M., Pazarlıoğlu, H. K., Tekir, M., Arslan, K., and Gedik, E., "Numerical investigation on turbulent flow and heat transfer characteristics of ferro-nanofluid flowing in dimpled tube under magnetic field effect", ***Applied Thermal Engineering***, 200: 117655 (2022).

41. Maxwell, J. C., "A Treatise on Electricity and Magnetism", ***Oxford: Clarendon Press***, (1873).
42. Weast, R. C., "Handbook of chemistry and physics: a ready-reference book of chemical and physical data", ***CRC Press***, (1971).
43. Bezaatpour, M. and Rostamzadeh, H., "Heat transfer enhancement of a fin-and-tube compact heat exchanger by employing magnetite ferrofluid flow and an external magnetic field", ***Applied Thermal Engineering***, 164: 114462 (2020).
44. Jafari, A., Tynjälä, T., Mousavi, S. M., and Sarkomaa, P., "Simulation of heat transfer in a ferrofluid using computational fluid dynamics technique", ***International Journal Of Heat And Fluid Flow***, 29 (4): 1197–1202 (2008).
45. Shah, R. K. and London, A. L., "Chapter XVII - Discussion—An Overview for the Designer and the Applied Mathematician", Laminar Flow Forced Convection in Ducts, ***Academic Press***, 385–420 (1978).
46. Incropera, F. P., DeWitt, D. P., Bergman, T. L., and Lavine, A. S., .
47. Wei, H., Moria, H., Nisar, K. S., Ghandour, R., Issakhov, A., Sun, Y.-L., Kaood, A., and Youshanlouei, M. M., "Effect of volume fraction and size of Al2O3 nanoparticles in thermal, frictional and economic performance of circumferential corrugated helical tube", ***Case Studies In Thermal Engineering***, 25: 100948 (2021).
48. Jiji, L. M., "Heat Convection", ***Springer Science & Business Media***, (2009).
49. Setia, H., Gupta, R., and Wanchoo, R. K., "Stability of nanofluids", (2013).
50. Giwa, S. O., Sharifpur, M., and Meyer, J. P., "Effects of uniform magnetic induction on heat transfer performance of aqueous hybrid ferrofluid in a rectangular cavity", ***Applied Thermal Engineering***, 170: 115004 (2020).

RESUME

Hani HAMIDO pursued his bachelor's degree in mechanical engineering at Aleppo University, beginning in 2005 and successfully graduating in 2009 with a GPA of 2.95.

Following the completion of his degree, Hani launched his professional career as a Mechanical Manufacturing Engineer at Dubies Establishment in Aleppo, Syria, contributing actively from 2009 to 2013. Subsequently, he ventured to Dubai and took on the role of Mechanical Maintenance Engineer at Dubai Municipality, serving from 2013 to 2014.

Seeking to embrace new challenges, Hani entered the dynamic oil and gas industry, joining Halliburton Company as a Project Engineer in the Abu Dhabi branch in 2014. In 2018, he transitioned to the role of Repair and Maintenance Engineer at Halliburton's Dubai branch. His unwavering dedication and deep expertise allowed him to make consistent contributions to a variety of projects until 2023. This milestone year saw him being appointed as Team Lead during his relocation to Halliburton Australia, marking an exciting new phase in his Halliburton journey.

Hani Hamido's steadfast commitment to continuous growth and pursuit of excellence motivated him to embark on a Master's degree program at Karabuk University in 2020. This decision further enriched his academic and professional achievements.